

**INVESTIGATING THE ROLES OF SRRM4 IN CONTRIBUTION TO
NEUROENDOCRINE PROSTATE CANCER PROGRESSION**

by

Yinan Li

M.D, Shanghai Jiaotong University, 2010

M.Sc, Shanghai Jiaotong University, 2013

A THESIS SUBMITTED IN PARTIAL FULFILLMENT OF

THE REQUIREMENTS FOR THE DEGREE OF

DOCTOR OF PHILOSOPHY

in

THE FACULTY OF GRADUATE AND POSTDOCTORAL STUDIES

(Reproductive and Developmental Sciences)

THE UNIVERSITY OF BRITISH COLUMBIA

(Vancouver)

October 2018

© Yinan Li, 2018

Committee Page

The following individuals certify that they have read, and recommend to the Faculty of Graduate and Postdoctoral Studies for acceptance, the dissertation entitled:

Investigating the roles of SRRM4 in contribution to neuroendocrine prostate cancer progression

submitted by Yinan Li in partial fulfillment of the requirements for

the degree of Doctor of Philosophy

in Reproductive and Developmental Sciences

Examining Committee:

Xuesen Dong, Reproductive and Developmental Sciences

Supervisor

Michael Cox, Experimental Medicine

Supervisory Committee Member

Colin Collins, Genome Science and Technology

Supervisory Committee Member

Honglin Luo, Pathology & Laboratory Medicine

University Examiner

Chinten James Lim, Experimental Medicine

University Examiner

Additional Supervisory Committee Members:

Yuzhuo Wang, Experimental Medicine

Supervisory Committee Member

Supervisory Committee Member

Abstract

While androgen receptor pathway inhibition (ARPI) has significantly increased the survival of metastatic prostate adenocarcinoma (AdPC), accumulating evidence suggests that AdPC can change to a more aggressive subtype, called treatment-induced neuroendocrine prostate cancer (t-NEPC). T-NEPC is androgen receptor (AR) indifferent, and shows a neuroendocrine-like phenotype. Few targeted therapy is currently available for t-NEPC. It is imperative to identify biomarkers for early detection of t-NEPC and molecular targets for drug development.

In this work, using whole transcriptome sequencing on t-NEPC from two independent patient cohorts, we have identified a t-NEPC specific splice signature that is predominantly controlled by the RNA splicing factor, serine/arginine repetitive matrix 4 (SRRM4). We have found that SRRM4 is highly expressed in t-NEPC and is strongly correlated with t-NEPC biomarker expression. Significantly, we have, for the first time, shown that SRRM4 can transform LNCaP adenocarcinoma cells into t-NEPC xenografts. We also confirmed that one of SRRM4 target genes was the RE1 silencing transcription factor (REST), a key regulator of neurogenesis. Moreover, The ARPI combined with a gain of SRRM4-induced adenocarcinoma cells to assume multicellular spheroid morphology, and this was essential in establishing progressive NEPC xenografts. We also identified a BHC80 splice variant, BHC80-2, that functions as a key facilitator of t-NEPC development. Functionally reprogrammed by the SRRM4, BHC80-2 does not confer the NEPC

phenotype to cancer cells, but rather stimulates cell proliferation and invasion to accelerate tumor progression. In contrast to the epigenetic role of BHC80 in histone demethylation, we defined a novel non-epigenetic action of BHC80-2, whereby cytosolic BHC80-2 proteins trigger the MyD88-p38-TTP pathway to increase the RNA stability of a set of tumor-promoting cytokines. Blocking BHC80-2 signaling suppresses NEPC cell spheroid growth, identifying BHC80-2 as a potential therapeutic target for t-NEPC.

Overall, my doctoral studies confirmed that SRRM4 is both a biomarker and a driver of t-NEPC by regulating tumor cell growth and metastasis in addition to its previously reported roles in neuroendocrine differentiation. Our studies not only enhance our understanding of the mechanisms of NEPC development, but also provide insights for personalized medicine-based strategies for prostate cancer patients.

Lay Summary

Prostate cancer affects one in every seven men in developed countries. The primary treatment for advanced prostate cancer patients is hormonal therapy. However, recent findings indicate that this treatment can facilitate tumor transformation into a more aggressive type of cancer, called treatment-induced neuroendocrine prostate cancer (t-NEPC). In this research, we have identified a gene named SRRM4, which is highly expressed in t-NEPC tumors. Significantly, our studies have, for the first time, shown that SRRM4 is a powerful driver of NEPC, and patients who have SRRM4 expression are more likely to progress into NEPC. I also identified a SRRM4-target gene called BHC80. In t-NEPC patients, the BHC80 gene generates an unusual variant called BHC80-2 which can facilitate t-NEPC progression. Therefore, SRRM4 has the potential to become a NEPC biomarker and a therapeutic target. This information may aid detection of t-NEPC and direct drug development for t-NEPC.

Preface

All the work presented in this dissertation was primarily completed by me under the supervision of Dr. Xuesen Dong. Together with Dr. Dong, I developed the projects and designed the experiments. All the in vitro experiments were performed by me except for the ChIP, RNA-seq and pathologic assays. I performed most of the in vivo experiments with the help of Mary Bowden and Hui Xue. RNA-seq analysis is performed by Dr. Nilgun Donmez, Dr. Cenk Sahinalp, and Dr. Colin Collins. Pathologic assays are performed by Dr. Qingfu Zhang, Dr. Ladan Fazli, and Dr. Jiaoti Huang. I contributed to all the other data collection and analysis. The content of this dissertation contains four original research papers. Chapter 3 is based on a manuscript published in Prostate [Yinan Li, Qingfu Zhang, Jessica Lovnicki, Ruiqi Chen, Ladan Fazli, Yuzhuo Wang, Martin Gleave, Jiaoti Huang, and Xuesen Dong (2018) SRRM4 Gene Expression Correlates with Neuroendocrine Prostate Cancer. doi: 10.1002/pros.23715.]. Chapters 4 and 5 are based on two research papers published in European Urology [Yinan Li, Nilgun Donmez, Cenk Sahinalp, Ning Xie, Yuwei Wang, Hui Xue, Fan Mo, Himisha Beltran, Martin Gleave, Yuzhuo Wang, Colin Collins, and Xuesen Dong (2017) SRRM4 Drives Neuroendocrine Transdifferentiation of Prostate Adenocarcinoma under AR Pathway Inhibition. 71(1):68-78.] and Oncotarget [Yinan Li, Ruiqi Chen, Mary Bowden, Fan Mo, Yen-Yi Lin, Martin Gleave, Colin Collins, and Xuesen Dong (2017) 8(40): 66878–66888.]. Furthermore, the research paper entitled “RNA Splicing of the BHC80 Gene Facilitates Neuroendocrine Prostate Cancer Progression” [Yinan Li, Ning Xie, Ruiqi

Chen, Ahn Lee, Emma A. Morrison, Ladan Fazli, Catherine A. Musselman, Yuzhuo Wang, Martin E. Gleave, Colin Collins, and Xuesen Dong] is incorporated into Chapter 6. This manuscript was prepared at the time of the online submission of my doctoral dissertation. During my PhD, I was also involved in several additional projects in collaboration with other laboratory members, and contributed to five peer-reviewed articles as co-author.

The reuse and reprint of all published work is with permission from the journals as indicated. The *in vivo* work was approved by the University of British Columbia Animal Care Committee (A14-0088). All other experiments were carried out in accordance with the University of British Columbia Biosafety Committee approved protocol number #B13-0187.

Table of Contents

Abstract.....	iii
Lay Summary	v
Preface.....	vi
Table of Contents	viii
List of Tables	xii
List of Figures.....	xiii
List of Abbreviations	xvi
Acknowledgements	xxi
Chapter 1: Introduction	1
1.1 Prostate cancer	1
1.2 Treatment-induced neuroendocrine prostate cancer	9
1.3 Development of T-NEPC.....	15
1.4 Thesis theme and rationale.....	30
1.5 Hypotheses and specific aims	32
Chapter 2: Materials and Methods	33
2.1 Sample collection and RNA sequencing.....	33
2.2 Bioinformatics analysis of RNA-Seq data.....	33
2.3 COMPAS pipeline summary	33

2.4 Tissue microarrays (TMAs).....	34
2.5 RNA <i>in situ</i> hybridization (RISH) and immunohistochemistry (IHC) analyses	35
2.6 Cell lines and cell culture.....	36
2.7 Transfection and RNA silencing.....	37
2.8 Antibodies and Western blot.....	37
2.9 Reverse-transcription and real-time qPCR	39
2.10 Construction of REST and BHC80 minigenes	47
2.11 RNA-immunoprecipitation (RNA-IP) assays	47
2.12 RNA-Protein interaction assay	48
2.13 Lentiviral approaches to constructing cell lines.....	49
2.14 Multicellular spheroid formation and immunofluorescence analysis.....	50
2.15 BrdU incorporation and colony formation assays	50
2.16 Renal capsule xenografts	51
2.17 Luciferase reporter assays.....	51
2.18 Immunofluorescence assays.....	51
2.19 Cell proliferation, migration, invasion, and colony formation assays	52
2.20 Human prostate cancer subcutaneous xenografts	53
2.21 RNA run-on assay and stability assay	53
2.22 Co-immunoprecipitation.....	54

2.23 Proximity Ligation Assay (PLA)	54
2.24 3D spheroid culture and high throughput screening system	55
2.25 Statistical analysis	56
Chapter 3: SRRM4 Gene Expression Correlates with Neuroendocrine Prostate Cancer ...	57
3.1 Introduction	57
3.2 Results	59
3.3 Discussion	73
Chapter 4: SRRM4 Drives Neuroendocrine Transdifferentiation of Prostate Adenocarcinoma under Androgen Receptor Pathway Inhibition.....	79
4.1 Introduction	79
4.2 Results	80
4.3 Discussion	95
Chapter 5: Establishment of a Neuroendocrine Prostate Cancer Model Driven by SRRM4	102
5.1 Introduction	102
5.2 Results	104
5.3 Discussion	115
Chapter 6: RNA Splicing of the BHC80 Gene Facilitates Neuroendocrine Prostate Cancer Progression	121
6.1 Introduction	121
6.2 Results	124

6.3 Discussion.....	144
Chapter 7: Closing Remarks.....	148
7.1 Conclusion	148
7.2 Research significance.....	151
7.3 Limitations and Future Directions	153
Bibliography	158

List of Tables

Table 2.1 Antibody information	38
Table 2.2 Realtime qPCR primer information	41

List of Figures

Figure 1.1 Prostate cancer progression	2
Figure 1.2 Prostate tissue structure	4
Figure 1.3 Basic prostate anatomy	4
Figure 1.4 Different subtypes of castration-resistant prostate cancer	11
Figure 1.5 Different pathological characteristics of neuroendocrine prostate tumors	12
Figure 3.1 COMPAS identifies a NEPC-specific signature in prostate tumor biopsies	60
Figure 3.2 Different spliced genes between AdPC and t-NEPC	61
Figure 3.3 SRRM4 is associated with the common NEPC-specific splicing signature	62
Figure 3.4 Validation of SRRM4 probes for RNA ISH assays	64
Figure 3.5 SRRM4 expression in castrate-resistant prostate tumors	66
Figure 3.6 SRRM4 expression correlates with t-NEPC	68
Figure 3.7 SRRM4 expression in PDXs	70
Figure 3.8 SRRM4 expression in treatment-naïve and NHT-treated AdPC tumors	72
Figure 4.1 SRRM4, REST, and REST4 expression in PCa tumors and cell lines	81
Figure 4.2 SRRM4 is an upstream regulator of REST	83
Figure 4.3 SRRM4 regulates alternative splicing of REST in prostate cancer cells	85
Figure 4.4 Androgen receptor pathway inhibition enhances SRRM4 actions to induce the NEPC phenotype	87

Figure 4.5 Roles of TP53 and RB1 depletion in SRRM4-induced NEPC phenotype.....	89
Figure 4.6 SRRM4 alters the morphology of epithelial prostate cancer cells	91
Figure 5.1 Comparison of RNA splicing and transcriptome of LnNE P0 cells with NEPC	106
Figure 5.2 Establishment of LnNE neuroendocrine prostate cancer xenografts	109
Figure 5.3 LnNE cell morphology and neuroendocrine phenotypes	111
Figure 5.4 LnNE cell proliferation and transfection efficacy	113
Figure 5.5 3D culture of LnNE cells.....	115
Figure 6.1 Expression of BHC80-2 splice variant is upregulated in NEPC	124
Figure 6.2 Validation of BHC80-1 and BHC80-2 probes	125
Figure 6.3 Expression of BHC80-2 splice variant is correlated with t-NEPC progression.....	127
Figure 6.4 SRRM4 expression is correlated with alternative splicing of the BHC80 in PCa cells	129
Figure 6.5 SRRM4 regulates alternative splicing of the BHC80 in PCa cells	131
Figure 6.6 BHC80-2 does not confer LNCaP cell NEPC phenotype	132
Figure 6.7 BHC80-2 increases PCa proliferation, invasion, and xenograft growth	134
Figure 6.8 Genes and cellular function regulated by BHC80-2.....	136
Figure 6.9 BHC80-2 regulates target cytokines expression through MyD88.....	138
Figure 6.10 BHC80-2 regulates the RNA stability of target cytokines through the MyD88-p38- TTP pathway.....	140

Figure 6.11 BHC80-2 directly interacted with Myd88 141

Figure 6.12 Blocking BHC80-2 signaling via MyD88 and CCL20 suppresses PCa spheroid
growth 143

List of Abbreviations

2D: two-dimensionality

3D: three-dimensionality

AdNE: prostate adenocarcinoma with abundant neuroendocrine cells

AdPC: prostate adenocarcinoma

AR: androgen receptor

ARPI: androgen receptor pathway inhibition

AS: alternative splicing

AURKA: aurora kinase A

BHC80: BRAF35/HDAC2 Complex Protein (80 KDa)

BPH: benign prostatic hyperplasia

BrdU: 5-Bromo-2'-deoxyuridine

BRN2: brain-specific Homeobox/POU domain protein 2

cAMP: cyclic adenosine monophosphate

CCL2: C-C motif chemokine ligand 2

CCL20: C-C motif chemokine ligand 20

CD: cytosine deaminase

CHGA: chromogranin A

CHGB: chromogranin B

CRPC: castrate-resistant prostate cancers

CTL: control

CSC: cancer stem cell

CXCL10: C-X-C motif chemokine ligand 10

DAPI: 4',6-diamidino-2-phenylindole

DHT: dihydrotestosterone

DMEM: dulbecco's modified eagle medium

EMT: epithelial-mesenchymal transition

ENZ: enzalutamide

ERK1/2: extracellular signal-regulated kinase 1/2

FBS: fetal bovine serum

FDR: false discover rate

GO: Gene ontology

GSEA: gene set enrichment analysis

H&E: hematoxylin and eosin

HDAC: Histone deacetylases

HP1 α : Heterochromatin protein 1 α HP1 α

IHC: immunohistochemistry

IL-6: Interleukin 6

IL-8: Interleukin 8

I κ B α : inhibitor of κ B α

IP: immunoprecipitation

KRAS: kirsten rat sarcoma 2 viral oncogene homologue

LBD: ligand-binding domain

LSD1: lysine demethylase 1A

MAPK: mitogen activated protein kinase

MEAF6: MYST/Esa1 associated factor 6

MTS:3-(4,5-dimethylthiazol-2-yl)-5-(3-carboxymethoxyphenyl)-2-(4-sulfophenyl)-2H-tetrazolium

Myd88: myeloid differentiation primary response 88

NE: neuroendocrine

NEPC: neuroendocrine prostate cancer

NES: normalized enrichment score

NF- κ B: nuclear factor kappa beta

NHT: neoadjuvant hormone therapy

N-myc: MYCN Proto-Oncogene, BHLH Transcription Factor

OS: overall survival

PBS: phosphate-buffered saline

PCR: polymerase chain reaction

PDX: patient derived xenograft

PEG10: paternally expressed 10

PH: pleckstrin homology

PI3K: phosphatidylinositol-3-kinase

PKB: protein kinase B

PSA: prostate-specific antigen

RB1: retinoblastoma transcriptional corepressor 1

REST: RE1 silencing transcription factor

REST4: RE1 silencing transcription factor splicing variant 4

RISH: RNA *in situ* hybridization

RNA-seq: RNA sequencing

RTK: receptor tyrosine kinase

RPMI: Roswell park memorial institute

SCG3: secretogranin III

SCID: severe combined immune deficient

SCNC: small cell neuroendocrine carcinoma

SD: standard deviation

SEM: standard error of the mean

ShRNA: short hairpin RNA

SH2: src-homology-2

SiRNA: small interfering RNA

SOX2: SRY-box 2

SRC: proto-oncogene, non-receptor tyrosine kinase

SRRM4: serine/arginine repetitive matrix 4

SYP: synaptophysin

TKI: tyrosine kinase inhibitor

TMA: tissue microarrays

TNF: tumor necrosis factor

TTP: tristetraprolin

TP53: tumor protein p53

TRAMP: transgenic adenocarcinoma of the mouse prostate

UGE: urogenital sinus epithelium

UGM: urogenital sinus mesenchyme

WT: wild type

Acknowledgements

First, I would like to express my deepest gratitude to my supervisor, Dr. Xuesen Dong, for giving me the opportunity to pursue this PhD project, and for his guidance and support throughout these years. His enthusiasm towards research, attitude to work, and vibrant personality enlightened me and kept me going strong. His supervision has shaped my professional life, enabling me to overcome academic challenges.

I would also like to express my sincere appreciation to the members of my supervisory committee: Dr. Colin Collins, Dr. Michael Cox, and Dr. Yuzhuo Wang. They have provided me with so much constructive advice for my project and career.

My sincere thanks go to all Dong lab members, including Mrs. Ning Xie, Dr. Liangliang Liu, Dr. Haolong Li, Ms. Yue Yu, Ms. Ahn Lee, Mr. Ruiqi Chen, Dr. Yu Gan, and Ms. Jessica Lovnicki, I am so glad to be a part of the team.

It is my honor to be a part of the Vancouver Prostate Centre, and I would like to thank our collaborators, Dr. Martin Gleave and Dr. Ladan Fazli from the Vancouver Prostate Centre for their generous help.

I wish to express my gratitude to the Reproduction and Development Sciences Program. I truly appreciate all the funding supporting my study, particularly from the Prostate Cancer Canada-Movember Trainee Award, and the China Scholarship Council.

Finally, I would like to thank my wife and family, who are dearest to my heart. I am so grateful for all of the support and love from you.

Chapter 1: Introduction

1.1 Prostate cancer

1.1.1 Overview

Prostate cancer (PCa) is the most common malignancy, and is the top-rank leading cause of cancer-related death in males worldwide. About 1.5 million patients were diagnosed with prostate cancer, and more than 336,000 deaths were PCa-related globally in 2015, according to the Global Burden of Disease Study^{1, 2}. Based on the Canadian Cancer Statistics of 2017, PCa affects one in every seven Canadian males, and is the third leading cause of cancer-related death in men (<https://www.canada.ca/en/public-health/services/chronic-diseases/cancer/canadian-cancer-statistics.html>). The incidence of this disease will increase with gains in life expectancy, creating a perpetual health and financial burden on our health system. It is of great importance used as a biomarker to improve PCa diagnosis, treatment, and management.

Although surgery and localized radiotherapy can cure the majority of early stage PCa, around 30% of patients will progress to an aggressive disease state³. The next generation of Androgen Receptor Pathway Inhibition (ARPI) therapies for locally aggressive or metastatic PCa, on average leads to remission lasting 2-3 years before the disease inevitably progresses to a treatment-resistant stage, which is associated with poor prognosis, and poses considerable therapeutic challenges^{4, 5}. Emerging evidence suggests that at least one quarter of acquired drug resistance is driven by

lineage plasticity and phenotype alternation of PCa cells. In this scenario, PCa cells have undergone cellular reprogramming to adapt to ARPI treatments, to lose prostate specific antigen (PSA) expression, and to acquire a continuum of neuroendocrine (NE) phenotype. These highly aggressive and lethal tumors, are termed treatment induced neuroendocrine prostate cancer (t-NEPC).

This thesis aims to provide a contribution to the understanding of the mechanisms of t-NEPC development, and to provide insights for personalized medicine-based strategies for PCa patients.

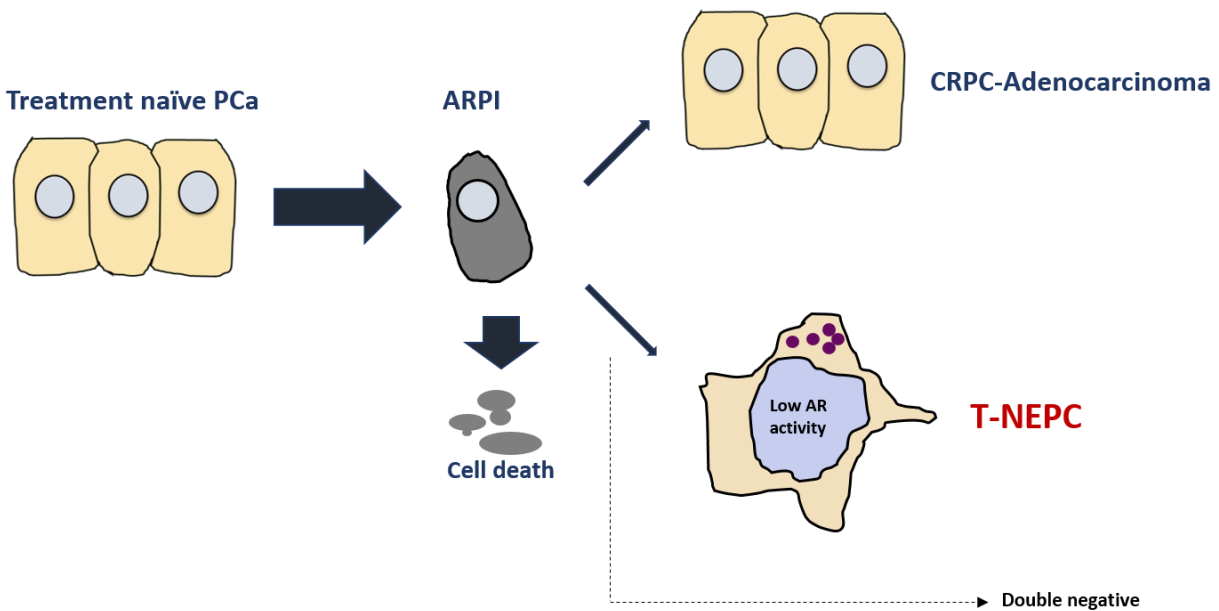


Figure 1.1 Prostate cancer progression under ARPI treatment

1.1.2 The prostate

Human prostate development is initiated during the first 10-12 weeks of gestation. During this

period, androgen activates the androgen receptor (AR) signaling of urogenital sinus mesenchyme (UGM), and promotes epithelium (UGE) budding, epithelial morphogenesis, and differentiation⁶.
7. After the maturation of the prostate stroma, the epithelial-mesenchymal interactions further induce the UGE to differentiate into several distinct cell lineages, including luminal cell and basal cell, while the UGM differentiates into prostatic smooth muscle cells and fibroblasts^{8,9}. The origin of the benign NE cells is still controversial¹⁰.

Cells of different lineages usually have different morphology, and express distinct lineage biomarkers. In the adult prostate, the luminal cells are columnar, and express cytokeratin 8 and 18. These cells are also expressed and secrete PSA. The basal cells are localized along the basement membrane of the ductal lumen, and express cytokeratin 5 and 14. In addition, NE cells are scattered within the basal epithelial cells, are mostly non-proliferating, and express NE peptides.

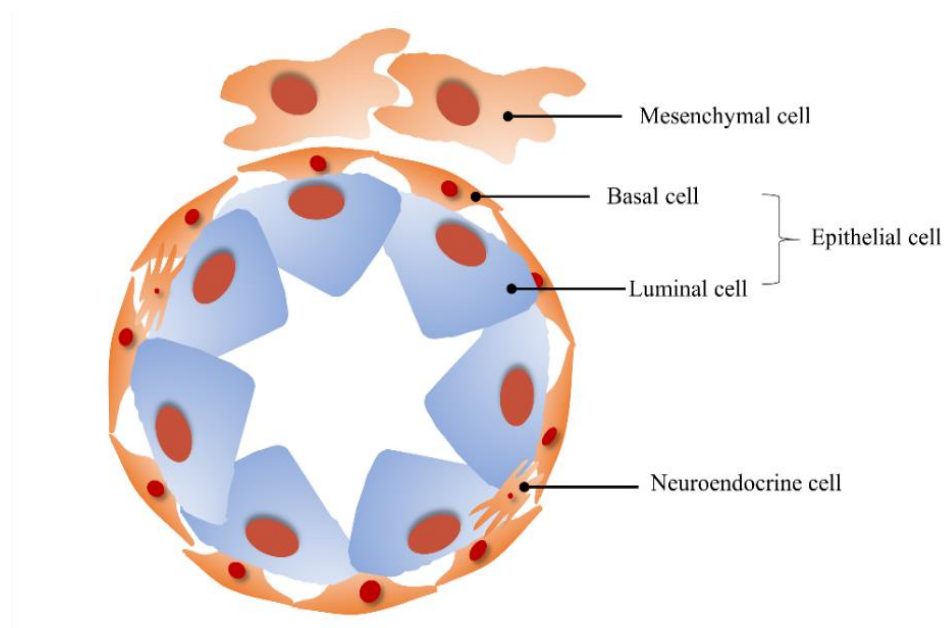


Figure 1.2 Prostate tissue structure

The adult prostate has three zones with different histological characters^{11, 12}. The peripheral zone, which includes lateral and posterior parts of the prostate, accounts for 70% of the prostatic tissue. Most PCa arise within this region¹³. The transition zone enfolds the urethra and is prone to developing benign prostatic hyperplasia (BPH)¹⁴. Finally, the central zone is between the peripheral and transition zones, and is comprised of 20-25% of the prostate.

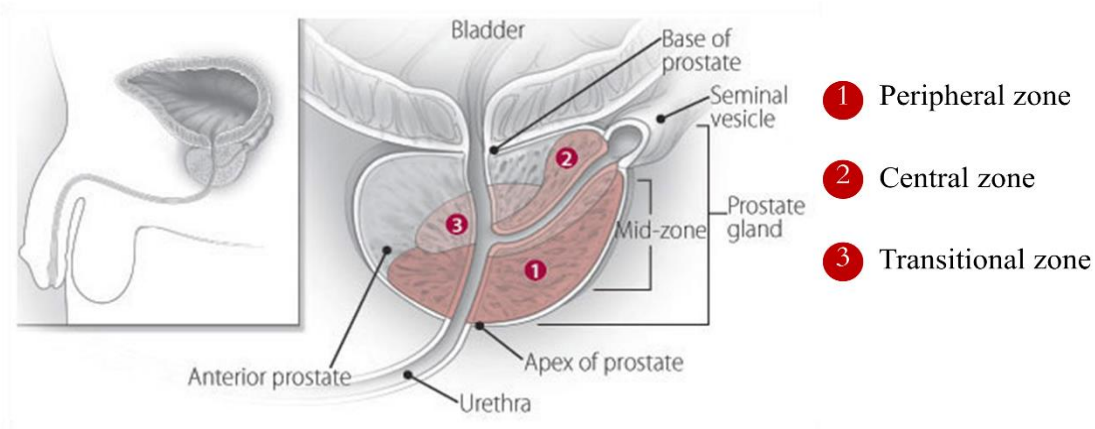


Figure 1.3 Basic prostate anatomy

Copied from <https://www.harvardprostateknowledge.org/prostate-basics> with permission

Functionally, the prostate gland can secrete prostate fluid, and helps to expel semen during ejaculation¹⁵. The prostate fluid contains various enzymes that increase the mobility of sperm; one of the most notable enzymes is PSA, which is used as a biomarker to diagnose PCa¹⁶. PSA secretion, as well as the growth and differentiation of the prostate, have been shown to be regulated by androgens and AR signaling¹⁷⁻¹⁹.

1.1.3 Prostate carcinogenesis

Three major risk factors, including age, race, and family history, are associated with PCa risk²⁰. Age is the most significant factor, as most PCa cases are diagnosed in patients over age 65^{21, 22}. During the aging process, Stochastic mutations, gene fusion, oncogene amplification, or rearrangement caused by DNA-replication errors, along with environmental factors, such as chronic inflammation, could lead to oncogenic cellular processes such as hyper-proliferation, cell de-differentiation or trans-differentiation, and disruption of biological barriers²³⁻²⁷. Moreover, men with a family history of PCa have around 6-12 times the risk of PCa, when compared to those who do not have a family history of PCa²⁸. It is also reported that black men have a 60% higher PCa risk, when compared to their counterparts globally²⁹. In addition, other factors such as germline mutations, and a high fat diet also contribute to PCa risk³⁰⁻³³.

1.1.4 Androgen receptor signaling and prostate cancer

The growth and survival of primary PCa depends on androgen and AR signaling. AR is a nuclear transcription factor belonging to the steroid receptors superfamily³⁴. The AR exerts its cellular and physiologic effects through binding to androgen using its ligand-binding domain (LBD), which allows it to be imported into the nucleus, where it recruits co-regulators to androgen-responsive elements, and subsequently results in either promotion or repression of the downstream target gene

transcription³⁵. Upon ligand binding, the AR can also activate Src through direct interaction³⁶, and promotes non-genomic action of the AR on gene transcription. In addition, the AR and its co-regulators can be phosphorylated, which leads to activation of the AR in androgen deprivation conditions³⁷.

1.1.5 Diagnosis and treatment of primary prostate cancer

Early stage PCa is usually asymptomatic due to its small size and slow growth, in contrast to invasive and metastatic PCa^{38,39}, which is characterized by frequent and painful urination, weight loss, fatigue, and pelvic or lower back pain. So far, digital rectal examination and serum PSA levels are the most widely used methods to scan for, and detect early stage PCa³⁹⁻⁴². PSA, also known as human kallikrein peptidase 3(KLK3), is a member of the kallikrein gene family, and is regulated by androgen and AR signaling⁴⁰. It is believed that elevated PSA levels in serum are probably caused by the disruption of the prostate cellular architecture, which diffuses PSA into blood circulation¹⁶. However, PSA has shown serious limitations and inconsistency as a diagnostic and prognostic marker for prostate cancer. In fact, PSA is not a cancer-specific, but an organ-specific marker. It can also rise due to other conditions such as BPH and prostatitis. Additionally, the correlation of PSA level with prostate cancer severity is rather weak, which undermines its use for disease grading⁴³.

According to the newest European Association of Urology (EAU) guideline, prostate biopsies, guided by ultrasound or magnetic resonance imaging (MRI), are suggested once PCa is suspected^{39, 41}. This systematic biopsy procedure would include a minimum of 12 core samples. Tissue samples from biopsies should be further evaluated via histopathological assessment by pathologists⁴¹. Immunohistochemistry (IHC) staining of specific biomarkers such as Ki-67 may help with the diagnosis and evaluation⁴⁴.

The Gleason Grading system is the most widely used histopathological grading and classification system of PCa. It includes 5 grades (1: well-circumscribed nodule of closely packed glands, 2: nodule with more loosely arranged glands, 3: small glands with an infiltrative pattern between benign glands, 4: large irregular cribriform glands, 5: solid nests of tumor with central comedonecrosis) based on tissue histology, followed by combining the primary pattern (most predominant) and secondary pattern (second most predominant) to produce Gleason scores ranging from 2-10^{45, 46}. Currently, Gleason scores higher than 6 are considered PCa, and Gleason scores ≥ 8 refer to a high-grade, aggressive disease with a poor prognosis^{45, 47}. In 2015, a new Gleason group system was suggested. The Gleason groups range from 1-5 (group 1: Gleason 5 and 6, group 2: Gleason 3+4, group 3: Gleason 4+3, group 4: Gleason 4+4 and group 5: Gleason 9 and 10) with 5 being the most aggressive, with the worst prognosis^{48, 49}. In addition to Gleason groups, the TNM system indicates the carcinoma staging, location, invasion, and metastasis of the tumor⁵⁰. Within

the system, T (1-4) refers to the tumor within and immediately adjacent to the prostate tissue, N (0-1) describes lymph node metastasis stage, and M (0-1) refers to the presence of distant metastasis. According to the newest guideline, nucleotide-based tests such as PCA3 level, Genomic Prostate Score, and Cell Cycle Progression Score may also be taken into consideration in PCa evaluation^{40, 51-56}.

According to the EAU guidelines, treatment options for low and intermediate risk PCa include active surveillance (particularly in low risk Gleason 6 PCa), surgery, and radiation therapy^{57, 58}. Patients who choose active surveillance are monitored with DRE and PSA testing twice or four times a year, and repeated prostate biopsy every year⁵⁹.

Patients with high-risk PCa (Tumor stage \geq T2c, Gleason group \geq 3, and/or PSA>20 ng/ml) and a life expectancy of at least 10 years are recommended to receive therapies such as surgery and radiation therapy with neoadjuvant hormone therapy (NHT)^{60, 61}.

1.1.6 Recurrent advanced prostate cancer and androgen pathway inhibition therapy.

Although surgery and radiation therapies effectively cure most localized PCa, about 20-30% of cases that have undergone these therapies will progress to advanced stages within 5 years³. PCa recurrence is defined by re-rising PSA levels after radical prostatectomy (biochemical relapse) or

by metastasis of the disease that is detected by MRI and positron emission tomography (PET) scanning⁶². First line treatment for locally advanced, recurrent, and metastatic PCa is ARPI⁶³⁻⁶⁵. ARPI targets AR-mediated functions by suppressing the production of androgens (such as abiraterone acetate)^{66, 67} and/or androgen binding to the AR ligand-binding domain (such as enzalutamide)⁶⁸⁻⁷⁰, to achieve medical or surgical castration. Despite being effective initially, virtually almost all patients will develop biochemical and clinical treatment resistance in approximately 2 to 3 years, leading to a lethal, castration resistant prostate cancer (CRPC) stage^{66, 68}.

1.2 Treatment-induced neuroendocrine prostate cancer

1.2.1 Castration resistant prostate cancer

CRPC is defined by consecutive rises in serum PSA levels and/or tumor metastasis following surgical or medical castration. Upon diagnosis, CRPC patients have approximately 2-3 years of median overall survival^{71, 72}. Even though recently approved ARPI therapies such as enzalutamide and abiraterone have shown improvements in the total survival of CRPC patients, the benefits are temporary, since resistance to these drugs eventually occurs. Clinical studies have revealed that the gain in median survival after docetaxel and enzalutamide is only 4.8 months, and after abiraterone is merely 3.9 months^{66, 68}. Several mechanisms have been proposed by which the CRPC tumors evade ARPI: 1) AR-dependent CRPC with alterations in the AR, such as AR gain-

of-function mutation, amplification, alternative splicing, and activation of co-actors that restore AR signaling⁷³⁻⁷⁹, and 2) AR-dependent CRPC with bypass or crosstalk mechanisms through glucocorticoid receptor (GR) overexpression, PI3K/AKT pathway alternation, and other mechanisms^{80, 81}. These tumors cover the majority of CRPC, and retain their AdPC phenotypes. However, it has been increasingly recognized that a subset of CRPC tumors can evade ARPI therapy through another mechanism, through which the tumors lose the luminal-epithelial phenotype, and show lineage plasticity, which makes the tumor bypass the dependency on the AR signaling. These tumors are AR “indifferent”. In fact, accompanied with the applications of more potent ARPI drugs, there is an increased incidence of tumor cells switching lineage from luminal-epithelial to neuroendocrine, during which tumor cells’ lose their luminal characteristics, and acquire NE features⁸². These tumors are usually highly aggressive and metastatic⁸³⁻⁸⁵. No effective therapies are currently available for this subtype of CRPC, besides platinum-based systemic chemotherapy⁸⁶. Another rare subtype of AR indifferent tumors, which was recently reported is a “double-negative” tumor. This kind of tumor shows no AR expression or characteristics of NE lineage. So far, how PCa cells choose their lineages to either AdPC or NEPC remains unknown.

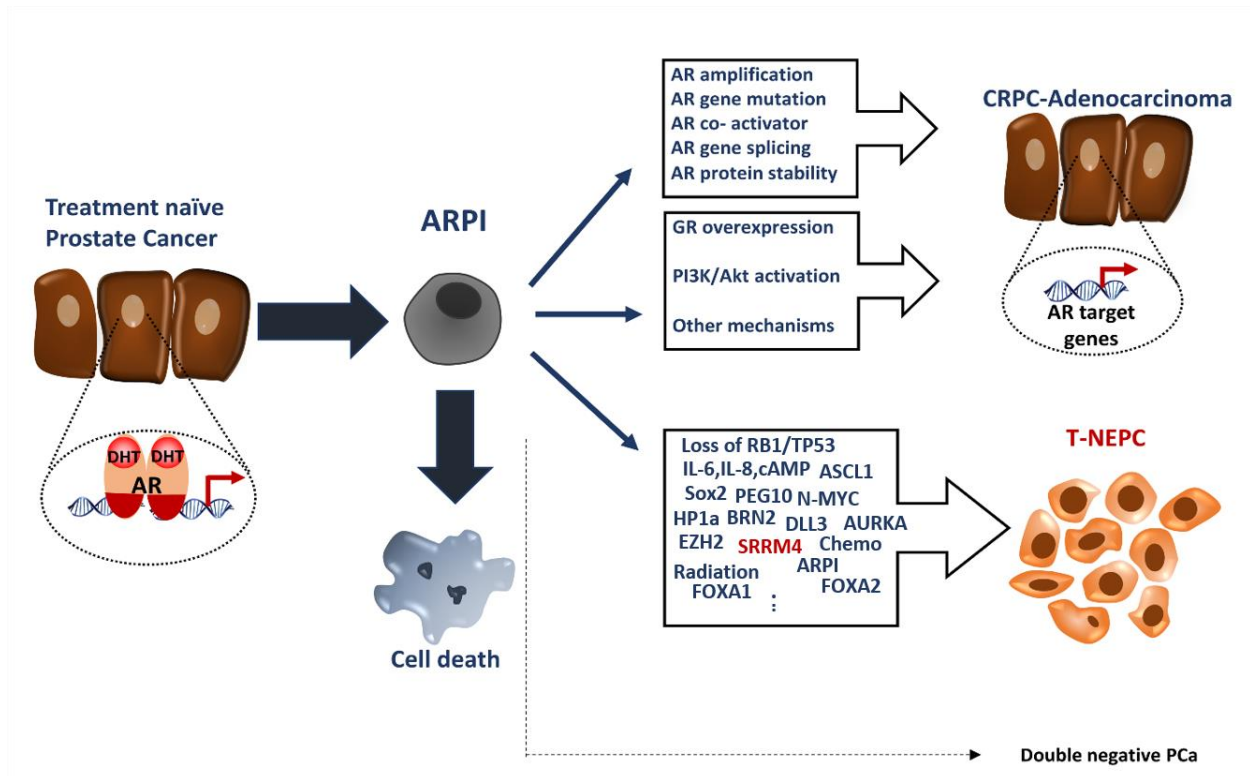


Figure 1.4 Different subtypes of castration-resistant prostate cancer

How CRPC tumors evade ARPI: 1) AR status alterations such as AR gain-of-function mutation, amplification, alternative splicing, and activation of co-actors that restore AR signaling. 2)

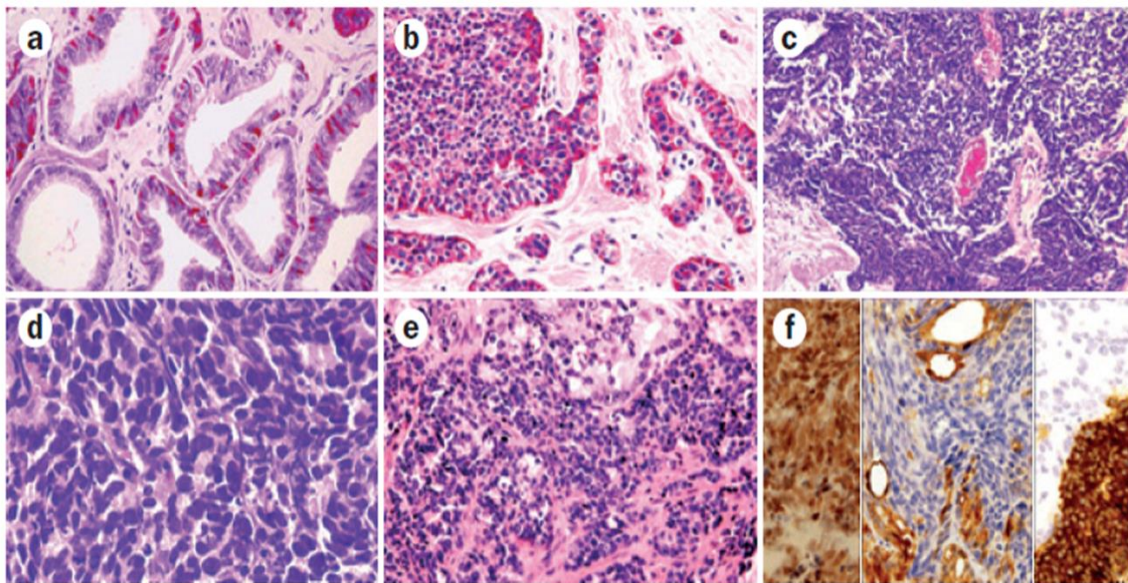
Bypass or crosstalk mechanisms through GR overexpression, PI3K/AKT pathway alternation, and other mechanisms. These tumors retain their AdPC phenotypes. 3) Switching lineage from luminal-epithelial to neuroendocrine. 4) Becoming a “double-negative” tumor. This kind of

tumor shows no AR expression or characters of NEPC.

1.2.2 Characteristics of t-NEPC

In a clinical setting, the definition of NEPC is based on the presence of small cell neuroendocrine

carcinoma (SCNC) morphological features, which include a proliferation of small cells with unique and strict morphological features, scant cytoplasm, finely granular ‘salt and pepper’ chromatin, absent or inconspicuous nucleoli, poorly defined borders, and a high mitotic count. The small cell morphology accounts for about half of diagnosed t-NEPC⁸⁷⁻⁸⁹. Morphological variations of NEPC also include usual prostate adenocarcinoma with NE differentiation, adenocarcinoma with Paneth cell NE differentiation, carcinoid tumor, large cell neuroendocrine carcinoma, and mixed neuroendocrine carcinoma-acinar adenocarcinoma^{82, 87, 90}.



Nadal, R. et al. Nat. Rev. Urol. 11, 213–219 (2014)

Figure 1.5 Different pathological characteristics of neuroendocrine prostate tumors

A) Adenocarcinoma of the prostate with focal neuroendocrine differentiation. **B)** Adenocarcinoma of the prostate with Paneth-cell-like changes. **C)** Primary prostatic carcinoid tumor. **D-E)** Prostatic small-cell carcinoma. **F)** Large-cell neuroendocrine carcinoma of the prostate.

Diagnosing t-NEPC by morphological characters can be challenging because the transition from AdPC to t-NEPC is not an acute process, and involves sequential molecular and morphological alterations, resulting in multiple intermediate transitional phenotypes^{88,91}. Early stages of t-NEPC may consist of scattered tumor cells expressing NE markers, admixed with AdPC cells with minor morphological changes. On the contrary, later stage t-NEPC often presents with SCNC morphology and NE marker expression throughout the tissue. However, even these distinct morphological characteristics of SCNC can still overlap with poorly differentiated Gleason pattern 5 AdPC that have a solid pattern without glandular structures with central necrosis^{89,92}. In addition, tumor cell morphology can be more complex when treated with ARPI, radiation, and chemical therapies. Under these circumstances, detecting NE markers such as synaptophysin (SYP), chromogranin A/B (CHGA/CHGB), CD56, and neuronal-specific enolase (NSE), using IHC techniques are often used to facilitate the diagnosis. NEPC is positive for one or more NE markers in almost 90% of cases⁹². Usually there is low, or no, PSA /AR expression in NEPC. However, during the NEPC trans-differentiation process, The AR and PSA can be positive⁹³. Through analyzing 604 samples from four different RNA-seq prostate cancer data sets, researchers have proposed a bioinformatics-based diagnosis system called integrative NEPC score by weighting expression levels of genes associated with NEPC⁹⁴. However, this method is highly dependent on the pathological diagnosis of the samples used to train the model. So far, there is no universal NE

marker profile that can be used as a “gold standard” to diagnose t-NEPC. These findings highlight the importance of identifying new reliable NE markers of t-NEPC.

1.2.3 T-NEPC is an emerging clinical challenge

Primary (*de novo*) NEPC is extremely rare and only accounts for ~0.5-2% of all PCa⁹⁵. However, our research focuses on treatment-induced NEPC (t-NEPC). T-NEPC is distinct from primary NEPC, because patients with these tumors usually have a history of, or concomitant, typical prostatic adenocarcinoma, and have received single or multiple rounds of ARPI, radiation therapy, or chemotherapy⁸⁷. It is estimated that t-NEPC accounts for 13-17% of total CRPC^{85, 88, 93, 96}. T-NEPC is an emerging clinical challenge for several reasons:

- 1) It is under-diagnosed, and it is therapy-induced. The diagnosis of t-NEPC requires the evaluation of histological features and NE markers of tumor biopsies. However, patients with metastatic PCa rarely undergo biopsies. In addition, PSA is a commonly used biomarker to monitor the efficacy of ARPI to AdPC. No/low levels of PSA in t-NEPC also often render it under-recognized until it is at a later stage of development.

- 2) T-NEPC is highly aggressive and metastatic. The tumors have a high Ki-67 index, and the majority of patients have lymph node/distal metastasis at the time of diagnosis⁹⁷. Therefore, the

median survival of t-NEPC patients is only ~ 7 months after the diagnosis is confirmed⁹⁸.

3) T-NEPC is also under-studied. Because it is under-diagnosed, t-NEPC has not drawn much attention to itself, until recent reports from Science, Cancer Cell, and Nature Medicine emerged on t-NEPC^{94, 99-102}, a few years after enzalutamide and abiraterone were utilized as clinical treatments¹⁰³. How t-NEPC develops remains largely unknown, although several targeted therapies for t-NEPC have been studied, as led by an aurora-A kinase (AURKA) inhibitor MLN8237 (NCT01799278) in phase II clinical trials. EZH2 inhibitors are also being evaluated in pre-clinical models for t-NEPC; beyond systemic chemotherapy, no targeted therapy is available in clinical application now. The lack of therapies reflects our limited knowledge of the molecular underpinning of t-NEPC development. To overcome these barriers for t-NEPC management, early detection of t-NEPC and identification of therapeutic targets are urgently needed.

1.3 Development of T-NEPC

1.3.1 T-NEPC is derived from AdPC

The finding of TMPRSS2:ERG gene fusion by fluorescent *in situ* hybridization confirmed that NEPC is prostatic in origin⁹³. However, a consensus on how t-NEPC is generated has not yet been reached. Multiple hypotheses have been proposed, including that t-NEPC originates from either:

1) PCa stem-like cells that retain traits of self-renewal, invasion, and resistance to apoptosis under

hormone therapy⁹¹, or 2) AdPC cells undergo NE differentiation, followed by t-NEPC tumor establishment^{94, 104, 105}, or 3) benign prostatic neuroendocrine cells acquire tumor genetic capacity⁹⁷. Using whole-exome sequencing technology, research has revealed that despite distinct pathologic and clinical differences, t-NEPC and AdPC cells in patients, as well as in PDXs, carry similar gene mutation landscapes, including the distribution of non-silent point mutations, polyploidy, and somatic copy-number genomic burden^{94, 104}. These findings support the idea that t-NEPC originates from AdPC, but is not likely from benign prostatic neuroendocrine cells.

There is less doubt on the opinion that AdPC can acquire the cancer stem cell (CSC) phenotype, but its involvement in the emergence of t-NEPC is being debated. So far, there is no direct evidence supporting the idea that t-NEPC arises from the expansion of resident CSCs. However, ARPI was shown to induce the NE marker expression of PCa cell lines through an intermediary stem-like state, highlighting that t-NEPC may be transdifferentiated from AdPC via a CSC intermediate stage.

1.3.2 The lineage plasticity of AdPC cells

Although global genomic features of AdPC and t-NEPC are similar, some specific genomic alternations are enriched in t-NEPC. T-NEPC has a high frequency of tumor protein 53 (TP53) and retinoblastoma 1 (Rb1) gene deletions/mutations (~70-90%) when compared with AdPC (~30-

50%)⁹⁴. Recent research results have demonstrated that the loss-of-function Rb1 and TP53 have been shown to enhance prostate luminal epithelial cells possessing lineage plasticity under ARPI^{100, 101, 105}. TP53/Rb1-deficient cells possess the flexibility to adapt to transitional and alternative lineages, from luminal to NE-like, basal, or mesenchymal lineage. Lineage plasticity conferred by TP53/Rb1 deficiency is also supported by the TRAMP transgenic mouse model. Upon the expression of the transforming region of SV40 large T antigen (SV40 Tag) in the TRAMP mouse model, AdPC were developed and transformed into t-NEPC as both Rb1, and TP53, and were inactive^{106, 107}. These mice initially developed well-differentiated AdPC by ~18 weeks, and then progressed to t-NEPC tumors by ~24 weeks¹⁰⁸⁻¹¹⁰. However, TP53 and Rb1 are also well known as tumor suppressor genes, whose deficiency is also common in AdPC and other non-neuroendocrine cancers in general. This phenomenon suggests that TP53/Rb1 deficiency alone is not sufficient to induce NEPC development. Supporting this idea are the DU145 cells, which are both AR-negative and have non-functional Rb1 and TP53, yet do not show NE morphology and NE marker expression. These results suggest that in addition to the canonical effects of TP53/Rb1 deficiency that promote cell survival and proliferation, a novel impact of it is to induce a multi-lineage plasticity state, which provides AdPC cells with a chance to transdifferentiate, but does not specifically drive them toward t-NEPC. Additional driver genes are still required to set the direction of NE differentiation of cancer cells toward t-NEPC tumorigenesis.

Epigenetic modifiers also play an important role in lineage plasticity. It has been reported that the DNA methylation status between AdPC and t-NEPC tumors is significantly different. In addition, the expression of a histone methyltransferase called EZH2 is upregulated in t-NEPC tumors^{94, 99, 111}. Recent findings have shown that increased EZH2 activity represses AR signaling and promotes an enhanced activation of the PI3K/AKT pathway to drive t-NPEC development¹⁰². Although further studies are required, these results suggest a potential mechanism by which the reprogramming of the epigenome can drive t-NEPC development.

The expression and function of transcription factors contributes greatly to the generation of t-NEPC as the transcriptome of AdPC and t-NEPC, and are quite distinct. In Rb1 and TP53 deficient LNCaP cells, upregulation of transcription factor SOX2 was observed¹⁰¹. SOX2 is a putative development factor that is essential for self-renewal and pluripotency. Knocking down SOX2 can halt the ARPI-induced lineage plasticity of Rb1 and TP53 deficient LNCaP cells¹⁰¹. Moreover, recent studies have reported that a POU-domain transcription factor, BRN2, can significantly promote NE marker expression and t-NEPC development together with SOX2 in CRPC cell lines¹¹². Heterochromatin protein 1 α (HP1 α) promotes NE transdifferentiation and reduces expression of AR and RE1 silencing transcription factor (REST) through repressing trimethylated histone H3 at Lys9 (H3K9me3) mark on their respective gene promoters¹¹³. To date, these findings

hint at the significance of genetic and epigenetic modifications conferred through the lineage plasticity of AdPC cells under ARPI treatment conditions.

1.3.3 Alternative splicing

Regardless of their largely similar genomic profiles, our primary research results have found that the transcriptome and splicing signature of t-NEPC is distinct, when compared to that of castration-resistant AdPC, indicating that RNA alternative splicing (AS) plays a crucial role in t-NEPC tumorigenesis¹¹⁴. AS is a process that enables a single gene to code for multiple protein isoforms. In this process, particular exons of a gene may be either included within, or excluded from, the mature mRNA produced by that gene to generate different splicing variants¹¹⁵. Despite the alternative splicing that occurs within the untranslated region, there are still about 70-88% of AS events that change the protein amino acid sequence, structures, and biological functions¹¹⁶⁻¹¹⁸. AS is a common phenomenon in eukaryotes, where it greatly increases the diversity of proteins that are encoded by the genome. Notably, in humans, about 30-95% of multi-exonic genes are alternatively spliced, which allows the human genome to direct the synthesis of many more proteins than would be expected from its twenty thousand protein-coding genes^{119, 120}, suggesting that AS is one of the most significant components of the functional complexity of the human genome.

AS is regulated by a system that includes trans-acting proteins and cis-acting binding motives. The trans-acting splicing factors can recognize and bind to the specific binding motives, and promote or reduce the usage of particular splicing sites¹²¹⁻¹²⁵. There are numerous modes of alternative splicing observed, of which the most common are exon skipping and inclusion. In these modes, a particular exon may be included in mRNAs under some conditions or in particular tissues, and omitted from the mRNA in others¹¹⁵. The majority of these changes appear to be in-frame¹¹⁸. Only 19% of the protein isoforms were shortened due to frame shift¹¹⁸. AS can have dramatic consequences on protein structure, localization, and function¹²⁶. Whereas differentially regulated AS events are significantly changed in functionally defined domains of tissue, including surface accessible and short linear interaction motifs¹²⁷⁻¹²⁹, AS events located in these regions are predicted to alter the protein functions and interactions¹³⁰.

Genome-wide analysis of AS is a challenging task. Next generation sequencing technologies have been used to conduct whole transcriptome analyses, and provide insights into alternative splicing. For example, results from the use of RNA-seq indicate that an estimated 95% of multi-exonic genes undergo alternative splicing, with a number of pre-mRNA transcripts spliced in a tissue-specific manner in humans¹²⁰. Expressed sequence tag alignment, combined with bioinformatics approaches, have also been developed to integrate RNA-seq data to predict alternatively spliced isoforms^{131, 132}. RNA-seq can also be used in *in vivo* detection of the transient middle product of

RNA splicing, the determination of branch site sequences, and the large-scale mapping of branch points in human pre-mRNA transcripts¹³³.

Abnormal variations in splicing are also implicated in disease. A large proportion of human genetic disorders result from splicing variants¹³⁴⁻¹³⁷. Both splicing factors express changes and nucleotide alterations in splice sites or cis-acting splicing regulatory motives of target genes, leading to differences in gene splicing modes and splicing variant expressions¹²². A study in 2005, involving probabilistic analyses indicated that more than 60% of human disease-causing mutations affect splicing-associated sites rather than directly affecting protein coding sequences¹³⁸. Another study in 2011, indicated that one-third of all hereditary diseases are likely to have a splicing component¹³⁹. Abnormally spliced mRNAs are also found in a high proportion of human cancer cells¹³⁵. Combined RNA-Seq and proteomics analyses have revealed striking differential expressions of splice isoforms from key proteins involved in cancer survival and proliferation pathways¹⁴⁰. Interestingly, PCa shows high amounts of aberrant exon skipping and inclusion¹³², indicating the possibility that PCa cells exploit alternative splicing processes to promote tumor growth and treatment resistance.

Among all human organs, neural tissues have the most complex repertoires of splice variants¹²⁰.¹⁴¹. This complexity reflects a growing list of alternative splicing events shown to have important

roles in neural differentiation. Neural-specific, or enriched splicing factors, such as Nova-1/2, Fox-1/2, and PTBP2 (nPTB) are reported to contribute to critical processes such as neuronal migration, synaptogenesis, and neurite outgrowth^{142, 143}. These splicing factors exert their function through regulating the splicing of downstream receptors and transcription factors^{144, 145}. Whether the similar mechanism also exists in NE differentiation of PCa, still needs to be demonstrated.

1.3.4 REST in NE differentiation

The repressor element 1 silencing transcription factor (REST) acts as a key transcription repressor of genes involved in neurogenesis. REST was identified in 1995, as a protein that binds to repressor element 1 (RE1, also known as neuron restrictive silencer element, NRSE) sequences^{146, 147}.

The REST gene structure in the protein coding region is conserved across humans, mice, and rats. The REST gene contain five exons and four introns. Exon 1 encodes untranslated regions. Exon 2 codes for the region from the N-terminal translation repressor recruitment region to the end of zinc finger 4 motif. Exon 3 is a short exon, encoding the spacer between zinc fingers 4 and 5 and the entire zinc finger 5 motif. The genomic fragment spanning exons 3 and 4 contains a neural specific exon N. Exon N of the human REST gene is 62bp long and is separated by a relatively large intron 3 from exon 3 and by a 2.5kb intron 4 from exon 4. In the mouse REST gene, exon N is 28bp long, flanked by introns 3 and 4 of 4.5 and 0.9kb in length, respectively. In both mouse REST and human REST genes, exon 4 contains the region of REST gene encoding zinc fingers 6–9 and C-terminal

transcription repressor recruitment region (Figure 1.6)¹⁴⁷.

REST binds to the 21bp RE1 site through eight C₂H₂ zinc fingers¹⁴⁷. Once associated with the chromatin, REST-mediated gene repression is achieved by the recruitment of two separate corepressor complexes, mSin3, and CoREST, in addition to other corepressors such as the histone H3 lysine 9 (H3K9) methylase, G9a, and the NADH-sensitive corepressor, CtBP26¹⁴⁸⁻¹⁵³. The mSin3 complex contains two class I histone deacetylases (HDACs), HDAC1 and HDAC2, the retinoblastoma-associated proteins RbAp48 (also known as RBBP4) and RbAp46 (also known as RBBP7), which are thought to interact with histones¹⁵⁴⁻¹⁵⁶.

Blocking REST function in vivo results in the upregulation of REST-repressed genes in non-neural tissues and neural stem and progenitor cells¹⁵⁷, whereas REST overexpression represses the expression of these genes in neuronal cells¹⁵⁸. In addition, loss of REST was associated with NEPC progression, in both clinical samples and animal models^{159, 160}. Knockdown of REST by siRNA also induced neuronal signatures in PCa cells that included NE markers such as SYP, NSE, and N-Cad, as well as EMT and stemness markers like Twist1 and CD44¹⁶¹⁻¹⁶³. Therefore, we propose the idea that as AdPC differentiates into t-NEPC, REST activity should be suppressed to allow for the expression of neuronal-specific genes. This suppression of activity is thought to arise in part from reduced REST transcript levels¹⁴⁷ and proteolytic degradation¹⁶⁴. However, the extent to

which these events affect REST activity, and whether additional mechanisms exist to downregulate REST in NE differentiation, is not known.

One important mechanism to compromise REST function is through AS. The neural specific exon N is important in the splicing regulation of REST function. Skipping of this exon is required to generate full-length REST protein in non-neural cells, whereas its inclusion between exon 3 and 4 leads to a frameshift that introduces a stop codon at the beginning of exon 4^{165, 166}. This splicing process generates a translating truncated protein isoform, named “REST4” (Figure 1.7). REST4 lacks four zinc fingers and the C-terminal repressor domain, both of which are required for full DNA-binding and repressive activity of REST. However, the extent to which AS regulation contributes to the control of REST activity and the splicing factors responsible for producing the REST4 isoform, were not completely determined.

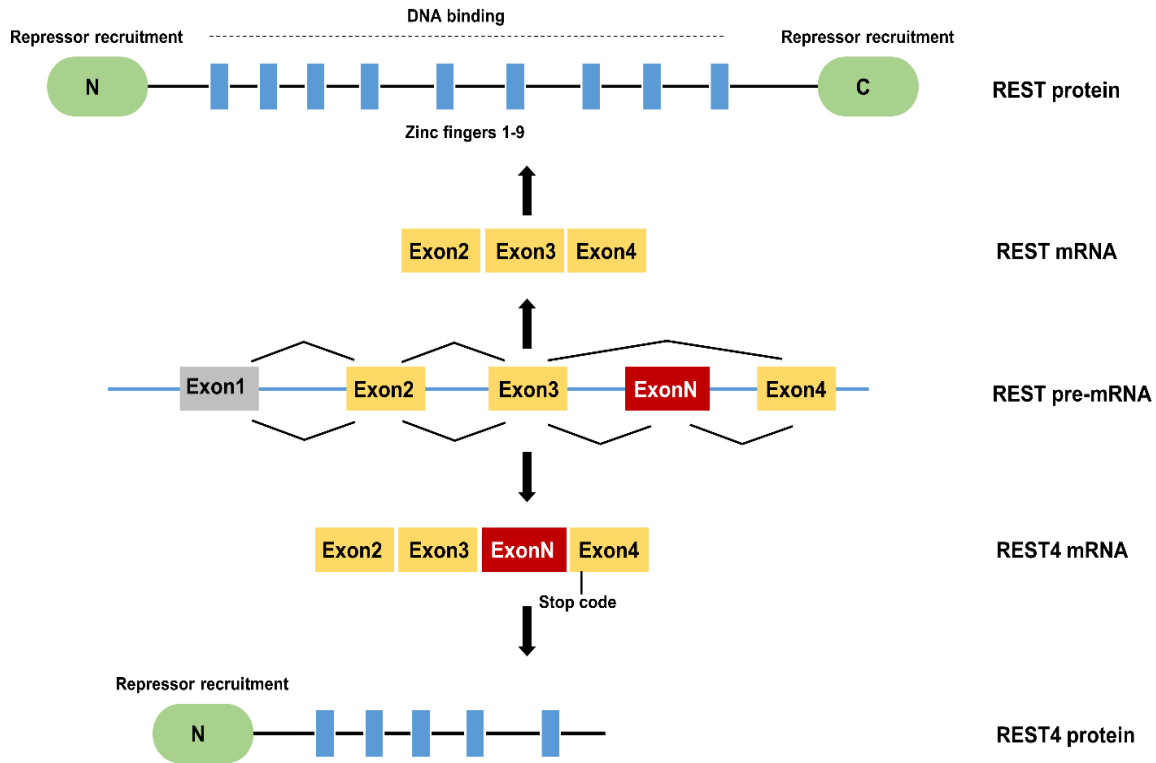


Figure 1.6 REST splicing isoforms

Alternative splicing of REST pre-mRNA. The red box indicates the neural-specific exon (Exon N). Skipping exon N is required to generate the REST protein, whereas exon N inclusion between exons 3 and 4 leads to a frameshift that introduces a stop codon at the beginning of exon 4. This splicing process generates the translating truncated protein isoform REST4.

It has been reported that transdifferentiation of PCa from AdPC to t-NEPC is associated with the loss of REST protein. REST has to be recognized as a master regulator in IL-6 induced NE transdifferentiation, as its transcription is significantly repressed upon IL-6 stimulation¹⁶⁷. Meanwhile, REST protein degradation induced by ARPI as well as PI3K/Akt inhibitors, can

facilitate a NE phenotype in AdPC cells¹⁶⁸. In conclusion, research to date supports the critical role of REST in the emergence of the NE phenotype. However, silencing REST alone is not sufficient to generate t-NEPC tumors, which indicates that other mechanisms may also take part in t-NEPC development.

1.3.5 Roles of NE differentiation in t-NEPC

Including loss-of-function of REST, AdPC cells can also undergo NE differentiation, induced by gain-of-function of N-Myc, BRN2, EZH2, HP1 α , and SOX2 or loss-of-function of the AR, and FoxA1^{101, 102, 104, 112, 169}. Additionally, AdPC cells can acquire transient NE phenotype, and NE-like morphology by cAMP, IL-6, ARPI, hypoxia, and radiation treatments *in vitro*^{167, 170-174}. However, only few of these factors enable the establishment of t-NEPC xenografts *in vivo*. These results emphasize the idea that AdPC cells can acquire NE differentiation through multiple mechanisms. Conversely, gaining NE marker expression and NE-like morphology are not sufficient for t-NEPC tumor development. As described above, t-NEPC is driven predominantly by epigenetic modifications, rather than by genetic changes^{94, 111}, suggesting that NE transdifferentiation is reversible once the driving factors are blocked or compromised¹⁰². In a clinical setting, NE marker expression is not associated with overall survival of t-NEPC patients, indicating that tumors with NE transdifferentiation are still different from highly aggressive t-NEPC. Other biological changes are needed for AdPC tumors with NE transdifferentiation to

progress into t-NEPC.

1.3.6 Roles of proliferation in t-NEPC

Development of NEPC tumors is not a quick process. It takes ~6 months in PDXs and ~5-6 years in patient tumors¹⁰⁴. However, PCa cells with neuroendocrine transdifferentiation were reported in 30-100% of adenocarcinomas¹⁷⁵⁻¹⁷⁷, indicating that gain of NEPC phenotype is not sufficient for cancer cells to become NEPC. Acquired growth advantage of NEPC over surrounding AdPC is essential. While ARPI is necessary for NE differentiation, it alone is insufficient, since only about 25% of tumors under ARPI treatment are transformed into t-NEPC⁹⁴. In fact, NE differentiation often occurs as an adaptive survival mechanism under selective pressure. *In vitro* studies have found that NE differentiation of PCa cells was often accompanied by reduced cell vitality under stimulation. (e.g. ARPI, IL-6, cAMP, hypoxia)¹⁷⁸⁻¹⁸⁰. These facts indicate that AdPC progression to t-NEPC requires not only NE differentiation, but also proliferation. Most AR-positive AdPC xenografts (e.g. LNCaP, LAPC4) are not destined to become t-NEPC by castration. NE-like cells from focal NE differentiation regions are non-proliferative, which is in contrast to those within overt NE differentiation regions that are highly proliferative in TP53/Pten knockout mice treated with castration surgery¹⁰⁵. These authors propose that a “proliferative switch” represents a molecular event in the emergence of t-NEPC. Furthermore, multiple factors including AURKA, PEG10, MEAF6, and Cyclin D1, have been implicated during t-NEPC progression¹⁸¹⁻

¹⁸⁴. AURKA is a mitotic kinase that plays important roles in early mitosis by regulating centrosome function and spindle assembly, thereby promoting cell cycle and proliferation¹⁸⁵. Upregulation of AURKA was found in almost all NEPC patients. Interestingly, AURKA overexpression did neither seem to be able to induce NE markers expression, nor have significant epigenetic impact to confer the NE phenotype to AdPC at the transcriptomic level⁹⁹. Furthermore, the placental gene PEG10 is a de-repressed gene during the adaptive response to ARPI, and is highly upregulated in NEPC patient samples and xenografts. PEG10 functionally drives the G0/G1 cell cycle progression in PCa cells in a TP53-dependent fashion while also promoting cell invasion through the upregulation of Snail expression via TGF- β signaling. However, PEG10 was not observed to exert an inductive effect on NE differentiation in AdPC cells¹⁸³. Instead of inducing NE differentiation of AdPC cells, these genes are more like facilitators of cell proliferation, invasion, and metastasis under ARPI. These findings suggest that AdPC cells may have to gain additional clonal expansion and tumor formation abilities in order to generate t-NEPC.

In summary, current evidence supports the theory that t-NEPC is derived from AdPC. While several genomic alternations confer AdPC AR-independent growth by inducing lineage plasticity of AdPC, in addition to having lineage plasticity, AdPC tumors may require the driver genes to eventually transform into NEPC and outgrow PCa cells for proliferation and expansion. Alternation of these driver genes are a strong indication of the early events that lead AdPC to

progress to t-NEPC, and therefore these genes may serve as t-NEPC biomarkers. Blocking the functions of these driver genes would also provide avenues for new therapies for t-NEPC.

1.3.7 Therapeutic approach of t-NEPC

Most often, a cisplatin-based combination chemotherapy has been used to treat t-NEPC¹⁸⁶. Although the optimal dose has not been established, a phase II study of carboplatin and docetaxel, along with second-line etoposide and cisplatin, in patients with SCNC suggests a high response rate of short duration to platinum-containing chemotherapies¹⁸⁷. However, patients become rapidly resistant to this approach. As the molecular mechanism for t-NEPC becomes gradually unveiled, targeting therapy may be possible.

The AURKA inhibitor danusertib was once used to treat PCa, but failed in a phase II clinical trial¹⁸⁸. However, it is not certain whether better response would have been achieved by focusing on t-NEPC patients, as the majority of t-NEPC tumors have amplified AURKA. Recently, a new clinical trial, evaluating the AURKA inhibitor alisertib, is on-going for patients with t-NEPC. In this trial, AURKA and MYCN co-amplification are being explored and used to select patients with high-risk PCa for early intervention of t-NEPC development¹⁸⁹.

MK-2206 is an oral AKT inhibitor. Within a phase I clinical trial containing a diverse population of 72 patients including breast, melanoma, pancreas, prostate, colon, esophageal, and small cell lung cancer, a partial response with a progression-free survival of 6 months was shown in a patient with t-NEPC, and minor responses were demonstrated in two patients with NE pancreatic cancers¹⁹⁰. However, more clinical data need to be collected for specific cancer types, and more homogenous cohorts need to be utilized to determine the clinical effects of MK-2206 on t-NEPC.

Targeting pluripotent stem cell transcription factors could provide opportunities for blocking cell lineage plasticity, thereby hindering NE transdifferentiation. Treatment with short hairpin RNA knockdown of SOX2 has been demonstrated to prevent tumor growth *in vivo*^{191, 192}.

So far, most supportive evidence for t-NEPC targets and corresponding drugs is derived from preclinical studies, or *in vivo* models. At the clinical level, there is no direct evidence, and all data are extrapolated from studies in CRPC. Thus, there is an urgent need for exploitation of emerging targets through the design and implementation of studies on t-NEPC.

1.4 Thesis theme and rationale

CRPC is the incurable stage of PCa. ARPI brings additional survival to CRPC patients. However, emerging evidence shows that the highly aggressive subtype t-NEPC becomes more prevalent

when patients are extensively treated with ARPI. T-NEPC is highly metastatic, with a median survival rate of less than a year. It expresses no/low levels of AR and AR-regulated biomarkers such as PSA, therefore it is resistant to ARPI, and difficult to be detected. It is therefore urgent to identify key factors or signals that drive t-NEPC formation, in order to better prevent, diagnose, and treat t-NEPC.

Using our bioinformatics tool “COMPAS” to analyze the whole transcriptome analyses of two patient cohorts, our preliminary work has identified a t-NEPC-specific RNA splice signature that is predominantly controlled by the RNA splicing factor, SRRM4. SRRM4 upregulation has been confirmed in t-NEPC patients and patient-derived xenografts (PDXs). In addition, several genes regulated by SRRM4, such as REST and BHC80, have been reported to play important roles in cell differentiation and tumor progression. However, analyses of SRRM4 in correlation with NEPC morphology, along with tumor progression from treatment-naïve to t-NEPC, remains unknown.

The overall goal of this study is to evaluate the role of SRRM4 in t-NEPC diagnosis, and to decipher the mechanism by which SRRM4 induces NE transdifferentiation, and facilitates t-NEPC progression.

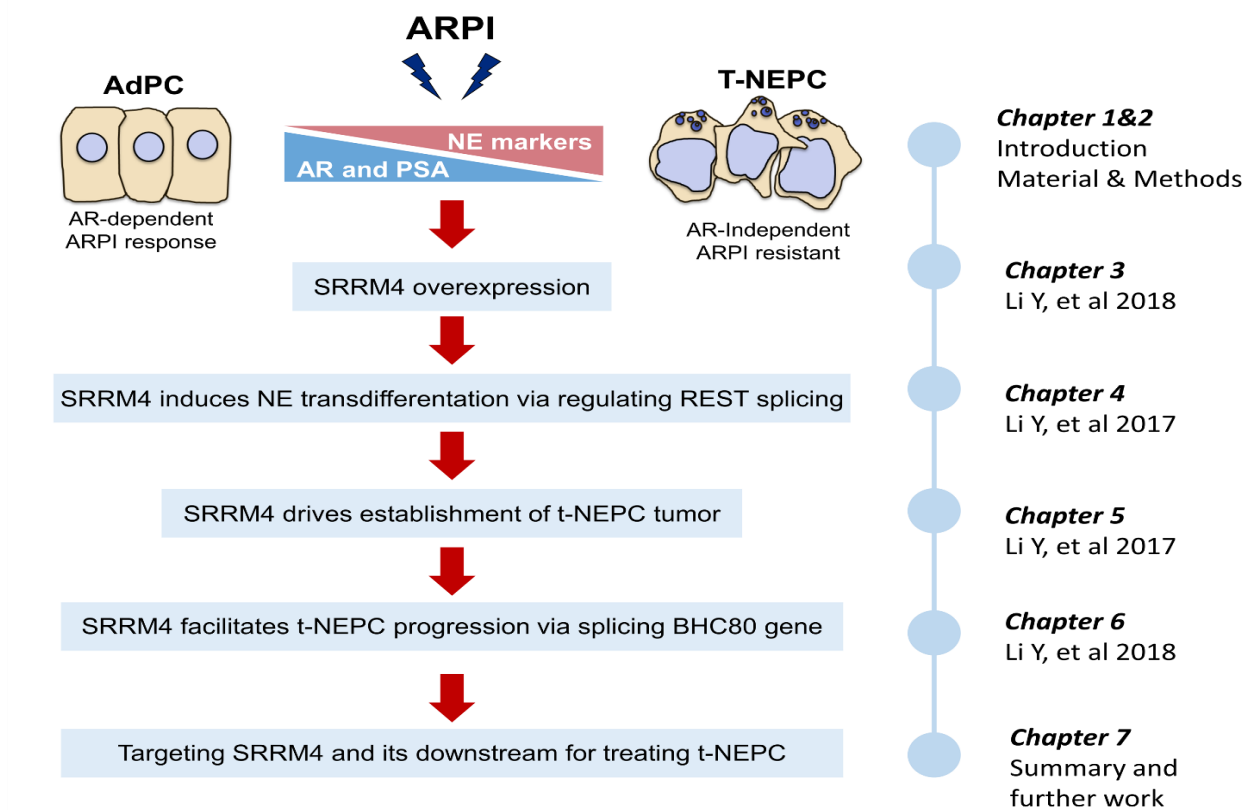


Figure 1.7 Diagram illustrating the outline of the thesis

1.5 Hypotheses and specific aims

Based on our previous publications and our substantial preliminary results, we hypothesized that increased SRRM4 expression in prostate tumors drives AdPC progression to t-NEPC. We have designed three specific aims to test this hypothesis:

Aim 1. To measure SRRM4 expression and to test its potential to be a diagnostic marker of t-NEPC

Aim 2. To confirm SRRM4 as a driver of t-NEPC by using PCa cell models

Aim 3. To decipher the mechanisms by which SRRM4 drives AdPC progression to t-NEPC

Chapter 2: Materials and Methods

2.1 Sample collection and RNA sequencing

For the VPC cohort, prostate tissue was obtained from cancer patients undergoing radical prostatectomy following a protocol approved by the Clinical Research Ethics Board of the University of British Columbia. All patients signed a formal consent form approved by the ethics board. RNA from 100µm sections of snap-frozen tissue was isolated using the mirVana Isolation Kit (Ambion Cat#:AM1560). RNA sequencing was performed on Illumina HiSeq 2000 at the BCCA Michael Smith Genome Sciences Centre according to standard protocols.

2.2 Bioinformatics analysis of RNA-Seq data

RNA-Seq reads were mapped with Star¹⁹³ using Ensembl gene annotations GRCh37.75 for the VPC cohort samples. Beltran cohort samples were previously mapped with TopHat¹⁹⁴ using Ensembl GRCh37.62. Gene expression and splicing analyses were performed using COMPAS. Gene expression values were quantile normalized in each cohort using the *preprocessCore* package in R.

2.3 COMPAS pipeline summary

COMPAS is a bioinformatics pipeline written in Perl and R. COMPAS takes SAM or BAM formatted files as input. These files can be generated by any splice-read mapper. COMPAS

processes pairs of samples together and detects alternatively spliced genes between the two samples using relative exon/junction counts. Each confident splicing event is reported along with the splicing index (i.e. PSI¹⁹⁵) and the relevant exon/junction coordinates. For each sample, COMPAS also reports the gene expression values as estimated from the mapped reads. A manuscript describing the full COMPAS algorithm, including a comparison to similar methods, is in preparation. COMPAS source is freely available for research use. The source code of COMPAS is available from <https://github.com/nlgndnmz/COMPAS>.

2.4 Tissue microarrays (TMAs)

Prostate tumor samples were retrieved from Vancouver Prostate Centre tissue bank and used to build several TMAs that had been previously reported^{196, 197}. A CRPC TMA contains 64 tissue cores from 32 patients who had received hormonal therapies and been diagnosed with CRPC. The recurrent tumors were removed by transurethral resection prostatectomy to relieve obstructive symptoms. Treatment-naïve TMAs contains 144 tissue cores from 72 patients who had undergone radical prostatectomy. A NHT TMA contains 174 tissue cores from 87 patients who received 0-12 month NHT treatment. This study also includes a patient derived xenograft (PDX) TMA containing 8 tissue cores from 4 NEPC and 18 cores from 9 AdPC PDXs that were pathologically evaluated previously¹⁰⁴.

2.5 RNA *in situ* hybridization (RISH) and immunohistochemistry (IHC) analyses

A SRRM4 specific RISH probe targeting the 496-835bp of SRRM4 mRNA (NM_194286.3), a BHC80-1 specific RISH probe targeting the 2048-2084bp of BHC80-1 mRNA (NM_001101802.1), a BHC80-2 specific RISH probe targeting the 1904-1946bp of BHC80-2 mRNA (NM_016621.3) and a negative control probe (targeting the *dapB* gene from bacteria) were designed by Advanced Cell Diagnostic (Hayward, USA). RISH assays were performed by using the BaseScope™ assay kit following manufacture's protocol. IHC was performed by using a Ventana Discovery XT autostainer (Ventana) as we reported^{196, 197}. All stained slides were scanned by a Leica SCN400 scanner and digital images were evaluated independently by three pathologists L.F., Q.Z., and J. H.

RISH signal presenting as red dots was evaluated under 40X magnification. SRRM4 RISH signal was scored as zero if no RISH signal; one if RISH signal was positive in <20% all cells within a core; and two if RISH signal is positive in >20% of the cells throughout the whole tissue core. RISH-positive cells with a score of one usually have ≤ 2 RISH dots/cell; RISH-positive cells with a score of two usually have multiple dots that can merge into dot clusters. IHC scores of CHGA, SYP, CD56, AR, and PSA were calculated by IHC signal intensity (no, low, medium, and high as 0-3) multiplied by the percentage of positive cells (0-100%). IHC scores ≥ 0.3 are considered as positive. Ki-67 index was scored by Aperio ImageScope software based on the intensity and the

percentage of IHC signals according to the manufactory's instruction (Leica Biosystems).

The histology of tumors is classified as AdPC, SCNC and AdPC with abundant NE cells (AdNE). AdPC contains tumor cells forming glandular structures. Compared to benign prostate glands, AdPC glands are smaller, more compact and homogeneous. The tumor cells are large, with vesicular nuclei and prominent nucleoli. AdPC have rare NE cells. SCNC contain only NE tumor cell populations that grow as solid sheets, cords or individual cells without glandular formation. The tumor cells demonstrate NE features including hyperchromatic nuclei, finely granular and homogenous chromatin pattern, and no nucleoli. Cells have scant cytoplasm and high nucleus/cytoplasm ratio. SCNC often contain areas of necrosis and crush artifact. Mitotic and apoptotic figures are frequent. AdNE are more similar histologically to AdPC than to SCNC, but cannot be classified as typical AdPC or SCNC. These tumors contain mixed cell populations with a large proportion (>10%) of NE cells.

2.6 Cell lines and cell culture

The LNCaP, PC3, 22Rv1, DU145, NCI-H660 and VCaP cell lines were purchased from ATCC (Manassas, VA, USA). LNCaP95 cells were a generous gift from Dr. Alan Meeker of Johns Hopkins University. C4-2, LNAI and 293T cell lines were generously provided by Drs. Rennie and Buttyan from the VPC. VCaP, PC3, DU145 and 293T cells were cultured in DMEM with 10%

FBS, whereas LNCaP, C4-2 and 22Rv1 cells were cultured in RPMI1640 medium with 10% FBS. LNAI and LN95 cells were maintained in phenol-free RPMI1640 medium with 10% charcoal-stripped serum (CSS) (Hyclone, Logan, UT, USA). The CSS medium does not contain androgen and is used to provide the androgen-deprivation condition. NCI-H660 was cultured in HITES medium (RPMI1640 medium plus 0.005mg/ml Insulin, 0.01mg/ml Transferrin, 30nM Sodium selenite, 10nM Hydrocortisone, 10nM beta-estradiol and 2mM L-glutamine) with 10% FBS. LnNE P0 cells are LNCaP cells with SRRM4 overexpression and TP53 knockdown. LnNE P0 to P5 cells were maintained in phenol-free RPMI1640 medium with 10% charcoal-stripped serum (CSS) (Hyclone, Logan, UT, USA).

2.7 Transfection and RNA silencing

Transient transfection of plasmid DNA was performed with the Lipofectamine 3000 (Invitrogen) according to the manufacturer's protocol. Transfection of siRNA oligos was performed with the siLentFect Lipid Reagent (Bio-Rad, Mississauga, ON, Canada) according to the provided protocols.

2.8 Antibodies and Western blot

Total cell proteins were extracted by lysis buffer containing 50 mM Tris pH8.0, 150 mM NaCl, 1% NP40, 0.5% sodium deoxycholate and 0.1% SDS with proteinase and phosphatase inhibitor

(Roche). Nuclear protein extraction kit (Sigma) was used to isolate cytoplasm and nuclear proteins according to the manufacturer's instruction. The protein lysis was separated on SDS-PAGE gel and immunoblotted with antibodies as indicated. Antibodies information are listed in the supplementary materials. Density of protein bands were measured using Image J software analysis (NIH, Bethesda, MD, USA). The values of each sample were expressed as a ratio of protein to the housekeeping protein.

Table 2.1 Antibody information

Name	Description	Cat No.	Company
Actin		A2066	Sigma
Flag-tag	M5	F4042	Sigma
REST/REST4	EPR2346Y	Ab75785	Abcam
RB	C-2	sc-74562	Santa Cruz
TP53	(C-19)-R	sc-1311-R	Santa Cruz
SRRM4		SAB2107518	Sigma
CHGB	C-19	sc-1489	Santa Cruz
SYP	D-4	sc-17750	Santa Cruz
NSE		MAB324	Millipore
SCG3	C-19	sc-1492	Santa Cruz
AR	N20	sc-816	Santa Cruz

E-cadherin	H-108	sc-7870	Santa Cruz
BHC80	F9	sc-376844	Santa Cruz
pp38		9211	Cell signaling
p38		9212	Cell signaling
TTP		sc-8458	Santa Cruz
MyD88	HFL-296	sc-11356	Santa Cruz
CCL20		MAB360	R&D
CCL2		MAB676-SP	R&D
CXCL10		AF-266-SP	R&D
TNF α		MAB610-SP	R&D

2.9 Reverse-transcription and real-time qPCR

Total cell RNA was extracted by TRIZOL reagent (Invitrogen, Burlington, ON, Canada) and tissue RNA was isolated by mirVana miRNA isolation kit (Invitrogen, Burlington, ON, Canada). All mRNA were treated with deoxyribonuclease to eliminate DNA resident. Reverse transcription was performed with random hexamers and superscript II (Invitrogen) according to the manufacture's instruction.

Regulated PCR was performed using a Taq DNA polymerase Kit following the manufacture's

instruction. Cycling process was 2 minutes at 94°C-followed by 30 cycles of 15 seconds denaturing at 94°C ,1 minute annealing at 60°C ,30 seconds extending at 68°C and then by 2 minutes at 68°C. The PCR products were run in 2% Agarose gel containing 0.001% Gel Star. All PCR assays were carried out using two independent cDNA syntheses.

Real-time qPCR was performed on the ABI PRISM 7900 HT system (Applied Biosystems) using the FastStart Universal SYBR Green Master mix (Roche) following standard protocol as we reported. All real-time qPCR assays were carried out in triplicates from three independent cDNA syntheses. Primer information is listed in the materials.

The relative quantification method has been described before using 18s rRNA as the internal control genes¹⁹⁸. For absolute quantification, PCR production of target genes were purified and quantified by NanoDrop (Thermo Scientific, Wilmington, DE, USA), and their copy numbers were calculated by copy number (molecules/ μ l)=concentration(g/ μ l)/(bp size of double-stranded product \times 660) \times 6.022 \times 10²³. A 10-fold dilution series of each product containing the purified of segments were used as the template for real-time PCR to generate a standard curve of log₁₀ copy numbers of these cDNA template at different dilutions versus the corresponding cycle threshold value (CT). The absolute quantity of target gene in query samples were calculated by the standard curve according to their real-time qPCR CT value. Primers information were listed in the

supplementary materials.

Table 2.2 Realtime qPCR primer information

GENE	Sequence
PTPRF(C) F	AAGCAGCATGGCCAGATCCG
PTPRF(C) R	AGGCCGCTGATAGTGGTTTCATAG
PTPRF(N) F	AAGCAGCATGGCCAGATCCG
PTPRF(N) R	GCCGCTGATAGTGGTTTCCTGG
MEF2D(C) F	GGGGTTAATGCATCACTTGACTG
MEF2D(C) R	TGGCTGAGTAAACTCGGCCGT
MEF2D(N) F	GGGGTTAATGCATCACTTGAACA
MEF2D(N) R	TGGCTGAGTAAACTCGGCCGT
SPTAN1(C) F	CCACCAACATCCAGCTTTCC
SPTAN1(C) R	GCTCCACGTTCAATGAGGGA
SPTAN1(N) F	ATCCCACCAACATCCAGAGCAAG
SPTAN1(N) R	GCTCCACGTTCAATGAGGGA
GIT1(C) F	TTCTACCTCTGTGGACGCAAG
GIT1(C) R	AATTCGGATAAGTCAAGGCTGTC
GIT1(N) F	CCACAGATGGCTGACAGATC
GIT1(N) R	TACACGTCCATGGCGAGTT

SH3GLB1(C) F	GCAGAAACTAGAAATTCATCTG
SH3GLB1(C) R	TCTGGTAATCTCTGCTTGAC
SH3GLB1(N) F	AGAGACTGGATTTGGATGCTGCAA
SH3GLB1(N) R	GTTATCTCCTTCAAGGCGAGCTGA
MEAF6(C) F	GAATAAAAACCGGCACAGGATTG
MEAF6(C) R	AAGGGAAGCAGGGCTCTACA
MEAF6(N) F	AATAAAAACCGGCACAGCCC
MEAF6(N) R	AAGGGAAGCAGGGCTCTACA
NSMF(N) F:	GTAGCCCCTGAACACCGAGAT
NSMF(N) R:	TCTGACGACATCCCTATTCGTA
NSMF(C) F:	CGTAGCCCCTGAACACCGCTT
NSMF(C) R:	TACAGCGTTGACCGTGTGTCT
MON2(N) F:	ATCCAACTATTTGCACCGGC
MON2(N) R:	GCTTTGTGACACGCTGTTTTT
MON2(C) F:	AAATGCAAAATATAATCAGGCG
MON2(C) R:	GCTTTGTGACACGCTGTTTTT
PTK2(N) F:	TACATCTCCAAATTGGCCTTCT
PTK2(N) R:	GCCCTCAAAAAGCTATGGAATA
PTK2(C) F:	ATGTACATCTCCAAATTGGCCT

PTK2(C) R:	GATACTTACACCATGCCCTCAAC
SC3GLB2(N) F:	GAGGGCACCACAGGCATAGT
3GLB2(N) R:	CAGCTCCCAGGGTGCCATAT
SC3GLB2(C) F:	GAGGGCACCACAGGCATAGT
SC3GLB2(C) R:	AGAAGCAGCTGGGCAGATTT
ABI1(N) F:	ATGCTTGGCTTTTAGCCACTT
ABI1(N) R:	TCACAAAATAATAGCACCTGCG
ABI1(C) F:	GGCTGGTTATTTCCATGCTTGA
ABI1(C) R:	TCACAAAATAATAGCACCTGCG
APBB1(N) F:	TACGTAGGCAAAGTCCCTCTCT
ABBB1(N) R:	CAGCTGGAGGATGAGACACTAA
APBB1(C) F:	GCTACGTAGGCAAAGTCCCTTC
ABBB1(C) R:	CAGCTGGAGGATGAGACACTAA
ATL2(N) F:	GATGACAGTCTCTGTCGCTGTG
ATL2(N) R:	CTGAAACACTATGGGAACAGAG
ATL2(C) F:	TTCCTCCATCAAATTATCACCC
ATL2(C) R:	TCTTGTGTAACCTTGTCATGGG
CAMTA2(N) F:	GCTGAAATCGCTTCTGTTCATA
CAMTA2(N) R:	GTACAAGCAGCTGACCTGGATT

CAMTA2(C) F:	GCTGAAATCGCTTCTGTTCATA
CAMTA2(C) R:	GTTACCGGAAGTACAAGCAGTT
ERGIC3(N) F:	CAGATACTATTGAGCAGTGCCG
ERGIC3(N) R:	AAGCTCTGCAAGTCATGGATCT
ERGIC3(C) F:	GAAGATGCAGGAGCAGAAGAAT
ERGIC3(C) R:	AGCTCTGCAAGTCATGGACGT
REST F:	TGCGTACTCATT CAGGTGAGA
REST R:	TCTTGCATGGCGGGT TACTT
REST4 F:	GCGTACTCATT CAGTGGGGTAT
REST4 R:	GATTAGAGGCCACATAACTGCAC
SRRM4 F:	CACAAGCGACGCAGGTCAT
SRRM4 R:	CGGTGGCGGTGAGACTTTC
SYP F:	GGCCCTTTGTTATTCTCTCGGTA
SYP R:	GGCCATTTCTGAGGCTAAACT
CHGB F:	CGAGGGGAAGATAGCAGTGAA
CHGB R:	CAGCATGTGTTTCCGATCTGG
SCGN F:	GGCCATTTCTGAGGCTAAACT
SCGN R:	GGGCTCCTGTTTTACTAACATCA
KCNH6 F:	GTCGCTCCCCAAAACACTTAC

KCNH6 R:	CGAAGAGTTCGCAGAAGCC
SYT4 F:	ATGGGATACCCTACACCCAAAT
SYT4 R:	TCCCGAGAGAGGAATTAGAACTT
ASCL1 F:	CCCAAGCAAGTCAAGCGACA
ASCL1 R:	AAGCCGCTGAAGTTGAGCC
SCG3 F:	GTCTTCATCAACTAGACGGGACT
SCG3 R:	ACAATCTTGTCAAACACGGCTC
NSE F:	CCGGGAACTCAGACCTCATC
NSE R:	CTCTGCACCTAGTCGCATGG
RB1 F:	TTGGATCACAGCGATACAAACTT
RB1 R:	AGCGCACGCCAATAAAGACAT
TP53 F:	CAGCACATGACGGAGGTTGT
TP53 R:	TCATCCAAATACTCCACACGC
NKX3.1 F	CCCACACTCAGGTGATCGAG
NKX3.1 R	GAGCTGCTTTCGCTTAGTCTT
KRT8 F	TCCTCAGGCAGCTATATGAAGAG
KRT8 R	GGTTGGCAATATCCTCGTACTGT
E-Cadherin F	ATTTTCCCTCGACACCCGAT
E-Cadherin R	TCCCAGGCGTAGACCAAGA

18s rRNA F:	TTGACGGAAGGGCACCACCAG
18s rRNA R:	GCACCACCACCCACGGAATCG
BHC80-1 F:	AGTCTTTGAGCCAGAGCGTAAG
BHC80-1 R:	CACTGCATTGTATTTTGGAGGA
CCL2 F:	CAGCCAGATGCAATCAATGCC
CCL2 R:	TGGAATCCTGAACCCACTTCT
CCL20 F:	GTGTGCGCAAATCCAAAAC
CCL20 R:	TTCCATTCCAGAAAAGCCAC
TNF F:	GAGGCCAAGCCCTGGTATG
TNF R:	CGGGCCGATTGATCTCAGC
CXCL10 F:	GTGGCATTCAAGGAGTACCTC
CXCL10 R:	TGATGGCCTTCGATTCTGGATT
TLR2 F:	ATCCTCCAATCAGGCTTCTCT
TLR2 R:	GGACAGGTCAAGGCTTTTTACA
CCL2 RNA-ChIP F:	TGAATTTTGTTTGTGATGTGAA
CCL2 RNA-ChIP R:	GCAATTTCCCAAGTCTCTGTA
CXCL10 RNA-ChIP F:	TTCCAAACACATACAGGAAGGT
CXCL10 RNA-ChIP R:	TTTGAAAACCATTCAGCACATT
TNF RNA-ChIP F:	GGAGCCAGCTCCCTCTATTTAT

TNF RNA-ChIP R: AGCCAAGGCAGCTCCTACAT
RNA-ChIP-BHC80(P1) F: ATGCTAGCCAATGAGGAACACT
RNA-ChIP-BHC80(P1) R: GAAGGGAACAAAAGGGAAAAAC
RNA-ChIP-Control(P2) F: TGCACCACCAACTGCTTAGC
RNA-ChIP-Control(P2) R: GGCATGGACTGTGGTCATGAG

C: Constitutive variant N: Neuro-specific variant

2.10 Construction of REST and BHC80 minigenes

The human genomic BAC clone was provided by The Centre for Applied Genomics (Hospital for Sick Children, University of Toronto). It was used as a template to amplify exon 3, exon N, exon 4 and their flanking intron regions of the REST gene (NM_005612.4) and exon 13- 15 plus their flanking intron regions of the BHC80 gene (NM_001101802.1) by Platinum Taq DNA Polymerase High Fidelity (Invitrogen). The REST minigene was then used as a template to construct mutant REST minigenes using a Q5 site-directed mutagenesis kit (NEB). The integrity of the final construct was confirmed by DNA sequence.

2.11 RNA-immunoprecipitation (RNA-IP) assays

Chromatin of LNCaP and 293T cell transfected with Flag-SRRM4 plasmid were cross-linked with formaldehyde(10ml PBS+270µl 1% formaldehyde) for 20 minutes at 37°C and sonicated in 300µl

buffer I (1% SDS, 10 mM EDTA, and 50 mM Tris, pH 8.0, plus protease inhibitor cocktail). After centrifugation, the supernatants was add to 2.7ml buffer II, 30 μ l of the mixture was saved as input. For immunoprecipitation, 2 μ g of Flag antibody or control IgG antibody were added to the purified chromatin sample and incubated overnight at 4 °C. Immunocomplexes were precipitated by adding 50 μ l of protein A/G agarose beads for 2 hours at 4 °C with agitation. Beads were washed sequentially for 5 minutes each in 1ml of buffers III-VI, as described previously. Immunocomplexes were eluted by adding 1600 μ l of elution buffer (1% SDS and 0.1M NaHCO₃) and 50 μ l RNase inhibitor to beads. 500 μ l of eluted immunocomplexes were added in 10 μ l 5M NaCl and subsequently heated for 2 hours at 64 °C to reverse formaldehyde-induced cross-links. RNA segments were isolated and collected by 1.5ml lysis buffer with 15 μ l 2-mercaptoethanol using Purelink RNA Mini Kit (Ambion) according to the manufacture's instruction and subsequence to reverse transcription and analyzed by real-time qPCR as described above. Data were calculated as a percentage of input.

2.12 RNA-Protein interaction assay

LNCaP (SRRM4) cell and 293T cell transfected with Flag-SRRM4 plasmid were lysis in NETN buffer (0.5% NP40, 1mM EDTA, 50mM Tris, and 150 mM NaCl with proteinase inhibitor). 0.4nmol biotin-labeled RNA oligonucleotides (Invitrogen) were banded onto 100 μ l of streptavidin beads (Pierce, Rockford, IL, USA) in a final volume of 500 μ l of binding buffer DG(20 mM

HEPES-KOH, pH 7.9, 80mM potassium glutamate, 0.1mM EDTA, 1mM DTT and 20% glycerol) at 4°C for 2 hours. The Flag-SRRM4 protein were purified by incubating cell lysate with the beads containing biotin-labeled RNA oligonucleotides at 4°C for 2 hours. Then the beads were washed with binding buffer DG and suspended in SDS loading buffer. Eluted proteins were analyzed by western blot and detected by anti-Flag antibody.

2.13 Lentiviral approaches to constructing cell lines

Lentiviral vector (pFUGWBW) was used as the backbone to construct expression vectors encoding mock and Flag-SRRM4 using the Invitrogen gateway system. Vectors were used to package lentivirus and infect LNCaP cells. After blasticidin selection, LNCaP (SRRM4-) and LNCaP (SRRM4+) cell lines were established. Using these two lines as the parental lines, the second round of lentivirus infection was performed with lentivirus encoding control shRNA, shRNA against RB1 or TP53 (Addgene). Following puromycin and blasticidin double selection, six LNCaP stable lines were generated: LNCaP (SRRM4-/shCtl), LNCaP (SRRM4+/shCtl), LNCaP (SRRM4-/shRB1), LNCaP (SRRM4+/shRB1), LNCaP (SRRM4-/shTP53) and LNCaP (SRRM4+/shTP53).

For BHC80 stable lines, pFUGWBW was used as the backbone to construct expression vectors encoding mock, Flag-BHC80-1, Flag-BHC80-2 and using the Invitrogen gateway system. Flag-BHC80-1 expression vector was used as template to construct mutant BHC80-1. Vectors were

used to package lentivirus and infect LNCaP, PC3 and TRAMP-C1 cells. All cell lines were cultured under blasticidin selection. All these cell lines were validated by real-time PCR and immunoblotting assays.

2.14 Multicellular spheroid formation and immunofluorescence analysis

LNCaP (SRRM4-/shCtl), LNCaP (SRRM4+/shCtl), LNCaP (SRRM4-/shRB1), LNCaP (SRRM4+/shRB1), LNCaP (SRRM4-/shTP53) and LNCaP (SRRM4+/shTP53) cells were cultured in phenol-free RPMI1640 medium containing 10% CSS for 4 weeks. Six random 5X fields were chosen, and cell imaging was captured and analyzed by Zeiss fluorescent microscope (Carl Zeiss, Thornwood, NY). The spheroid numbers were counted according to the diameter. Cell spheroids described above were fixed in 4% paraformaldehyde.

2.15 BrdU incorporation and colony formation assays

Cell proliferation was measured with a bromodeoxyuridine (BrdU) assay kit (Millipore, Cat#: 2750). In the colony formation assays, 2×10^4 cells were seeded in 0.7% soft agar in a 6-well plate. Cells were allowed to grow for 10 days to form colonies. Colonies were stained with crystal violet, photographed by a digital camera, and colony numbers (diameter >0.1mm) were counted.

2.16 Renal capsule xenografts

LNCaP (SRRM4-/shCtl), LNCaP (SRRM4+/shCtl), LNCaP (SRRM4+/shRB1) and LNCaP (SRRM4+/shTP53) was implanted into both renal capsules of three Nude mice to generate 6 tumors (2×10^6 cells/per line). All mice underwent castration surgery the next day after implantation. The animal protocol was approved by the Institutional Animal Care and Use Committee at the University of British Columbia. Serum samples were collected one day after castration, as well as every two weeks when tumors became palpable until week six. Serum SYP concentrations in each mouse serum were measured by ELISA kit (USCNK, Cat#: SEA425Hu). Xenograft tissues were fixed and stained with hematoxylin and eosin as well as SYP, Flag-SRRM4, AR and PSA antibodies.

2.17 Luciferase reporter assays

Cells were transfected with PSA-luciferase reporter plasmid with the renilla reporter as a control for transfection efficiency. Luciferase activities were determined using the luciferin reagent (Promega, Madison, WI) according to the manufacturer's protocol. Transfection efficiency was normalized by renilla luciferase activity.

2.18 Immunofluorescence assays

Cells were fixed in 4% paraformaldehyde, permeabilized in 0.25% Triton X-100 and blocked with

1% BSA for 1 hour at room temperature. Cells were then incubated with the primary antibody, washed with PBS with 0.1% Triton X-100, and incubated with FITC-conjugated secondary antibody (1:1000 in PBST containing 1% BSA). Cell imaging was captured by Zeiss fluorescent microscope (Carl Zeiss, Thornwood, NY).

2.19 Cell proliferation, migration, invasion, and colony formation assays

Cell proliferation assay were performed using the MTS (Promega) reagent according to the manufacture's protocol. Briefly, 20 μ l of combined MTS/ phenazine methosulfate (PMS) solution was added into each well of a 96 well assay plate containing $\sim 1 \times 10^5$ cells/well in a final volume of 100 μ l culture medium, and the plate was incubated at 37 °C for 2 hours. Subsequently, the absorbance at 490nm was recorded on a microplate reader. Cell proliferation rates were calculate as relative fold change of OD490. For migration assays, a monolayer wound were created when cells reached 100% confluence. Cell migration were subsequently captured at time point 0h and 24h after wound scratch. Migration ability of cells were calculated as the migration distance from 0h to 24h. Cell invasion assays were carried out by using BD BioCoat Matrigel Invasion chambers (BD Biosciences, USA) according to manufacturer's protocol. Invasion rate were calculated as the percentage of cell invade through the Matrigel. In the colony formation assays, about 2×10^4 cells were seeded in 0.7% soft agar in a 6-well plate. Cells were allowed to grow for 10 days to form colonies. Colonies were stained with crystal violet, photographed by a digital camera, and colony

numbers (diameter >0.1mm) were counted.

To collect conditioned mediums, LNCaP and PC3 cells overexpressing control, BHC80-1 or BHC80-2 were cultured until 90% confluent and then replenished with RPMI medium for LNCaP cells and DMEM medium for PC3 cells. After 48 hours, the conditioned mediums (CM) were collected and the same amount of CM were used for cell invasion and proliferation assays in the presence of control, CCL2, TNF α , CXCL10 and CCL20 neutralize antibody.

2.20 Human prostate cancer subcutaneous xenografts

To construct LNCaP xenografts, each LNCaP cell line (2×10^6 cells/per line) was implanted subcutaneously in bilateral flanks of 6-8 week old male nude mice. Tumor volume ($V = \text{length} \times \text{width} \times \text{high} \times 0.5236$) was measured weekly. Serum PSA levels were determined by ELISA. Mice were castrated, when tumor volume reached 200mm^3 . TRAMP-C1 xenografts were constructed by implanting TRAMP-C1 (2×10^6 cells/per line) cells subcutaneously in bilateral flanks of C57/bl6 mice. Tumor volume were measured weekly. All animal procedures were under the guidelines of the Canadian Council on Animal Care.

2.21 RNA run-on assay and stability assay

Nuclear run-on assays were performed as we described¹⁹⁹. Briefly, totally 1×10^7 cells per cell line

were lysed and centrifuged to collect the nuclei. In vitro transcription was performed in a buffer containing 10mM of Tris•HCl (pH 8.0), 5mM of MgCl₂, 0.3mM of KCl, 2.5mM of NTP and biotin-16-UTP mix from Roche (Laval, QC) for 45 min at 30°C. Biotinylated nascent RNA transcripts were precipitated by streptavidin beads. Purified RNA was used as templates for real-time PCR analyses. For mRNA stability assay, each cell lines were cultured for 24 hours before treated with 1uM of Actinomycin D (Act D). Total RNA was collected after 0-6 hours of treatment. The percentage of remaining mRNA was calculated as fold change normalized to 18S rRNA. Results were plotted as mean ± S.D. from three independent repeats.

2.22 Co-immunoprecipitation

Cell lysates were extracted by NETN buffer containing 0.5% NP40, 1mM of EDTA, 50mM of Tris, and 150mM of NaCl plus proteinase and phosphatase inhibitor (Roche). Pre-cleared lysates were incubated with Flag or MyD88 antibody and the associated proteins were immunoblotted by antibodies as indicated. Experiments were repeated at least three times and one set of the representative blots was shown.

2.23 Proximity Ligation Assay (PLA)

PLA assays were performed using the Duolink *in situ* red starter kit mouse/rabbit (Sigma, Oakville, Canada). LNCaP(BHC80-1), LNCaP(BHC80-2) and LNCaP(BHC80-1m) cells were fixed with

4% paraformaldehyde and permeabilized by 0.2% Triton-X100. Fixed cells were incubated with primary antibodies overnight at 4°C. Secondary probe, ligation and amplification reactions were performed following manufacturer's instructions. Fluorescence images were captured by Zeiss fluorescent microscope (Carl Zeiss, North York, Canada).

2.24 3D spheroid culture and high throughput screening system

The 3D spheroid culture of LNCaP and NCI-H660 cells were performed using GravityPLUS™ Hanging Drop System (INSPERO, ISP-06-001). On the GravityPLUS™ spheroid culture plate, a 40ul cell suspension containing 2000 cells was dispensed into the access hole at each cell culture site of plates to form a hanging drop. The growth medium was replenished every other day. The amounts of replenished medium were calculated by the evaporation map provide by the manufactory. After spheroid formation, these micro-tissue spheroids were transferred into the GravityTRAP™ culture plates. Spheroids were treated with control or increasing doses of MyD88 inhibitor or the CCL2 neutralize antibody. Images of spheroids were captured by Zeiss fluorescent microscope (Carl Zeiss, Thornwood, NY) and the sizes of spheroids were measured using Imagine-J software. Cell viability assay were performed using the MTS (Promega) reagent according to the manufacture's protocol.

2.25 Statistical analysis

Statistical analysis was performed using the SPSS 17.0 software. Results generated from in vitro experiments are expressed as mean \pm SDs and results from in vivo murine studies are presented as mean \pm SEMs. Student's t test and one-way ANOVA followed by Tukey's test were applied to compare data among groups. SRRM4 and BHC80 RISH scores in correlation with NE markers, Ki-67, AR, and PSA IHC scores were analyzed by Pearson's Chi-square analysis. Patient overall survival was measured from the date of the CRPC diagnosis to the date of death or latest follow-up. Survival curves were generated by using the Kaplan-Meier method and compared using the log-rank test.

Chapter 3: SRRM4 Gene Expression Correlates with Neuroendocrine Prostate Cancer

3.1 Introduction

While the usage of novel ARPI drugs like abiraterone and enzalutamide has significantly improved the total survival of patients with CRPC, emerging evidences indicates that AdPC can escape from ARPI therapies and progress into t-NEPC^{83, 85, 98, 99}, which is responsible for almost one fourth of prostate cancer-related deaths⁸⁵. Progression into t-NEPC is obscure, as it cannot be reflected by rising levels of serum PSA. Once the t-NEPC diagnosis is confirmed, patient median survival is less than 7 months⁹⁸. It is therefore important to identify new biomarkers for early detection of t-NEPC, and therapeutic targets for drug development.

T-NEPC is traditionally diagnosed based on tumor histologic features. This is a challenging task, even for pathologists, because the transition of AdPC to NEPC is not an acute process, and involves sequential morphological and molecular alterations, resulting in multiple intermediate transitional phenotypes^{87, 88, 91}. In addition, tumor cell morphology and tissue pattern can be more complex when treated with ARPI, radiation, and chemical therapies. Under these circumstances, NE markers are often used to facilitate the diagnosis. T-NEPC may express one or multiple NE markers, including SYP, CD56, and CHGA⁹². However, there is no universal NE marker profile that can be used as a gold standard to diagnose t-NEPC, as expression of current NE markers is inconsistent. In addition, NE marker expression is not associated with the outcome and therapy

response of t-NEPC⁹⁸. These findings highlight the importance of identifying new reliable NE markers of t-NEPC.

RNA-seq can elucidate molecular mechanisms of t-NEPC development⁹⁹. Although recent work has focused on identifying the genomic and transcriptomic profiles of NEPC, analyses of AS have lagged. Access to RNA-seq data from independent (Vancouver Prostate Centre [VPC] and Beltran) cohorts allowed us to decipher NEPC-specific AS signatures. The VPC cohort contained three patient samples, and nine PDXs¹⁰⁴. These PDX models had remarkable fidelity with respect to genome, transcriptome, and responses to ARPI in relation to the patient tumors. The Beltran 2011 cohort contained clinical samples from 27 AdPC, and 5 NEPC patients. Together, these cohorts generated an RNA-seq data set for analyzing NEPC-specific AS signatures. In our primary research, we have performed whole transcriptome analyses of RNA-seq data from two independent patient cohorts^{99, 160}. We also developed a computational tool named COMPAS to decipher the splicing pattern of t-NEPC. Using this bioinformatics tool, we have identified a t-NEPC specific splice signature that is predominantly regulated by the RNA splicing factor SRRM4. In addition, Both SRRM4 mRNA and protein expression is significantly increased in t-NEPC patient tumors and PDXs¹⁵⁹. These findings suggest that SRRM4 may be used as a potential biomarker of t-NEPC. Unfortunately, current commercially available antibodies against SRRM4 are not suitable for immunohistochemistry, thereby hindering the validation of this hypothesis.

Here, we developed RNA *in situ* hybridization assays to measure SRRM4 expression on prostate cancer TMA. Our results indicated that SRRM4 expression has high sensitivity and specificity to detect NEPC among CRPC. SRRM4 can be co-expressed with the AR and PSA in non-classical AdPC tumors. These tumors are morphologically different from classical AdPC tumors, and usually show NE features, implying that SRRM4 may be a predictive marker for early stage t-NEPC before the NEPC phenotype becomes fully developed. We also reported that subpopulations of cancer cells in ~16% treatment-naïve AdPC expressed low levels of SRRM4, and that SRRM4 expression increases in these AdPC treated with long-term NHT. These findings suggest that t-NEPC may arise from clonal expansion of SRRM4-positive AdPC cells under the selection pressure of AR pathway inhibition.

3.2 Results

3.2.1 COMPAS identifies a neuroendocrine prostate cancer-specific alternative splicing signature induced by SRRM4

In the VPC cohort, t-NEPC samples exhibited distinct alternative splicing profiles. Among 1,036 alternative splicing events from 916 genes predicted by COMPAS, 106 events showed statistically significant differences between NEPC and AdPC samples (Benjamini-Hochberg corrected, FDR <0.01). In the Beltran cohort, among the 1023 alternative splicing events from the 889 genes predicted, 58 alternative splicing events showed statistically significant differences (Benjamini-

Hochberg corrected, $FDR < 0.01$) (Figure 3.1A-B). This cohort was sequenced to significantly lower read depth than the VPC cohort; therefore, our power to detect alternative splicing was reduced for low abundance transcripts. Two tumors from this cohort were also diagnosed as “prostate cancer with neuroendocrine differentiation,” indicating mixed phenotypes.

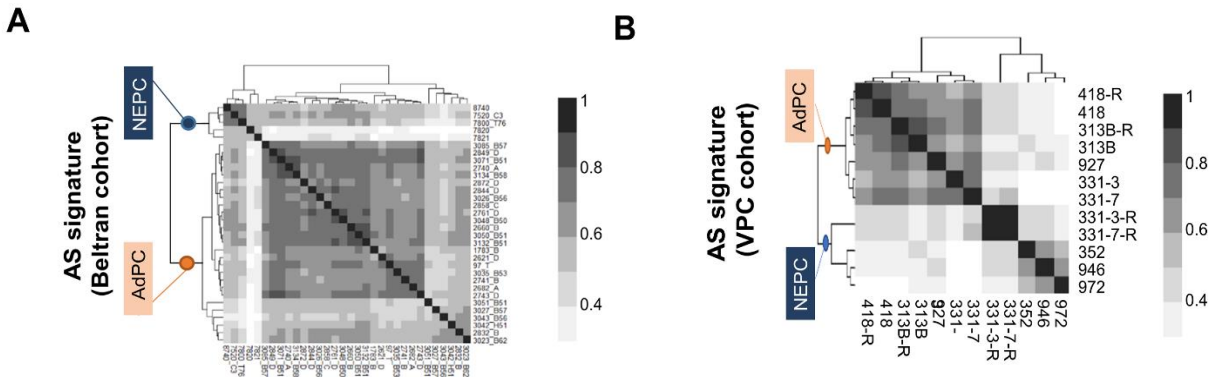


Figure 3.1 COMPAS identifies a NEPC-specific signature in prostate tumor biopsies

(A-B) RNA-seq data of Beltran and VPC cohorts were analyzed by the COMPAS software and AS indexes of these two cohorts were calculated. Heat maps shows Spearman correlation values using the AS index of samples from the (A) Beltran and (B) VPC cohort based on the entire set of splicing predictions. The splicing signatures of NEPC groups in both cohorts are significantly different from that of the AdPC groups. Samples with similar splicing signatures are classified together.

The VPC and Beltran cohorts shared 24 NEPC-specific AS events (Figure 3.2). Gene ontology (GO) analysis of these genes revealed biological processes including cell surface receptor-linked signal transduction, vesicle-mediated and intracellular transport, and secretion and establishment

of cellular localization. Cellular component GO terms were enriched in the leading edge, cell projection, and cytoskeleton, suggesting these genes may regulate cell morphology (FDR <0.05). None of these 24 genes exhibited a significant change in overall expression between NEPC and AdPC samples (Figure 3.2), emphasizing the complementary role of alternative splicing in transcription regulation during NEPC transdifferentiation.

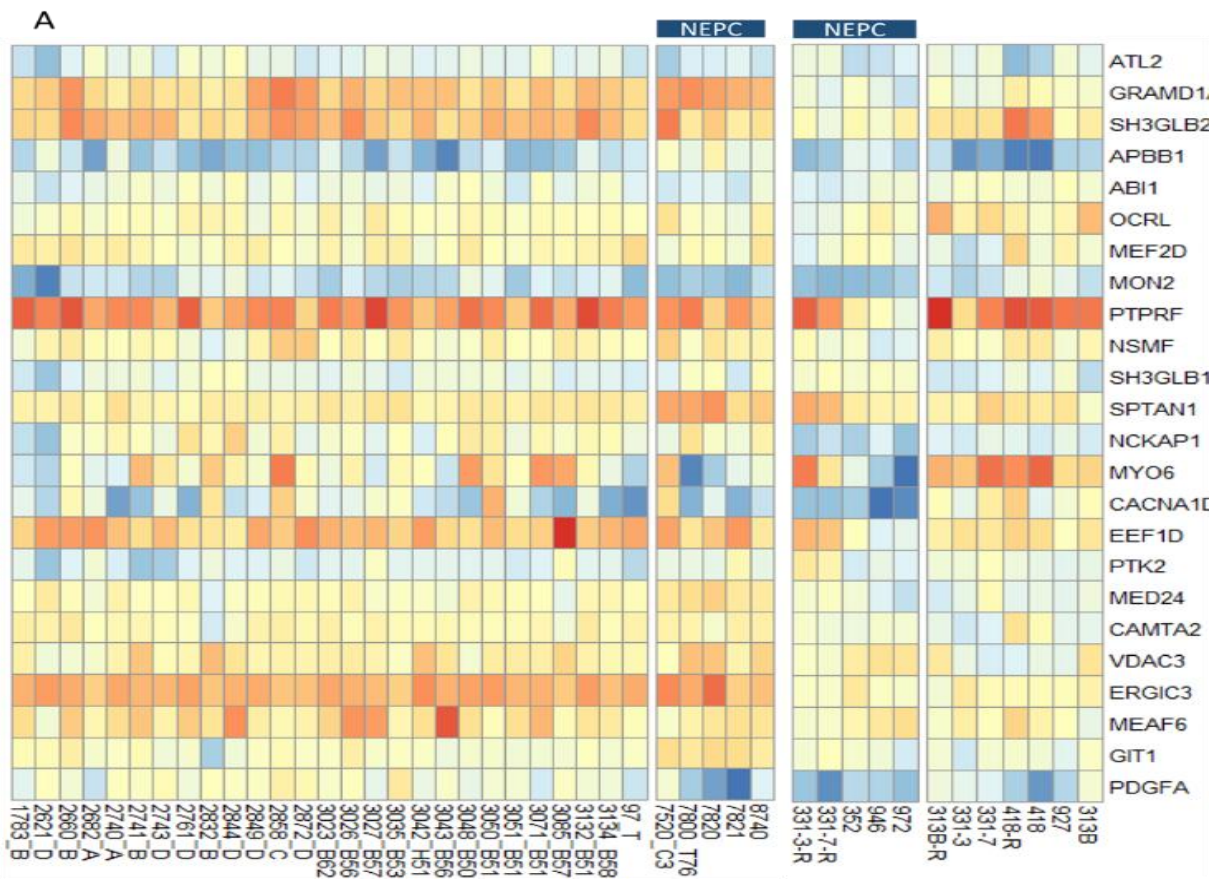


Figure 3.2 Different spliced genes between AdPC and t-NEPC

RNA-seq data of Beltran (left two groups) and VPC (right two groups) cohorts were analyzed by the COMPAS software and total gene expression were calculated. A heat map shows the normalized gene expression estimated by RNA-Seq data on the common NEPC splicing signature

genes in the Beltran and the VPC cohorts. Normalization is performed separately within each cohort. None of these genes show a significant difference in overall expression between NEPC and AdPC samples.

Although the functions of these NEPC splice variants are mostly unknown, most of these genes were reported to be regulated by the splicing factor SRRM4 in N2A neuroblastoma and 293T embryonic kidney cell lines (Figure 3.3A)²⁰⁰. Comparing their results with our VPC and Beltran NEPC signatures separately, we obtained even higher rates of overlap (36 and 21 in the VPC and Beltran cohorts, respectively). Moreover, several genes from our alternative splicing signature were also reported in Bronx Waltzer mice carrying mutant SRRM4²⁰¹. In addition, SRRM4 is one of the most significantly upregulated genes in NEPC in both the VPC and Beltran cohorts (Figure 3.3B). These findings suggest an important role for SRRM4 in t-NEPC.

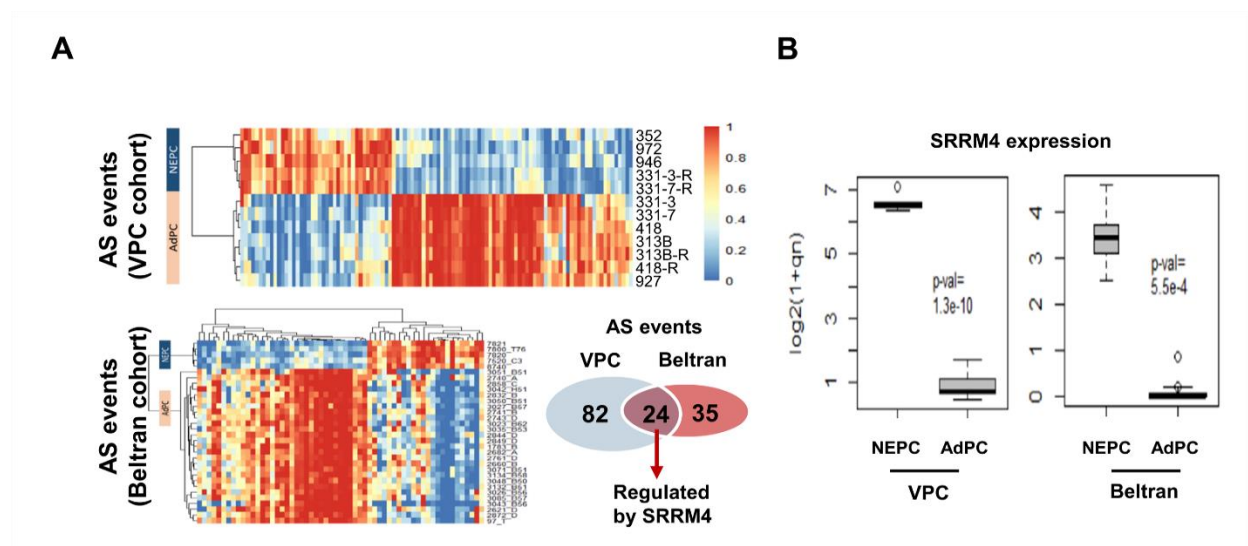


Figure 3.3 SRRM4 is associated with the common NEPC-specific splicing signature

(A-B) RNA-seq data of VPC and Beltran cohorts were analyzed by the COMPAS software. Both overall gene expression level and gene AS events in each cohort were calculated. (A) NEPC-specific AS signatures are generated based on 106 differential AS events from 104 genes between NEPC and AdPC samples from the VPC cohort and 59 differential alternative splicing events from 59 genes between NEPC and AdPC samples from the Beltran cohort (Benjamini-Hochberg corrected, $FDR < 0.01$) (B) Comparison of overall gene expression of SRRM4 between NEPC and AdPC samples using RNA-Seq data from the VPC and Beltran cohorts. The widths of the boxplots are scaled by the relative fraction of the samples in the respective group (i.e. NEPC or AdPC).

Although RNA-seq results demonstrated upregulation of SRRM4 mRNA level in t-NEPC. It is still important to identify the relationship between SRRM4 and pathological characters of PCa. Unfortunately, current commercially available antibodies against SRRM4 are not suitable for immunohistochemistry, thereby hindering the validation of this hypothesis. So we introduce RNA *in situ* hybridization technology to detect SRRM4 mRNA in PCa tissues.

To test the specificity of the SRRM4 probe for RISH, we applied several control experiments (Figure 3.4). RISH assays were performed: 1) on SRRM4-negative tissues from LNCaP, PC3, DU145 xenografts, and AdPC PDXs; 2) on SRRM4-positive tissue slides from xenografts of LNCaP, PC3, and DU145 cells infected with lentivirus encoding SRRM4 protein, and tissues from

NCI-H660 xenografts, NEPC PDXs, and human brain tissues; and 3) using a negative control RNA probe that does not cross-react to any human RNA. These results confirmed that the RISH signal is specific to SRRM4, and reflects SRRM4 protein expression as well as its splicing activity. The RISH signal is quantitative, as described in the Methods section.

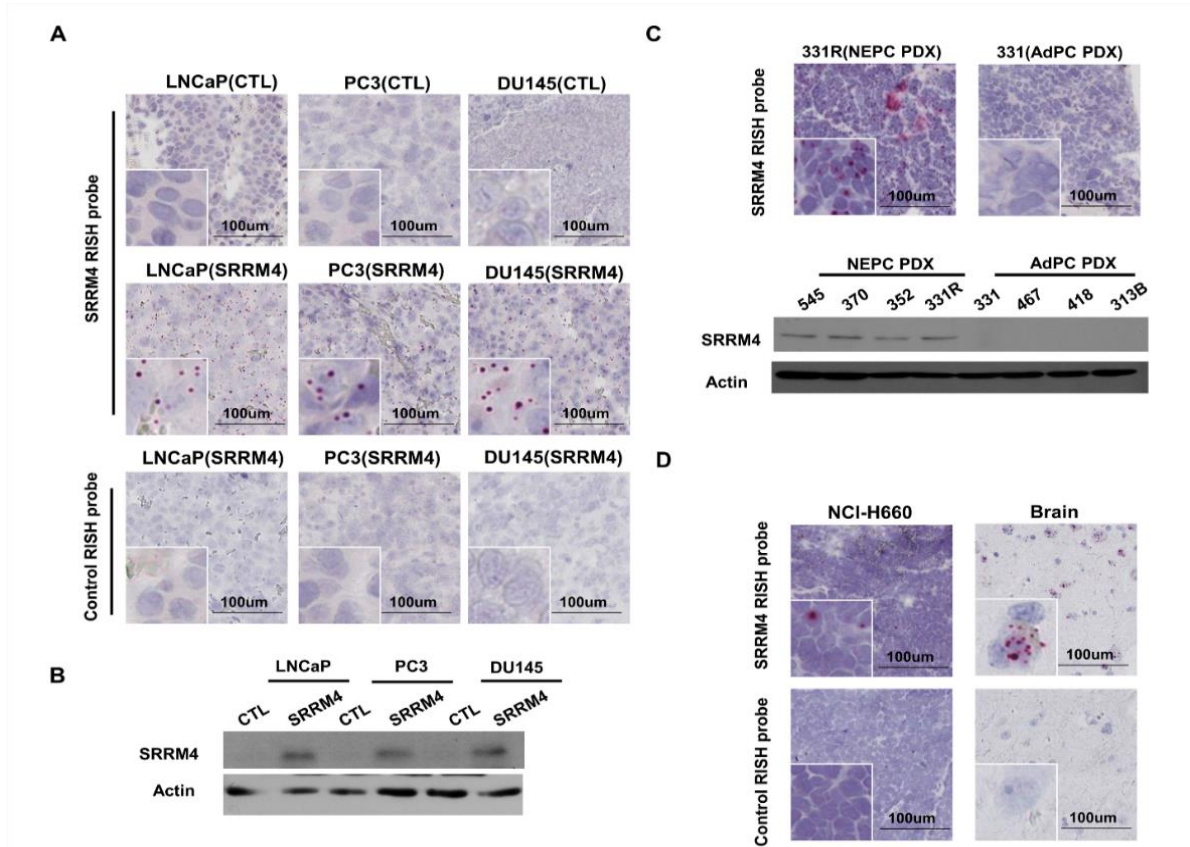


Figure 3.4 Validation of SRRM4 probes for RNA ISH assays

(A) LNCaP, PC3 and DU145 cells infected with lentivirus encoding SRRM4 protein or control (CTL) were used to generate xenografts. A SRRM4 specific RISH probe targeting the 496-835bp of SRRM4 mRNA (NM_194286.3) and a negative control probe (targeting the *dapB* gene from bacteria) were designed by Advanced Cell Diagnostic. RISH assays were performed by using the

BaseScope™ assay kit following manufacture's protocol. Xenografts with SRRM4 overexpression show positive signal (red dots) detected by SRRM4 RISH probe. Xenografts without SRRM4 overexpression or detected by negative control RISH probe show negative signal. **(B)** Total protein lysis from above xenografts were immunoblotted with the SRRM4 antibody to validate the overexpression of SRRM4 protein. **(C)** SRRM4 RISH assays were also performed on NEPC and AdPC PDXs tissue slides. Total protein lysis was extracted from 4 NEPC and 4 AdPC PDXs and immunoblotted with the SRRM4 antibody to validate the upregulation of SRRM4 protein in NEPC PDXs. **(D)** Tissue slides from NCI-H660 (NEPC cell line) xenografts and brain tissue were used to perform RISH assays using control and SRRM4 probes. NCI-H660 (NEPC cell line) xenografts and brain tissue show positive signal detected by SRRM4 RISH probe.

3.2.2 SRRM4 expression in castrate-resistant tumors correlates with t-NEPC

In CRPC tumors, SRRM4 was detected in 27% (17/64) of tissue cores. It is highly expressed in all SCNC that are CHGA, SYP, and CD56 triple positive, and AR and PSA double negative (Figure 3.5 and 3.6A). SRRM4 is also positive in all AdNE cores, of which four are also AR-positive. Interestingly, SRRM4 is positive in five AdPC cores that are AR-positive, of which four express at least one NE marker. SRRM4 is co-expressed with AR and PSA in some AdNE and AdPC with NE marker expression, suggesting that these tumors may be an intermediate transition stage of t-NEPC.

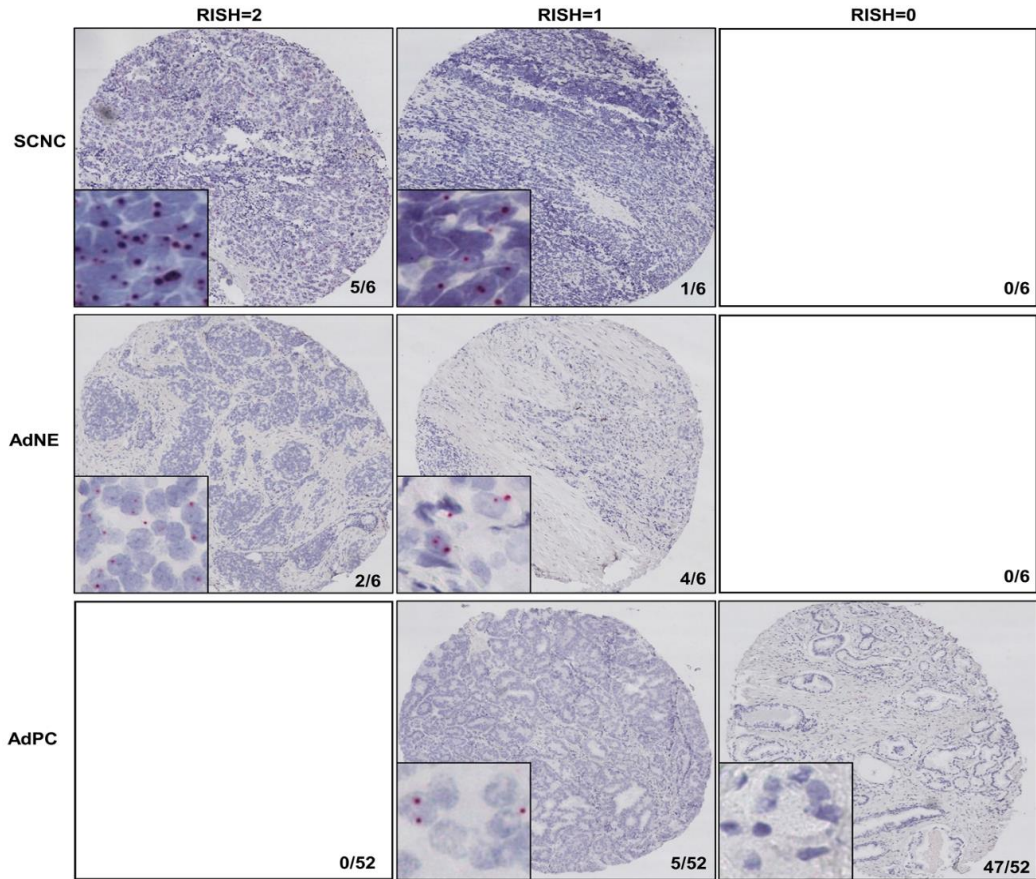


Figure 3.5 SRRM4 expression in castrate-resistant prostate tumors

A CRPC TMA contains 64 tissue cores from 32 patients who had received hormonal therapies and been diagnosed with CRPC. The recurrent tumors were removed by transurethral resection prostatectomy to relieve obstructive symptoms. SRRM4 RISH assays performed on this TMA. SRRM4 RISH signal was scored as zero if no RISH signal; one if RISH signal was positive in <20% all cells within a core; and two if RISH signal is positive in >20% of the cells throughout the whole tissue core. The histology of tumors is classified as AdPC, SCNC, and AdPC with abundant NE cells (AdNE). AdPC contains tumor cells forming glandular structures and has rare NE cells. SCNC contain only NE tumor cell populations that grow as solid sheets, cords or

individual cells without glandular formation. AdNE are more similar histologically to AdPC than to SCNC, but cannot be classified as typical AdPC or SCNC. These tumors contain mixed cell populations with a large proportion (>10%) of NE cells. Representative RISH and IHC images are presented.

Statistical analyses demonstrate that SRRM4 expression is highly enriched in SCNC and AdNE (Figure 3.6A-C). SRRM4 RISH signal is highly and positively correlated with not only the number of NE markers (Pearson correlation $r=0.836$; $p<0.0001$), but also the IHC scores of SYP, CD56 and CHGA (Pearson correlation $r=0.883$, 0.675 and 0.881 respectively; $p<0.0001$) (Figure 3.6D-E). SRRM4 expression negatively and weakly correlates with AR ($r=-0.544$, $p<0.0001$) and PSA ($r=-0.310$, $p=0.013$) IHC scores. If NEPC is defined as SCNC and AdNE, the sensitivity of SRRM4 to detect t-NEPC is 1.00 (95% CI: 0.75-1.00) and the specificity is 0.9 (95% CI: 0.76-0.96) (Figure 3.6F), indicating that all NEPC are SRRM4-positive, and 10% SRRM4-positive tumors are not NEPC. However, it is unknown whether these 10% SRRM4-positive tumors will later develop into t-NEPC. High Ki67 index in SCNC is consistent with their highly proliferative features (Figure 3.6C). However, AdNE have much lower Ki67 index, suggesting that these tumors may have undergone NE differentiation but not gained high proliferation capacity. Median overall survival for patients with SRRM4-positive tumors is 12.3 months, and is 23 months for patients with SRRM4-negative tumors (log-ranked test, $p=0.029$) (Figure 3.6G). These findings were

consistent to 7 and 10 month overall survival (OS) of t-NEPC (4) and de novo NEPC patients (20), and ~19 month OS of CRPC (21). These results indicate that SRRM4 is a potential biomarker to detect t-NEPC in CRPC, and patients with SRRM4-positive tumors have poor OS rates similar to NEPC patients. Because SRRM4 had been demonstrated to be able to drive t-NEPC xenograft formation, and gain of SRRM4 expression is observed in SCNC, AdNE and AdPC with NE marker expression, we propose that SRRM4 upregulation may be an early event during t-NEPC development.

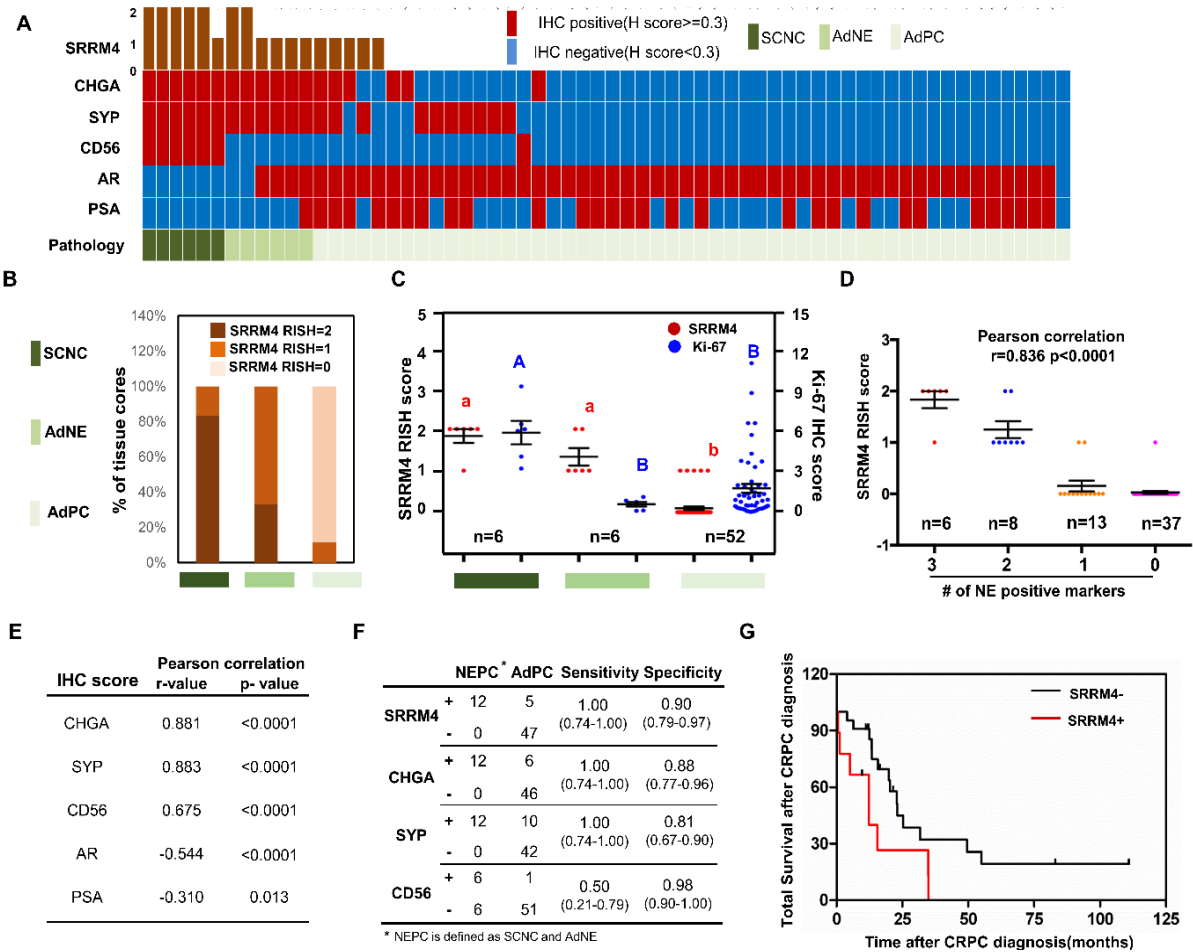


Figure 3.6 SRRM4 expression correlates with t-NEPC

(A) RISH and IHC scores, as well as tumor histology of the CRPC TMA were evaluated. Each column represents one of the 64 tissue cores from 32 patients. IHC scores of CHGA, SYP, CD56, AR, and PSA were calculated by IHC signal intensity (no, low, medium, and high as 0-3) multiplied by the percentage of positive cells (0-100%). IHC scores ≥ 0.3 are considered as positive. (B) Castrate-resistant tumor cores were grouped according their histology into SCNC, AdNE and AdPC. Distribution of SRRM4 RISH scores in each tumor group are plotted. (C) Scatterplots show SRRM4 RISH scores and Ki-67 indexes of each tumor cores in association with tumor morphology. (D) Scatterplots show SRRM4 RISH scores in association with the numbers of positive NE markers. SRRM4 correlation with NE marker numbers were calculated by Pearson's Chi-square test. (E) SRRM4 expression in correlation with CHGA, SYP, CD56, AR and PSA IHC scores was calculated by Pearson's Chi-square test. (F) The sensitivity and specificity of SRRM4 with CHGA, SYP and CD56 to detect t-NEPC were calculated as described²⁰². T-NEPC is defined as tumors with SCNC and AdNE histology. All data are presented as Mean \pm standard error (SEM). Values without a common letter are significantly different, $p < 0.05$. (G) Kaplan-Meier curves plot overall survival of CRPC patients by SRRM4 status (log-rank $p = 0.0294$).

3.2.3 SRRM4 expression correlates with t-NEPC in patient-derived xenograft models

Similar SRRM4 RISH staining was observed in PDX TMA. SRRM4 is strongly expressed in all 8 NEPC cores, poorly expressed in 3 AdPC cores that are both SYP- and AR-positive, and absent

in all 15 SYP-negative and AR-positive AdPC cores (Figure 3.7). The correlation of SRRM4 with NE markers and AR/PSA status in PDXs are significantly stronger than that observed in clinical samples, possibly reflecting more heterogeneity with multiple intermediate stages of AdPC transition to t-NEPC in patients that are not recapitulated in PDXs. These results further support the notion that SRRM4 could be a diagnostic biomarker of t-NEPC in CRPC.

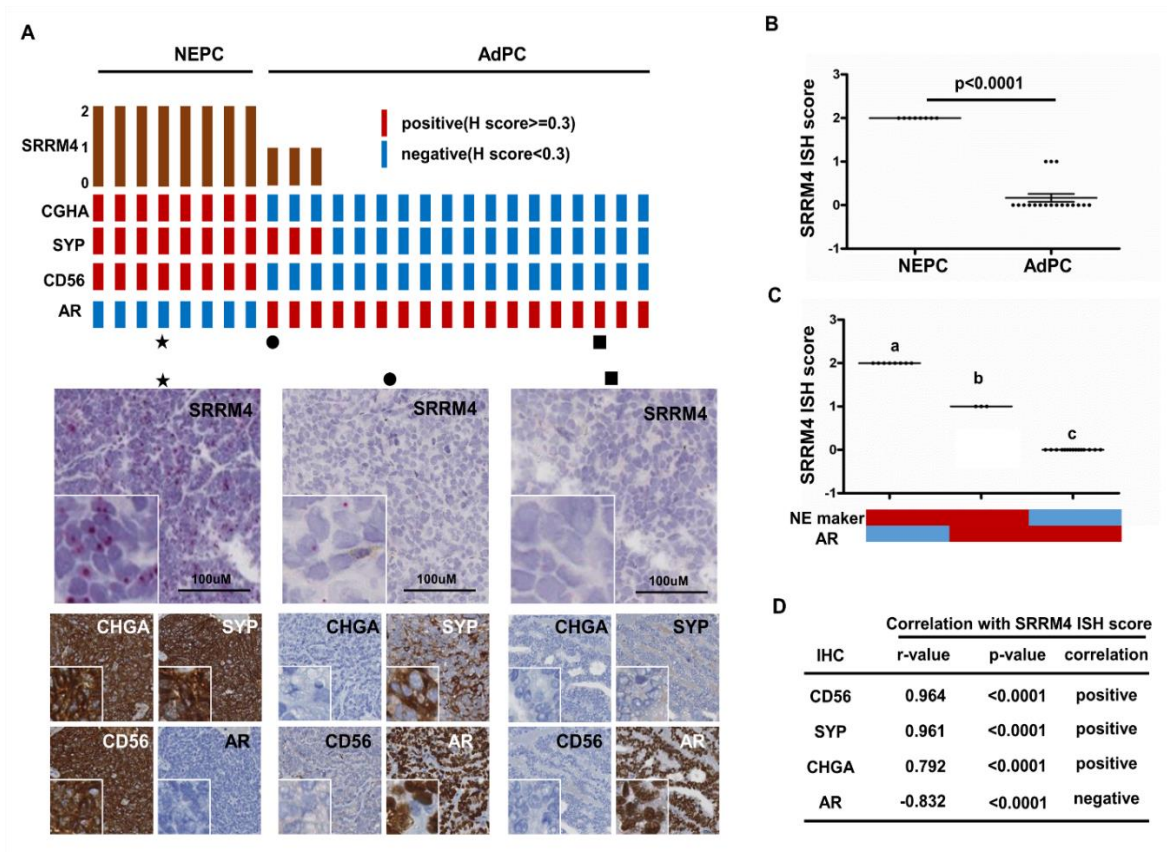


Figure 3.7 SRRM4 expression in PDXs

(A) SRRM4 RISH assays and IHC assays using CHGA, SYP, CD56, and AR antibodies were performed on a PDX TMA. This TMA containing 8 tissue cores from 4 NEPC and 18 cores from 9 AdPC PDXs. Histology evaluation of AdPC and NEPC PDXs were previously described¹⁰⁴.

Each column represents one of the 26 tissue cores from 13 PDXs. IHC scores ≥ 0.3 are considered as positive. Representative RISH and IHC images are presented. **(B-C)** Scatterplots show SRRM4 RISH scores in association with NEPC (B), and NE marker and AR expression status (C). **(D)** The correlation of SRRM4 expression with CHGA, SYP, CD56, and AR expression was calculated by Pearson's Chi-square test. All data are presented as Mean \pm SEM. Values without a common letter are significantly different, $p < 0.05$.

3.2.4 Low SRRM4 expression is detected in a minority treatment-naïve AdPC

SRRM4 was detected in subpopulations of ~16% (23/144) of treatment-naïve AdPC tissue cores (Figure 3.8A). However, all positive cores have low levels of SRRM4 with RISH scores of 1. SRRM4 expression is similar among tumors with different Gleason scores (Figure 3.8B). However, SYP and CHGA were detected in many AdPC tissue cores that were positively correlated with SRRM4 levels (Pearson correlation $r=0.570$ and 0.409 ; $p<0.0001$) (Figure 3.8C). These results indicate that SRRM4 can be expressed at low levels in a portion of cells within treatment-naïve AdPC.

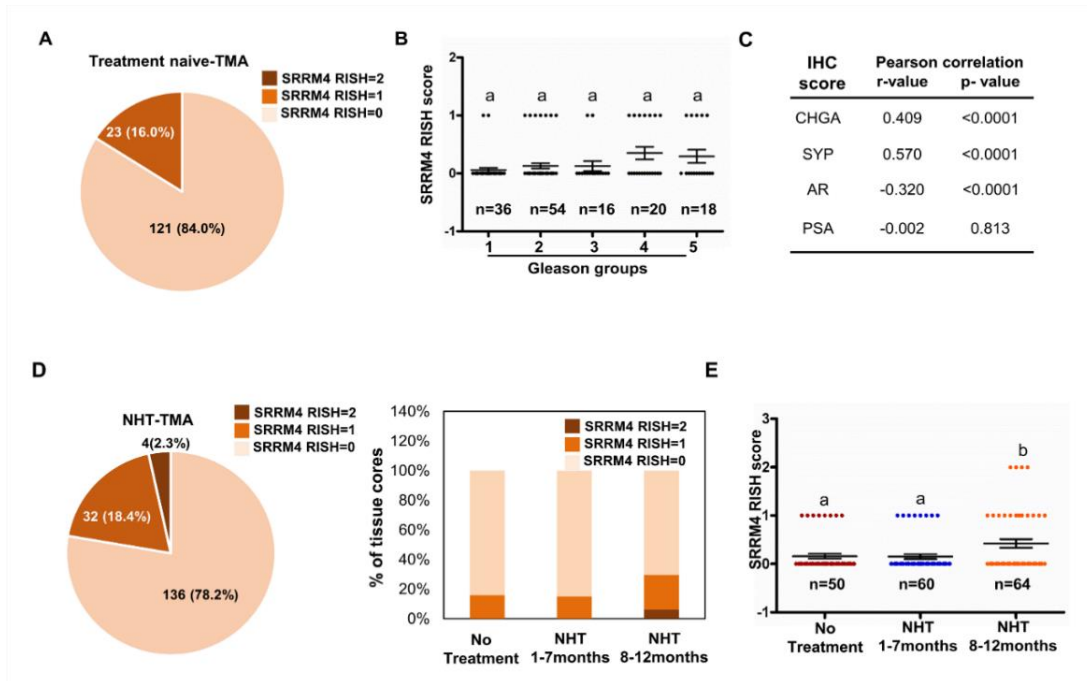


Figure 3.8 SRRM4 expression in treatment-naïve and NHT-treated AdPC tumors

(A) SRRM4 expression was measured by RISH assays on the treatment-naïve AdPC TMA. The treatment-naïve TMAs contain 144 tissue cores of different Gleason groups from 72 patients who had undergone radical prostatectomy. SRRM4 positivity is plotted using a pie chart. (B-C) The association of SRRM4 expression with tumor Gleason groups was calculated by one-way ANOVA followed by Tukey's test (B), and with the expression of CHGA, SYP, AR and PSA was calculated by Pearson's Chi-square test (C). (D) SRRM4 expression were measured by RISH assays on the NHT TMA. This NHT TMA contains 174 tissue cores from 87 patients who received 0-12 month NHT treatment. Distribution of SRRM4 RISH scores is plotted by a pie chart and a column chart. (E) The association of SRRM4 expression with duration of NHT were calculated by one-way ANOVA followed by Tukey's test. All data are presented as Mean±SEM. Values without a

common letter are significantly different, $p < 0.05$.

3.2.5 NHT upregulates SRRM4 expression in AdPC

In the NHT TMA, SRRM4 is positive in 16% (8/50) treatment-naïve tumor cores, 15% (9/60) cores of tumors treated with ≤ 7 month NHT, but 30% (19/64) of cores of tumors treated with > 7 month NHT (Figure 3.8D). SRRM4 RISH scores increase from 0.160 ± 0.076 in treatment naïve and 0.150 ± 0.046 in ≤ 7 month NHT, to 0.375 ± 0.047 in > 7 month NHT tumor cores (Figure 3.8E). There are four cores in the > 7 month NHT treatment group that have gained overt SRRM4 expression with RISH scores of two. These results indicate that SRRM4 expression can be induced in AdPC by long-term androgen deprivation therapy.

3.3 Discussion

To develop resistance to anti-AR therapies, metastatic AdPC can either re-activate its AR signaling and progress into AR-driven castrate-resistant AdPC, or alternatively, bypass AR dependency and progress into anaplastic tumors or t-NEPC for survival. While AdPC progression to t-NEPC reflects the phenotypic plasticity of tumor cells, the process is stochastic and contextual, making the detection or prediction of t-NEPC challenging. Through analyzing the transcriptome and splicing signatures of t-NEPC tumors, we find that splicing factor SRRM4 contributes to the t-NEPC-specific splicing signature. RISH results indicate that SRRM4 has high sensitivity and

specificity to detect t-NEPC in CRPC, emphasizing that SRRM4 may be a diagnostic biomarker of t-NEPC. Expression level of SRRM4 is significantly correlative with NE marker expression in SCNC and AdNC tumor cells, suggesting that SRRM4 may associate with NE differentiation. CRPC patients with SRRM4-positive tumors have shorter patient OS, implying that SRRM4 might be a poor prognostic biomarker. Furthermore, enhanced SRRM4 expression co-exists with AR and PSA in AdNE and AdPC with NE markers, supporting the idea that gain of SRRM4 expression may be both an early molecular event that predicts AdPC progression to t-NEPC, and contributes to tumor cell lineage plasticity.

Low SRRM4 expression in scattered AdPC cells can be detected in some treatment-naïve tumors. However, these tumors retain their AdPC phenotypes, likely due to the presence of AR signaling. The NHT TMA analysis indicates that androgen deprivation therapy induces SRRM4 expression, while overt SRRM4 expression is detected in SCNC with high Ki67 index and AdNE. These results suggest that SRRM4-positive cells become enriched during t-NEPC development. Under castration conditions, SRRM4 supports the transformation of AdPC cells into t-NEPC xenografts, in part by suppressing functions of REST and FoxA1^{114, 169}. SRRM4 target genes also include MEAF6, which functions to accelerate cell proliferation when spliced by SRRM4¹⁸¹, and the SH3GLB1 gene that was reported to confer cells' anti-apoptotic properties^{203, 204}. While androgen deprivation induces apoptosis of castrate-sensitive AdPC cells, the proportion of SRRM4-positive

cells increases during prolonged NHT (Figure 3.8). These findings suggest that gain of SRRM4 function may confer growth advantage to AdPC cells after castration, and support AdPC cell transformation to t-NEPC. Tumors will retain an AdPC phenotype if cancer cells re-activate AR signaling by either enhancing androgen synthesis^{73, 205} or via ligand-independent modes of AR activity¹⁹⁶.

Because SRRM4 antibodies suitable for IHC are currently unavailable, the RISH technique is unique in its ability to measure SRRM4 expression and histology simultaneously in tumor specimens. RISH allows for detection of SRRM4 in low cell populations within a tumor that are otherwise undetectable by RNA-sequencing and microarray assays, because these global gene profiling techniques use RNA samples extracted from tumor homogenates. Consistent with previous RNA-seq/microarray analysis reporting SRRM4 upregulation in t-NEPC^{94, 114, 159}, our RISH assays detect high SRRM4 levels in SCNC and AdNE. RISH also detect low SRRM4 expression in some treatment-naïve AdPC cells, and SRRM4 upregulation in AdPC treated with long-term NHT. These findings suggest that t-NEPC development may be initiated from sub-clonal populations of SRRM4-positive AdPC cells with typical adenocarcinoma morphology and classical ligand-dependent AR signaling. The functions of SRRM4 in these cells may be sequestered under hormone-naïve conditions. However, AR pathway inhibition selects SRRM4-positive cells with survival privilege over other androgen-dependent AdPC cells. Subsequently,

SRRM4 promotes both NE differentiation of AdPC and cell proliferation^{114, 169, 181}, which drives t-NEPC development.

The mechanisms that control SRRM4 gene expression in prostate cancer remain unknown. In neural cells, REST overexpression suppresses, while REST depletion induces, SRRM4 expression²⁰⁶. However, we failed to observe similar regulatory actions of REST in prostate cancer cells, and SRRM4 genomic alteration is not associated with t-NEPC¹¹⁴. However, we cannot exclude other genomic alterations that may indirectly induce SRRM4 expression. Recent studies reported that loss-of-function of TP53 and RB1 genes, and N-Myc gene amplification are associated with t-NEPC^{99, 101}. Whether such genomic alterations induce SRRM4 expression warrants further investigation.

In conclusion, SRRM4 expression is highly correlated with t-NEPC, and poor t-NEPC patient survival. It may be used as a diagnostic and/or prognostic biomarker of t-NEPC.

3.3.1 Hazard risk of SRRM4 expression in t-NEPC development

About 25% of CPRC tumors under ARPI treatment will finally transform into t-NEPC. This value is much smaller than the 30-100% prostate tumors that contain NE marker-positive cells. These results emphasize that NE marker expression is not sufficient to predict t-NEPC development. It

raises an urgent need to predict whether a tumor will develop into t-NEPC before stronger ARPI therapies are administered, since ARPI treatments on tumors with the potential of developing into t-NEPC can facilitate this progression. However, the study of t-NEPC hazard risk factors is very challenging because acquiring specimens of metastatic t-NEPC, at the end of follow-up, to detect the endpoint, is beyond our current ability. In our study, we tried to use “PSA-negative recurrence” as a compensatory endpoint. We compared the rate of PSA-negative metastasis of SRRM4-positive tumor specimens versus SRRM4-negative tumors which are under ARPI treatment after radical prostatectomy. Although the PSA-negative metastatic rate of SRRM4-positive tumors is higher, the difference is not significant because of the small size of SRRM4-positive tumor group (data not shown). In addition, neither NE marker expression, nor Gleason score is associated with PSA-negative recurrence in our patient cohort (data not shown). Further study with larger patient sample size and using histological analysis to identify patient endpoint is needed to study the hazard risk of SRRM4 expression in t-NEPC development.

High frequency blood surveillance is another way to predict t-NEPC. Two retrospective analyses have reported that serum CHGA level is a potential prognostic marker in prostate cancer patients treated with abiraterone and enzalutamide. High serum CHGA level (more than three times the upper normal value) is a hazard risk factor for shorter progression-free survival in patients treated with abiraterone, and for overall survival in patients treated with enzalutamide^{207, 208}. However,

the effects of serum NE markers on detecting t-NEPC have not been validated. Now detection of circulating nucleotides shows high sensitivity and specificity in tumor diagnosis. Using novel “liquid biopsy” technology to detect SRRM4 mRNA in circulating tumor cells and exosomes, may contribute to the detection of early stage t-NEPC.

3.3.2 The role that SRRM4 plays in t-NEPC development

RNA-seq data show both SRRM4 mRNA and NE marker expression are increased in t-NEPC PDXs and patient tumors, which is consistent with our RISH and IHC staining results. These results emphasize that SRRM4 may contribute to t-NEPC development. Other research has demonstrated that SRRM4 is important in neuronal progenitor cell differentiation and neural system development. Knockdown of SRRM4 in developing zebrafish is shown to impair neurite outgrowth and branching of trigeminal ganglia²⁰⁹. Meanwhile, in utero knockdown of SRRM4 in mice prevented differentiation of neuronal progenitors in the cortex²⁰⁶. More importantly, SRRM4 negatively regulates the REST transcriptional repressor via activation of a neural-specific splicing switch during neurogenesis, and loss of SRRM4 promotes REST-mediated repression of neurogenesis²⁰⁶. This mechanism is also found in small cell lung cancer²¹⁰. In the next chapter, we will perform comprehensive studies to analyze whether SRRM4 has the biological capacity to induce NE transdifferentiation through splicing of REST in prostate adenocarcinoma cells.

Chapter 4: SRRM4 Drives Neuroendocrine Transdifferentiation of Prostate Adenocarcinoma under Androgen Receptor Pathway Inhibition

4.1 Introduction

Next-generation ARPI therapies that suppress AR signaling in CRPC have improved patient outcomes²¹¹. However, emerging evidence suggests that lethal t-NEPC becomes more prevalent in patients treated with first- or second-line AR pathway inhibitors^{83, 84}. NEPC cells lose their granular structure, and present small cell neuroendocrine-like morphology⁹⁹. They express typical neuroendocrine markers such as CHGA/CHGB, SYP, and NSE, but no or low levels of AR and AR-regulated genes^{88, 104, 183}. Because AR signaling is required for epithelial cell differentiation during prostate development, ARPI likely triggers developmental reprogramming of AdPC to t-NEPC through a transdifferentiation mechanism¹⁸³. Although ARPI improves overall survival for men with metastatic CRPC, it may result in treatment-induced progression to NEPC as a resistance mechanism.

Although the expression of several genes is correlated with t-NEPC^{101, 102, 169, 184}, less of them were confirmed as driving t-NEPC transdifferentiation. We reported loss of REST in t-NEPC²¹². REST is highly expressed in embryonic stem cells and non-neuronal cells. It acts as a negative master regulator of neurogenesis by suppressing genes required for neural cell differentiation²¹³. One mechanism for cells to compromise REST function during neural differentiation is through

alternative splicing of REST into REST4²⁰⁰. The exon N becomes inserted between exons 3 and 4, resulting in translation of a truncated and functionally reprogrammed REST4 protein. These findings indicate that although transcriptomic studies can identify genes such as REST, which are associated with t-NEPC progression, analyzing NEPC-specific AS signatures to identify RNA splice factors may lead to currently unrecognized mechanisms of t-NEPC progression, and novel therapeutic approaches. Loss-of-function of RB1 and TP53 genes, as well as gain-of-function of AURKA were also reported in t-NEPC^{100, 182}. These genes are known as cell cycle regulators. Whether they can confer cancer cells with an NEPC phenotype has not been established. In Chapter 3, we found that splicing factor SRRM4 is highly expressed in t-NEPC tumor tissues, and correlates with NE marker expression. SRRM4 has been reported to regulate REST splicing in neural cell differentiation and development. In this study we demonstrated that, in the context of ARPI, SRRM4 can drive transdifferentiation to t-NEPC.

4.2 Results

4.2.1 SRRM4 is an upstream regulator of REST gene functions in prostate cancer cells

We analyzed the SRRM, REST, and REST4 mRNA expression in samples of VPC cohort and showed that in t-NEPC tumor samples, elevated SRRM4 expression was negatively associated with the expression ratio of REST: REST4. (Figure 4.1A). These results were consistent with those from NCI-H660 (NEPC line) and VCaP cells that express elevated levels of SRRM4 and REST4

proteins and low levels of REST protein (Figure 4.1B). Consistently these cells expressed enhanced REST4 messenger RNA (mRNA) levels, but extremely low levels of REST (Figure 4.1C).

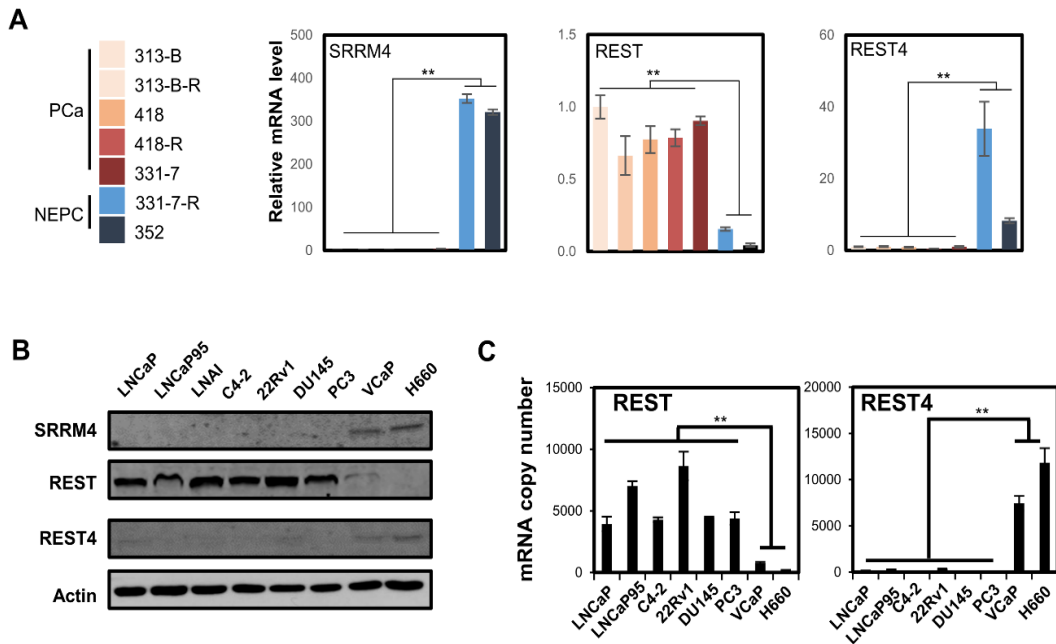


Figure 4.1 SRRM4, REST, and REST4 expression in PCa tumors and cell lines

(A) Total RNA of xenografts from the VPC cohort were isolated. SRRM4, REST and REST4 mRNA levels were measured by real-time qPCR. (B-C) Total RNA and protein lysates of different prostate cancer cell lines, including AdPC cell lines (LNCaP, LNCaP95, LNAI, C4-2, 22Rv1, DU145, PC3), AdPC cell lines with gene amplification (VCaP), and NEPC cell lines (H660) were also collected. (B) Immunoblotting assays were used to measure protein levels of SRRM4, REST and REST4. (C) Real-time PCR assays were used to measure REST and REST4 mRNA levels. Results (n=3) were presented as Mean \pm standard deviation (SD). **p < 0.01.

To determine whether SRRM4 regulated REST expression, we overexpressed SRRM4 in LNCaP cells (Figure 4.2A). There was a 30% decrease in REST, but a 130-fold increase in REST4 mRNA levels. SRRM4 depletion in VCaP cells resulted in a 10-fold increase in REST and a 90% decrease in REST4 mRNA levels (Figure 4.2B). Consistent REST and REST4 protein expression regulated by SRRM4 was also confirmed (Figure 4.2C). To determine whether REST regulated SRRM4 expression, two small interfering RNAs (siRNAs) were used to deplete REST. The exon 2 siRNA depleted REST and REST4 expression. Exon 4 siRNA depleted REST but induced a 50-fold increase of REST4. Regardless, minor changes of SRRM4 mRNA and no change of SRRM4 protein levels were observed (Figure 4.2D-E). Overexpression of REST4, but not REST, caused a twofold increase in SRRM4 mRNA levels and no change in SRRM4 protein levels (Figure 4.2F-G). Gain-of-function of SRRM4 and loss-of-function of REST resulted in a similar induction of t-NEPC biomarkers (Figure 4.2H); however, SRRM4 exerted stronger effects. REST4 did not significantly alter the expression of t-NEPC biomarkers. These results suggest that a key mechanism through which SRRM4 induces the NEPC phenotype is reprogramming of REST function by AS and that SRRM4 is an upstream negative regulator of REST function.

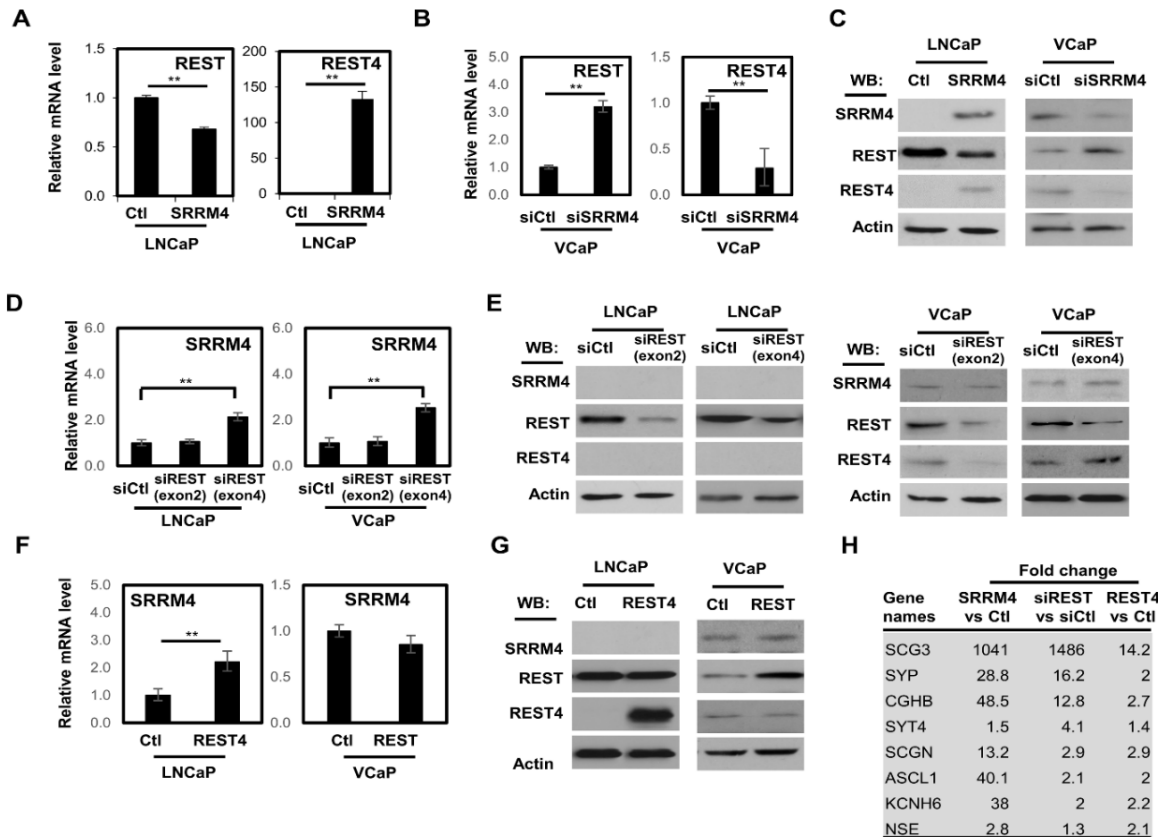


Figure 4.2 SRRM4 is an upstream regulator of REST

(A-C) LNCaP cells were transfected with control or SRRM4 expression plasmid. VCaP cells were transfected with control or SRRM4 siRNA for 48 hours. Total RNA and protein lysates were collected and used to measure REST and REST4 mRNA levels by real-time qPCR (A-B) and SRRM4, REST, and REST4 protein levels were determined by immunoblotting assays (C). (D-E) LNCaP and VCaP cells were transfected with control or REST siRNAs against exon 2 or exon 4. Total RNA and protein lysates were collected and used to measure SRRM4 mRNA levels by real-time qPCR (D) and SRRM4, REST, and REST4 protein levels were determined by immunoblotting assays (E). (F-G) LNCaP and VCaP cells were transfected with control, REST, or REST4 expression vectors. REST, REST4, and SRRM4 mRNA levels (F) and protein levels

(G) were detected by real-time qPCR and immunoblotting assays respectively. (H) LNCaP cells were transfected with control or SRRM4 expression vector (left panel), control or REST siRNA (middle panel), or control or REST4 expression vector (right panel). Total RNA was collected and used to measure mRNA levels of neuroendocrine prostate cancer biomarkers using real-time qPCR. All qPCR results (n=3) were presented as the mean \pm SD **. Values without a common letter are significantly different.

4.2.2 Molecular mechanisms through which SRRM4 regulates AS of REST

RNA chromatin immunoprecipitation showed that SRRM4 recognized the region near the 3' splice site of REST intron 3 (designated as the P1 region) (Figure 4.3A-B). In contrast, SRRM4 enrichment to the control intron region (designated as P2) was extremely low (<0.01% in Figure 4.3B). It has been reported that the UGC motif is predicted to be a consensus SRRM4 recognition site near RNA splicing sites²⁰⁹. RNA pulldown assays confirmed that purified SRRM4 protein from LNCaP or 293T cells interacted directly with a UGC motif in REST intron 3 (Figure 4.3C). A REST minigene was constructed in which the exon N and its flanking approximately 300-base pair nucleotides were inserted in between exon 3 and 4 of the REST gene (Figure 4.3D). This minigene is similar to the endogenous REST gene with respect to its response to SRRM4 overexpression (Figure 4.3E). Site-directed mutagenesis of all sites (M1–M4) around the UGC motif in the P1 region (Figure 4.3F) indicated SRRM4-mediated exon N inclusion relied on the G

within the UGC motif (Figure 4.3G). These results demonstrated that SRRM4 binds the UGC motif and induces exon N inclusion for REST4 splicing.

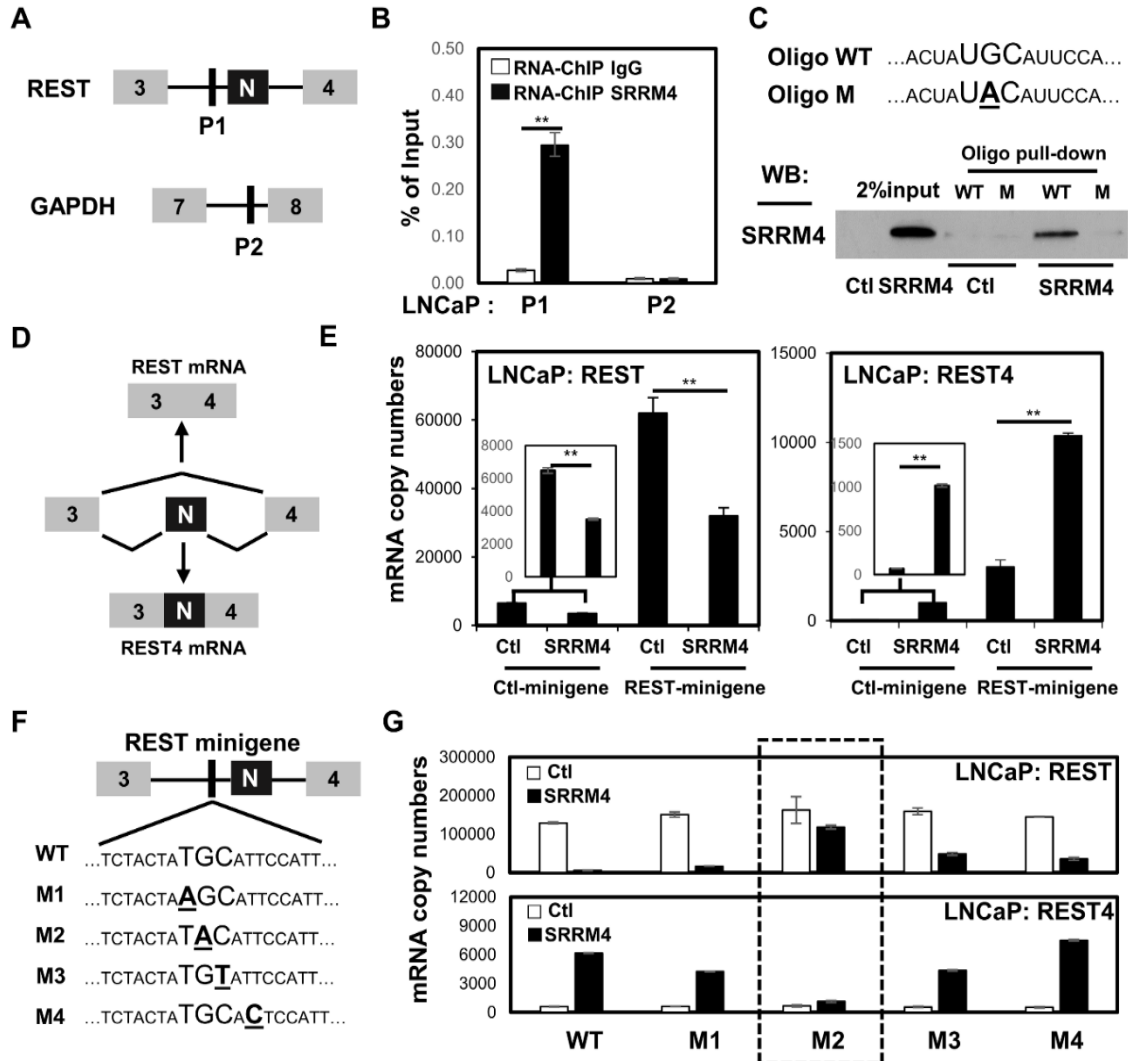


Figure 4.3 SRRM4 regulates alternative splicing of REST in prostate cancer cells

(A) A schematic diagram shows the regions (P1, P2) that were amplified in RNA-ChIP assays. (B) LNCaP cells were transfected with Flag-SRRM4 plasmids. RNA-ChIP assays were performed using Flag antibody or control IgG. Eluted RNA fragments were used as templates for real-time qPCR. Primers indicated in (A) were used to amplify the target regions. Signals were calculated

as percentage of input. (C) LNCaP cells were transfected with Flag-SRRM4 plasmids. Biotin labeled oligoes containing wild type (WT) or mutant (M) UGC motif in P1 region were used to pull down SRRM4 protein. Only in proteins pulled down by using the UGC (WT) oligo can SRRM4 be detected by immunoblotting. (D) A schematic diagram shows the REST minigene structure and the AS variants derived from the minigene. (E) LNCaP cells were transfected with control or REST minigene reporter in the presence of $-/+$ SRRM4. Total RNA was extracted to measure REST and REST4 mRNA levels by real-time PCR. Expressions level of both endogenous and exogenous REST4 mRNA were significantly increased by SRRM4. (F) Site-directed mutagenesis was performed around the UGC motif in the REST minigene. (G) LNCaP cells were transfected with control, REST minigene, or REST minigene with M1–M4 mutations in the presence of $-/+$ SRRM4. Total RNA was collected and used to measure REST and REST4 mRNA levels by real-time PCR. Only M2 mutant abolished SRRM4-induced REST4 mRNA expression. All results were derived from two independent experiments that were performed in triplicate. Data are presented as Mean \pm SD. $**p < 0.01$ compared with controls.

4.2.3 AR pathway inhibition enhances SRRM4 to induce the neuroendocrine prostate cancer phenotype in prostate cancer cells

To study interactions between SRRM4 and ARPI, LNCaP and VCaP cells were cultured in androgen depletion medium and treated with dihydrotestosterone (DHT) or the ARPI drug

enzalutamide (ENZ). AR inhibition did not alter REST, REST4, or SRRM4 mRNA levels (Figure 4.4A) but reduced REST protein expression (Figure 4.4B). These results indicated that ARPI reduced REST post-transcriptionally, as reported²¹². Overexpression of SRRM4 by lentivirus induced the NEPC phenotype, and it became stronger with enzalutamide (Figure 4.4C). These results together indicate that SRRM4 and ARPI target AS and protein expression of the REST gene, respectively, and that contributes additively to NEPC transdifferentiation.

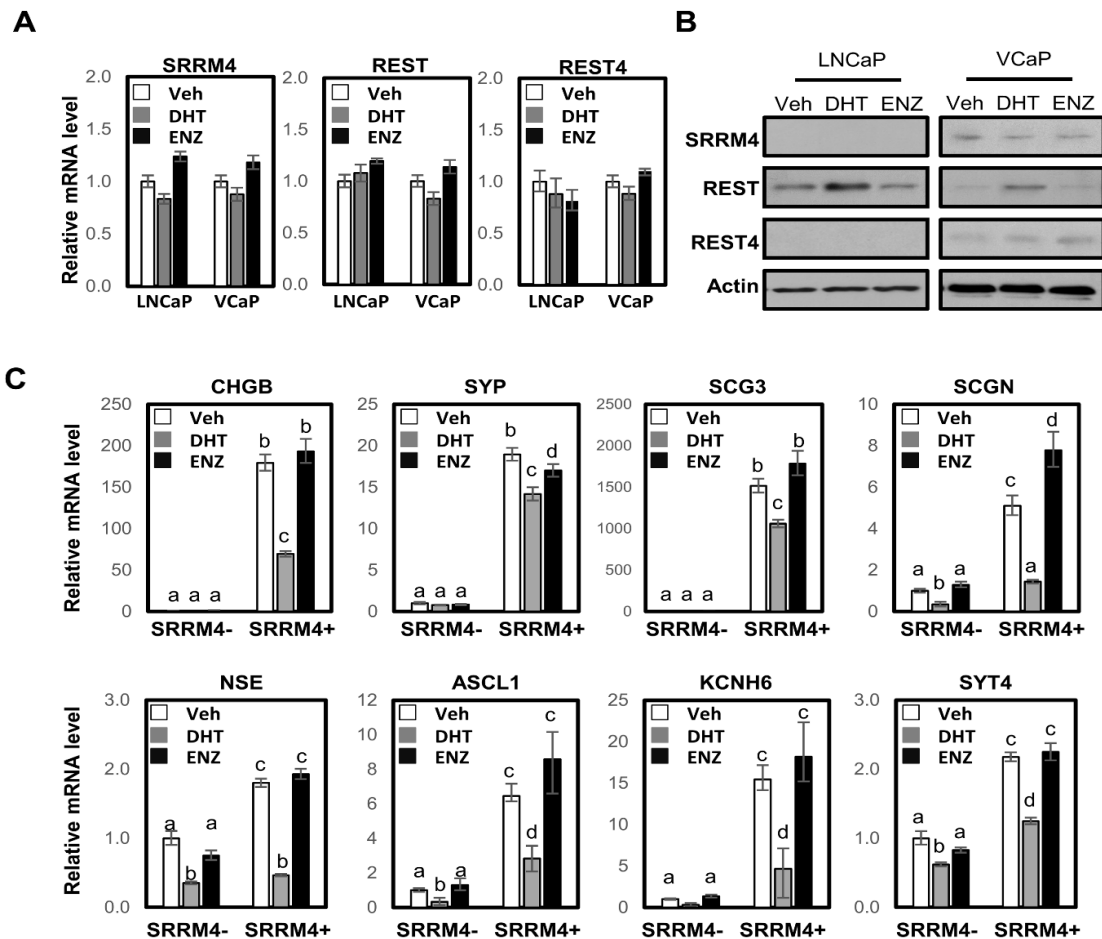


Figure 4.4 Androgen receptor pathway inhibition enhances SRRM4 actions to induce the NEPC phenotype

(A-C) LNCaP and VCaP cells (A and B) or LNCaP (CRL) and LNCaP (SRRM4) cells (C) were cultured in medium containing 10% charcoal-stripped serum(CSS) for 48 h before being treated with vehicle, dihydrotestosterone (DHT) , or ARPI drug enzalutamide (ENZ). The CSS medium does not contain androgen and is used to provide the androgen-deprivation condition. (A) Total RNA were collected. SRRM4, REST, and REST4 mRNA levels were detected by real-time qPCR. (B) Total protein were collect. SRRM4, REST, REST4, and actin protein levels were detected by immunoblotting. (C) Total RNA were collected. NEPC biomarker expression in mRNA was measured by real-time PCR. Both SRRM4 expression and ARPI induce NE biomarkers expression. All results were presented as Mean \pm SD. (n = 3; values without a common letter are significantly different, $p < 0.05$).

4.2.4 RB1 and TP53 loss-of-function enhance SRRM4-induced neuroendocrine prostate cancer transdifferentiation

We depleted RB1 or TP53 by shRNA in LNCaP cells and then introduced exogenous SRRM4 by lentivirus. When cells were cultured in fetal bovine serum medium, eight NEPC biomarkers were upregulated by SRRM4, the effects of which were enhanced by RB1 or TP53 depletion (Figure 4.5A). SRRM4 in combination with loss-of-function of RB1 or TP53 showed a dramatically stronger propensity to upregulate NEPC biomarkers under ARPI. CHGB, NSE, SYP, and secretogranin III protein levels were enhanced by SRRM4 and further increased by ARPI and/or

RB1 or TP53 knockdown (Figure 4.5B). Nevertheless, RB1 or TP53 knockdown alone or in combination with ARPI did not significantly affect NEPC biomarker expression if SRRM4 was absent (Figure 4.5C), suggesting that these two genes are facilitators of the NEPC phenotype. In summary, SRRM4 becomes a more potent driver of NEPC transdifferentiation under ARPI. Loss-of-function of RB1 and TP53 may facilitate this process.

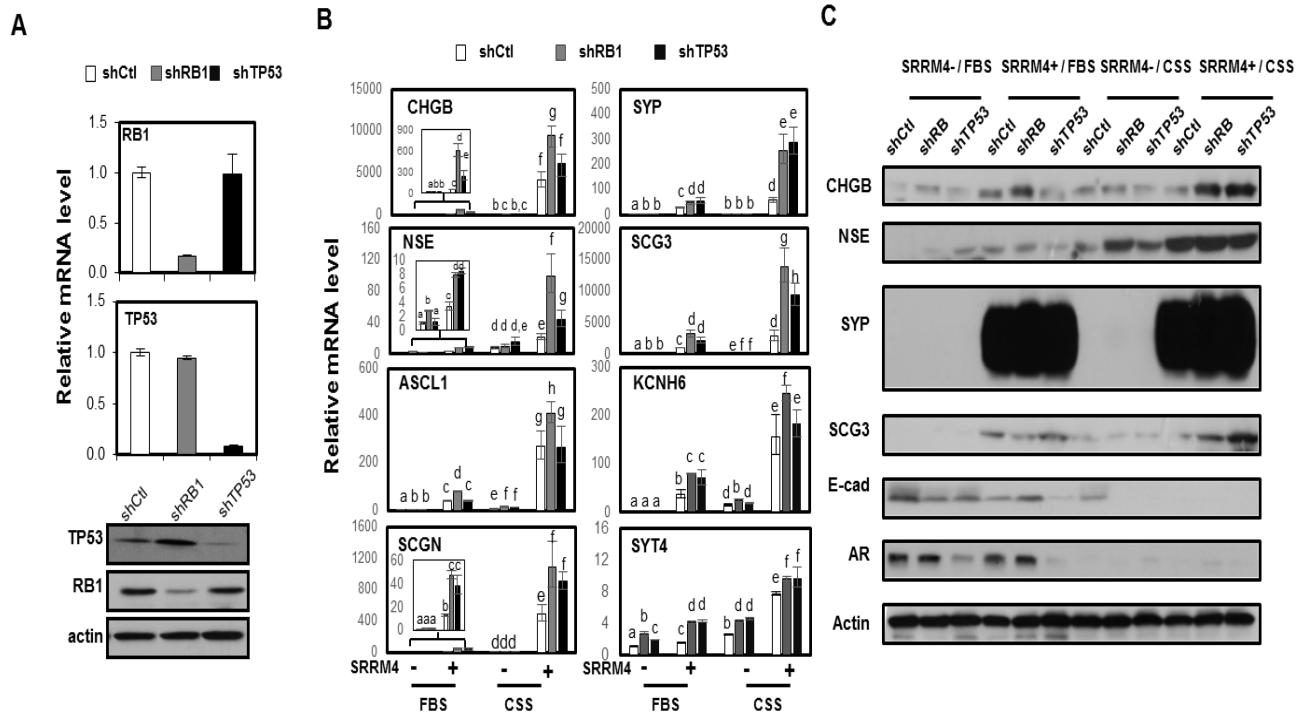


Figure 4.5 Roles of TP53 and RB1 depletion in SRRM4-induced NEPC phenotype

(A) LNCaP(shCtl), LNCaP(shRB1) and LNCaP(shTP53) cells were cultured in RPMI1640 medium containing 10% FBS. Total RNA and protein lysates were collected and used to detect TP53 and RB1 mRNA levels by real-time PCR and protein levels by immunoblotting. (B-C) LNCaP(SRRM4-/shCtl), LNCaP(SRRM4+/shCtl), LNCaP(SRRM4-/shRB1), LNCaP(SRRM4+/shRB1), LNCaP(SRRM4-/shTP53), and LNCaP(SRRM4+/shTP53) cells were

cultured in RPMI 1640 medium containing either 10% fetal bovine serum or 10% CSS for 4 week. Total RNA and protein lysates were collected and used to measure NEPC biomarker expression by real-time PCR (**B**) and by immunoblotting (**C**). Both TP53/RB1 depletion and SRRM4 expression induce NE biomarkers expression. All results were presented as MeanSD. Values without a common letter are significantly different, $p < 0.05$.

4.2.5 SRRM4 alters the morphology of epithelial prostate cancer cells and establishes neuroendocrine prostate cancer xenografts

Under AR inhibition, LNCaP cells changed their epithelial spear morphology to compact cell bodies with extended fine branches, but still grew as an adherent monolayer (Figure 4.6A). Gain of SRRM4 led to formation of 3D multicellular spheroids with strong SYP expression. The sizes and numbers of these spheroids were statistically greater in TP53-depleted cells (Figure 4.6A). DHT reversed these morphologic changes and upregulation of NEPC biomarkers (Figure 4.6B), indicating that the NEPC phenotype was not yet stably established at approximately 4 wk.

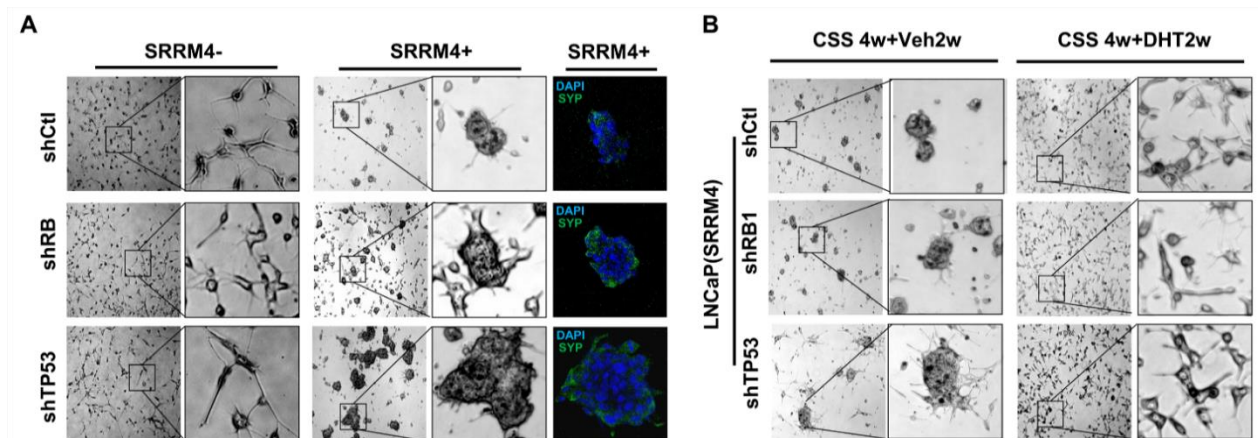


Figure 4.6 SRRM4 alters the morphology of epithelial prostate cancer cells

(A) LNCaP cells with $-/+SRRM4$, $-/+shRB1$ or $shTP53$ were cultured in medium containing 10% CSS for 4 week. Spheroids were fixed, immunostained with SYP antibody, and examined by fluorescence microscope. (B) LNCaP($SRRM4+/shCtl$), LNCaP($SRRM4+/shRB1$), and LNCaP($SRRM4+/shTP53$) cells were cultured in: 1) phenol-free RPMI1640 medium containing 10% CSS for 4 weeks followed by phenol-free RPMI1640 medium with 10% CSS plus vehicle for another 2 weeks, and 2) phenol-free RPMI1640 medium with 10% CSS for 4 weeks followed by phenol-free RPMI1640 medium with 10% CSS plus 10nM DHT for another 2 weeks. Multicellular spheroid formations were examined by microscopy.

Because TP53 and RB1 are cell cycle regulators, we cultured LNCaP cells in both 2D and collagen-embedded 3D culture conditions to show that TP53, but not RB1, enhanced BrdU incorporation regardless of SRRM4 overexpression (Figure 4.7A). Our colony formation assays further demonstrated that RB1 and TP53 can enhance anchorage-independent cell growth in the absence of SRRM4 (Figure 4.7B). SRRM4 can also stimulate colony formation, supporting its role for NEPC progression. This SRRM4 function was strengthened by depletion of TP53 but not RB1.

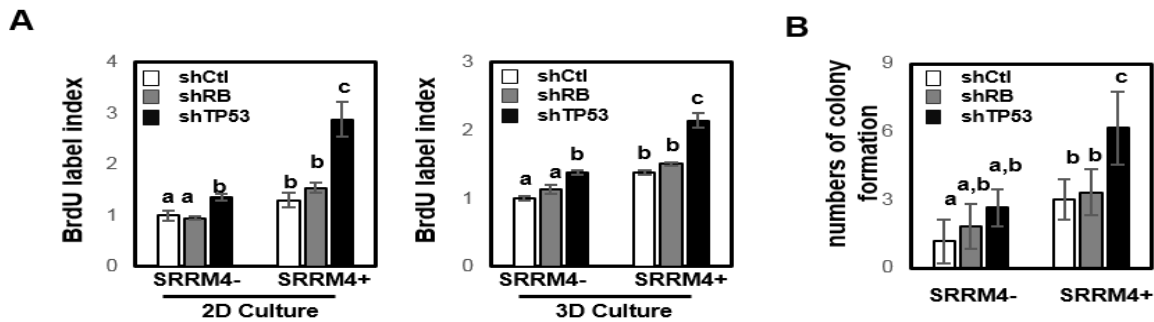


Figure 4.7 TP53 and RB1 loss enhance SRRM4 promoted cell growth and colony formation

(A) LNCaP cells with $-/+$ SRRM4, $-/+$ shRB1 or shTP53 were cultured in medium containing 10% CSS in six-well plates (2D) or in collagen-embedded 3D conditions. BrdU incorporation rates were calculated as described in the materials and methods. Gain of SRRM4 increased BrdU incorporation in LNCaP(shTP53) cells under both 2D and 3D conditions. (B) Colony formation assays were performed on LNCaP cells with $-/+$ SRRM4, as indicated. Colonies were stained with crystal violet, and colony numbers were counted. Gain of SRRM4 increased colony formation of LNCaP(shTP53) cells. All results are presented as Mean \pm SD ($n = 3$; values without a common letter are significantly different, $p < 0.05$). These data were analyzed by one-way analysis of variance followed by Tukey's multiple comparison tests.

Current evidence suggests that AR inhibition, cAMP, or Il-6 can induce neuroendocrine transdifferentiation of LNCaP cells under 2D culture conditions; however, this is limited to upregulation of NEPC biomarkers^{167, 171, 214-216}. No study has shown that LNCaP xenografts can be transformed into t-NEPC tumors after ARPI. When exogenous SRRM4 was introduced into

LNCaP cells in the presence of RB1 or TP53 knockdown in castrated nude mice, SRRM4 established NEPC xenografts with strong SYP expression detected by both enzyme-linked immunosorbent assay on serum samples and by immunohistochemistry (Figure 4.8). In SRRM4-established NEPC tumors, TP53 depletion consistently showed enhanced NEPC transdifferentiation. Interestingly, these NEPC xenografts heterogeneously expressed the AR and PSA (Figure 4.8C). Indeed, many cells in SRRM4+/SYP+ tumors are AR- and PSA-negative, whereas all cells in SRRM4-/SYP - xenografts are AR and PSA-positive. These results support the idea that SRRM4 drives transdifferentiation of AdPC to NEPC, accompanied by AR signaling being stochastically diminished.

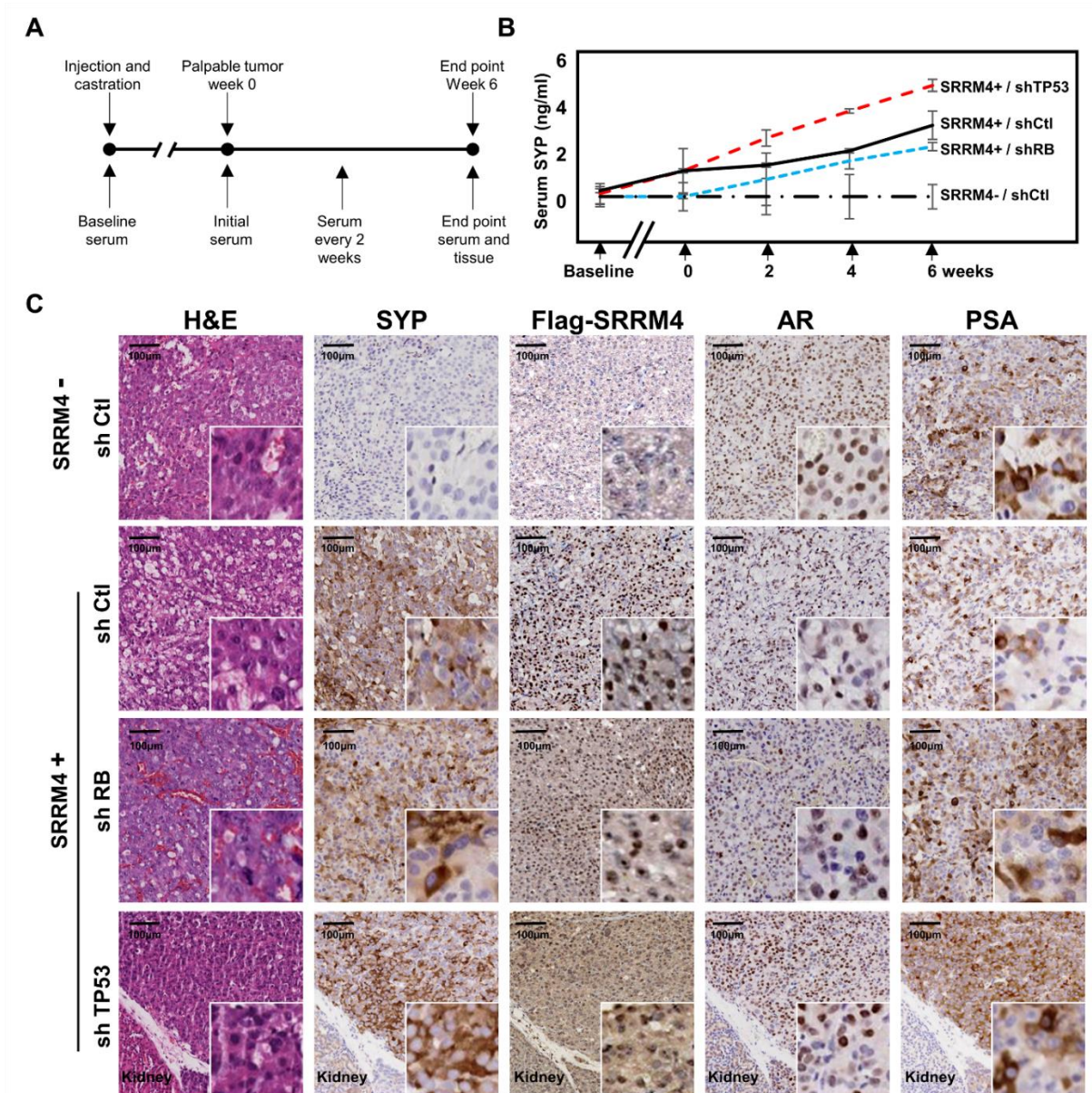


Figure 4.8 SRRM4 drives transdifferentiation of LNCaP xenografts to neuroendocrine prostate cancer tumors.

(A-C) Exogenous SRRM4 was introduced into LNCaP cells in the presence of RB1 or TP53 knockdown by lentivirus infection. These cells were used to generate xenografts in castrated nude mice. (A) Schematic diagram shows the time points of serum and tissue collection from mice

bearing these LNCaP xenografts. **(B)** Serum SYP concentrations from mice bearing LNCaP(SRRM4⁻/shCtl), LNCaP(SRRM4⁺/shCtl), LNCaP(SRRM4⁺/shRB1), and LNCaP(SRRM4⁺/shTP53) xenografts (six grafts in three mice) were measured by enzyme-linked immunosorbent assays and were repeated in triplicate. Mice bearing SRRM4-positive xenografts show high serum SYP levels **(C)** IHC of these xenografts were performed with indicated antibodies. Hematoxylin and eosin staining was also carried out. SRRM4-positive cells show strong SYP IHC staining. Scale bars = 100 μ m.

4.3 Discussion

It is anticipated that NEPC will become more prevalent with widespread adoption of potent ARPI for CRPC. Consequently, better understanding of the molecular mechanisms by which NEPC develops is necessary to design therapeutic strategies for NEPC. Our finding that SRRM4 drives AdPC transdifferentiation to NEPC through AS of multiple genes including REST is novel. Importantly, ARPI in the context of TP53 depletion exponentially escalates SRRM4-driven NEPC transdifferentiation. Our findings suggest that ARPI, genomic abnormality (eg, TP53 and RB1 genes), and reprogrammed transcription/AS programs (e.g., by SRRM4 and REST) can combine to drive NEPC progression.

Consensus on the epidemiology of NEPC has not been reached⁸⁸. Multiple hypotheses have been

proposed including that NEPC originates from: (1) adenocarcinoma cells through transdifferentiation, (2) clonal selection of pluripotent stem-like prostate epithelial cells, or (3) benign neuroendocrine cells. Accumulating evidence favors the first hypothesis. Genetic characterization of NEPC tumors^{93, 217} and PDXs showed a high degree of similarity to their adenocarcinoma counterparts. Androgen depletion, cAMP, or cytokines can also stimulate adenocarcinoma cells to express NEPC biomarkers^{167, 171, 214}. Although elevated SRRM4 expression was reported to be correlated with NEPC progression¹⁵⁹, we demonstrated for the first time that SRRM4 is a causal factor that not only can induce adenocarcinoma cells to express NEPC biomarkers but also can alter cellular morphology and, even more importantly, transform AdPC into NEPC xenografts in vivo. SRRM4 is a regulator of neural-specific exon networks required for embryonic stem cells to transdifferentiate into neural cells²⁰⁰. Many SRRM4-targeted genes (e.g., REST and BHC80) in neural cells were also identified in NEPC, suggesting that SRRM4 is functionally active in NEPC^{104, 160}. It is noteworthy that several SRRM4 target genes are epigenetic histone modifiers, transcription factors, and RNA splicing factors. These findings indicate that SRRM4 can be a regulator to reprogram AdPC transcriptomes into NEPC transcriptomes through AS alone. They highlight the importance of AS in determining tumor progression, something often overlooked in global transcriptome analyses.

Although SRRM4 regulates REST splicing, knockdown of REST does not affect SRRM4

expression, indicating that SRRM4 is an upstream regulator of REST in prostate cancer cells. As a global regulator, SRRM4 has much broader functions. Although REST knockdown stimulates NEPC biomarker expression, it does not alter LNCaP cell morphology and is not sufficient to establish NEPC xenografts, indicating that loss-of-function of REST is adequate to confer NEPC phenotype but not sufficient to induce NEPC transdifferentiation. Our results demonstrate that SRRM4 is a powerful driver of NEPC transdifferentiation.

The prerequisite condition for SRRM4 to establish NEPC tumors is ARPI, since SRRM4 cannot cause morphologic changes in LNCaP cells and cannot induce NEPC xenografts when androgens are present. Our study also showed that enhanced SRRM4 expression and ARPI can block REST function through AS and protein degradation, respectively²¹² (Figure 4.4). These findings explain interdependent and additive effects of SRRM4 and ARPI for NEPC progression.

Our results indicated that SRRM4 induction of the NEPC phenotype is enhanced by RB1 or TP53 depletion (Figure 4.5). When combined with ARPI, SRRM4 functions are further enhanced by TP53 loss (Figures 4.5, 4.6, and 4.7). Based on these results and others, we propose a model of AdPC transdifferentiation to NEPC involving two types of gene regulators in two steps. The first type of genes including AR, SRRM4, and REST function as cell-differentiation regulators. They control epigenetics, transcription, and AS to confer an NEPC phenotype. ARPI releases AR-

induced epithelium differentiation, thus providing an opportunity for cells to reset differentiation to NEPC. SRRM4 reprograms REST function through AS and globally regulates neural-specific epigenetic histone modifiers, transcription factors/cofactors, and RNA splicing factors that are necessary for the NEPC phenotype. Nevertheless, this phenotypic transition cannot be detected until the transdifferentiated NEPC cells lock in their phenotypes. The second type of genes includes TP53, RB1, and AURKA cell cycle regulators. Genetic alterations of these genes facilitate NEPC transdifferentiation by bypassing cell cycle checkpoints. Cells bearing these genetic alterations also gain selective growth advantage under ARPI. This step is significant because it enriches NEPC cell numbers and biomarkers above a critical threshold allowing pathologic detection; however, loss-of-function of RB1 or TP53 likely does not play a direct role in NEPC transdifferentiation because these genes also exist in many AdPC tumors. Consistent with this, we showed that TP53 or RB1 depletion did not change NEPC biomarker expression (Figure 4.5). Consequently, genomic heterogeneity may predispose some prostate cancer cells to stably establish an NEPC phenotype once they transdifferentiate. This partially explains variations in NEPC marker expression in different prostate tumors²¹⁸.

4.3.1 Mechanism of SRRM4 overexpression

The mechanisms of induction of SRRM4 remain unknown. No NEPC-specific mutations were found in the SRRM4 promoter, thus induction of SRRM4 gene expression may involve epigenetic

mechanisms involving histone post-translational modifications, DNA methylations and regulation effects of microRNA.

When located in a gene promoter, DNA methylation typically acts to repress gene transcription. It has been reported that DNA methylation profiles are distinct between castration-resistant AdPC and t-NEPC, associated with differentially methylated promoters and downstream transcriptional changes^{94, 219}. We have checked the methylation states of -100~2000bp upstream of SRRM4 transcription initiation site using CpG bisulfite conversion method and demonstrated DNA methylation states of this region is significantly higher in LNCaP cell than in NCI-H660 cell (data not shown). This result suggests that DNA methylation may participate in regulation of SRRM4 expression. Unfortunately, DNA methylation states of this region in AdPC and t-NEPC PDXs did not show significant difference (data not shown). However, we cannot exclude the possibility that DNA methylation in other regions of SRRM4 gene can affect SRRM4 gene transcription.

Histone modification also contribute to gene transcription. The histone methyltransferase EZH2 is upregulated in NEPC and EZH2-suppressed target genes downregulated. A recently research has elucidated a mechanistic link between N-myc and EZH2 in which they cooperate to drive histone methylation, suppress AR signaling, and drive a NEPC phenotype¹⁰². However combined overexpression of EZH2 and N-myc did not alter SRRM4 expression in LNCaP cells (data not

shown).

MicroRNAs function via base-pairing with complementary sequences within mRNA molecules and results in silencing of target mRNA molecules^{220, 221}. Through analyzing SRRM4 mRNA sequence using bioinformatics tools, we have found several microRNAs which are predicted to be able to target SRRM4 mRNA. One of these candidates is miR-138-5p which has been considered as a tumor suppressor in bladder and colorectal cancers^{222, 223}. Analyzing the regulation effect of miR-138-5p on SRRM4 mRNA is beyond the scope of this thesis.

In summary, multiple temporal steps that include epigenetic modifications, including those involving SRRM4, may be required before the NEPC phenotype is stably established; however, such a hypothesis cannot fully explain why not all tumors or all cancer cells within a tumor eventually develop into NEPC. We hypothesize that some uncharacterized mutations in AdPC genomes may be prerequisite for and cooperate with SRRM4-regulated and other epigenetic changes for NEPC. These questions warrant further investigation.

4.3.2 SRRM4-driven t-NEPC xenografts

Several *in vitro* and *in vivo* alternations can confer AdPC cells the NE phenotype; however, few of them can finally drive AdPC cells to establish t-NEPC tumors. Our study have for the first

time showed that alternative splicing can transform LNCaP xenografts into t-NEPC tumors. Histological analysis shows NE markers are co-expressed with AR and PSA regardless the weaker staining than AdPC xenograft. In addition, androgen treatment can reverse both NE markers expression and morphological changes of LNCaP(SRRM4) cell. These results suggest the transdifferentiation of LNCaP(SRRM4) cell is not stable. Development of NEPC tumors is not rapid. The LTL331 PDX progressed to NEPC approximately 6 month after castration. It also took 6 years for the original tumor that gave rise to the LTL331 xenograft to recur in the patient as NEPC, emphasizing continuous ARPI treatment is a precondition for fully development of t-NEPC tumors. Since one month of castration is not sufficient to diminish AR and PSA expression, in next chapter, we will study the effect of long-term ARPI on SRRM4-driven NEPC cell lines.

Chapter 5: Establishment of a Neuroendocrine Prostate Cancer Model Driven by SRRM4

5.1 Introduction

Although new generation ARPI therapies are effective in prolonging the survival of patients with metastatic CRPC^{211, 224}, emerging evidence indicates that t-NEPC is becoming more prevalent due to the selection pressure of ARPI^{88, 94, 104, 114}. T-NEPC has been reported in up to ~25% of patients who had received either first- or second-line anti-AR therapies⁸⁵, and this rate of occurrence is predicted to rise with the widespread use of ARPI. Besides systemic chemotherapy regimens, no targeted therapy has yet been approved for t-NEPC patients. This is in part due to the limited NEPC cell and tumor models available for studying the molecular underpinnings of t-NEPC progression.

Whole transcriptome sequencing technology applied on prostate tumor samples had identified many genes whose expression were highly correlated with t-NEPC progression^{94, 99, 160}. These findings require experimental validation on whether these genes can drive NEPC progression; and furthermore, whether a driver gene could be used as potential therapeutic target for the disease. These molecular mechanistic studies require cell or xenograft models that have transcriptome, morphology, and cellular physiology similar to those of NEPC tumors in patients. Such NEPC models should also be easily manipulated so that gain- and loss-of-function approaches can be applied to dissect signal cascades regulated by the genes of interest. The latter requirement is

challenging for patient derived xenografts, patient organoids, and genetically engineered mouse models. Among *in vitro* NEPC cell models, the NCI-H660 line is relatively well characterized²²⁵⁻²²⁷. It is AR-negative, expresses high levels of neuroendocrine markers, and grows as suspending cell clusters, and has a morphology distinct from adherent luminal epithelial cells, such as LNCaP or PC3 cells. When grafted into immune compromised mice, the NCI-H660 line can form NEPC xenografts that progress rapidly⁹⁹. However, its slow growth rate *in vitro* and low efficacy to be transfected by plasmids or siRNA limit its applications. Several LNCaP-derived cell models were reported to acquire neuroendocrine phenotypes when treated with androgen depletion, IL-6 or cAMP^{170, 171}. However, it has not been established whether these phenotypical alterations are sustainable during prolonged treatments, and whether xenografts derived from these cells can be established, and whether or not they will show similar gene signatures to NEPC globally.

Our previous studies using whole transcriptome analyses of RNA-seq data from two independent patient cohorts^{99, 160} have identified an NEPC-specific splice signature¹¹⁴ that is predominantly regulated by the RNA splicing factor, SRRM4. We report that through generating neuronal-specific splice variants of target genes, SRRM4 can induce neuroendocrine phenotypes and neuronal-like cellular morphology in AdPC cells, and transform AdPC cells into NEPC xenografts. These findings suggest that exogenous expression of SRRM4 in adenocarcinoma cells such as LNCaP cells may enable the establishment of t-NEPC cell and xenograft models.

5.2 Results

5.2.1 RNA splicing and transcription profiles of LnNE P0 cells

Although exogenous SRRM4 can transform LNCaP cells into NEPC xenografts under androgen depletion conditions¹¹⁴, several questions remain to be answered: 1) whether LNCaP cells overexpressing SRRM4 have global RNA splicing features and transcriptomes similar to those of NEPC in patients; 2) whether the neuroendocrine phenotype is sustainable during prolonged castration treatment, and the transformed LNCaP cells can be developed into an NEPC cell and xenograft model with stabilized NEPC molecular profile and morphology; and 3) whether the AR expression and or AR signaling will be silenced, mimicking NEPC. To address these questions, we applied RNA sequencing to profile the whole genomic transcription in LNCaP cells overexpressing SRRM4 or SRRM4 plus TP53 knockdown¹¹⁴. These two cell lines showed very similar phenotypes to each other with 15.2% (908/5925) - 18.1% (1110/6127) genes differentially expressed at the mRNA level (Benjamini-Hochberg corrected FDR<0.01). The differentially expressed genes were not relevant to NEPC as demonstrated by Gene Set Enrichment Analysis (GSEA) using the Beltran 2016 data set (NES=1.10, FDR=0.39)⁹⁴. Since cells with TP53 depletion showed a faster tumor establishment rate, we therefore named the LNCaP cells with SRRM4 overexpression plus TP53 knockdown as LnNE P0 in the following experiments.

The LnNE P0 cells exhibited splicing profiles distinct from LNCaP cells, but similar to NEPC

tumor samples from the VPC cohort containing 6 AdPC, 5 NEPC and 1 AdPC with neuroendocrine differentiation samples¹¹⁴. There were 882 different splicing events from 606 genes between NEPC and AdPC samples (Benjamini-Hochberg corrected, FDR<0.01) within the VPC cohort. Based on these differentially expressed splicing isoforms, Spearman correlation and hierarchical clustering showed that LnNE P0 cells (n=3 repeats) were similar to NEPC tumors, while LNCaP cells (n=3 repeats) were clustered into the AdPC tumor group (Figure 5.1A). These results support our previous findings that the NEPC-specific RNA splicing signature is predominantly controlled by SRRM4.

There were 905 genes differentially expressed at the mRNA level (Benjamini-Hochberg corrected, FDR<0.01) between NEPC and AdPC samples from the VPC cohort¹¹⁴ and 364 genes differentially expressed (Benjamini-Hochberg corrected, FDR<0.01) in the Beltran cohort containing 34 AdPC and 15 NEPC samples⁹⁴. Based on these gene expressions, Spearman correlation and hierarchical clustering showed that both LnNE P0 and LNCaP cells were classified in the AdPC group. However, the transcriptome of LnNE P0 was more similar to the NEPC profile than those of other AdPC samples including the AdPC with neuroendocrine differentiation samples in both cohorts (Figure 5.1B-C). In contrast, the transcriptome of LNCaP cells was more distal to the NEPC profile. Since SRRM4 is an RNA splicing factor and the LnNE P0 splicing features are NEPC-like, these results together indicate that SRRM4 mediates RNA splicing

programs that drive the transformation of LNCaP transcriptome towards the NEPC transcriptome. Further GSEA assays showed that the top ranked genes upregulated in NEPC tumors from both VPC (NES=2.02, FDR<0.0001) and Beltran 2016 (NES=2.22, FDR<0.0001) cohorts were also significantly correlated with the expression profiles of the LnNE P0 cells (Figure 5.1D-E). Together these findings indicate that LnNE P0 cells possess an NEPC specific RNA splicing signature and confirms that SRRM4 drives LnNE transformation to NEPC.

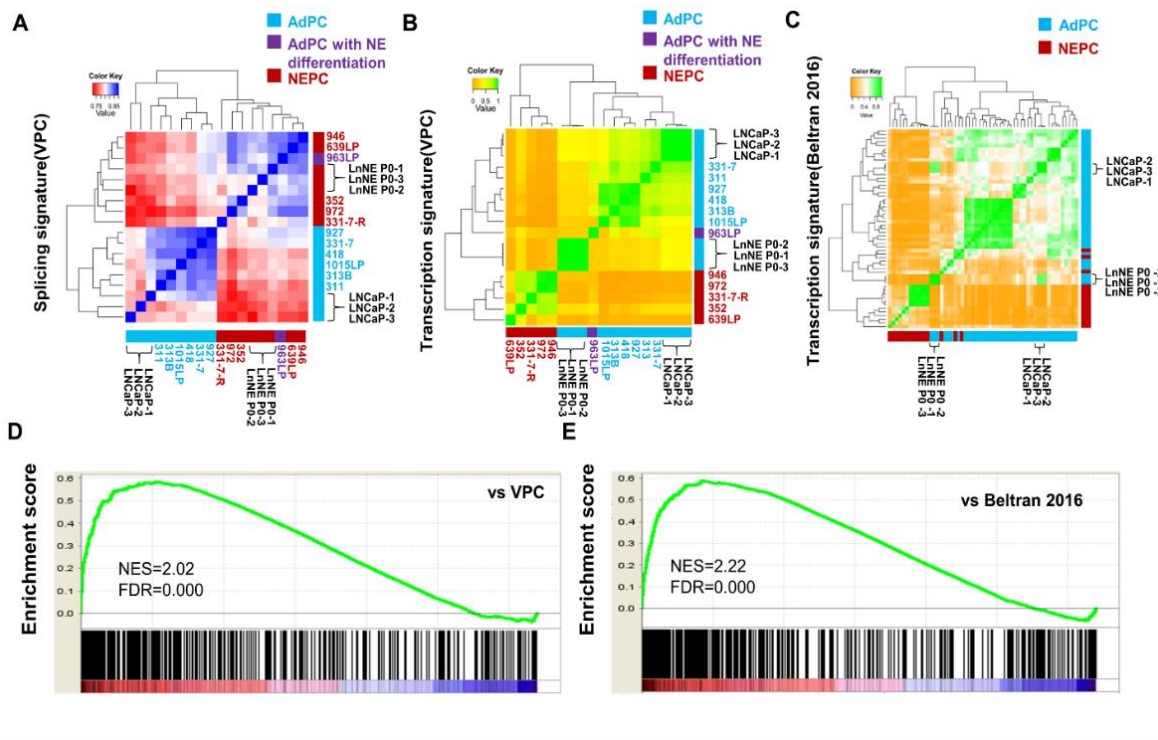


Figure 5.1 Comparison of RNA splicing and transcriptome of LnNE P0 cells with NEPC

(A-C) Total RNA of triplicated LNCaP and LnNE P0 samples were isolated and used for RNA-seq to measure AS events and transcription levels of each gene. RNA-seq data of LNCaP and LnNE P0 cells were analyzed combined with those of samples from VPC and Beltran 2016 cohorts.

(A) RNA-seq data from LNCaP and LnNE P0 cells were compared with NEPC-specific RNA AS events from the VPC cohort. Spearman correlation and hierarchical clustering using the pheatmap package in R showed the correlations of LnNE P0 splicing signature with that of NEPC patient samples splicing signature of LnNE P0 cells correlated with NEPC. (B-C) RNA-seq data from LNCaP and LnNE P0 cells were compared with NEPC specific transcripts from the VPC cohort (B) and Beltran 2016 cohort (C). Spearman correlation and hierarchical clustering showed that the LnNE P0 transcriptome was closer to those of the NEPC compared to those of parental LNCaP cells. (D-E) GSEA results showed the correlation of the LnNE P0 expression profiles with the top up regulated genes from (D) VPC cohort and (E) Beltran 2016 cohort.

5.2.2 NEPC progression of LnNE xenografts

To determine whether long-term androgen depletion can further promote NEPC progression of LnNE P0 xenografts, we inoculated LnNE P0 cells into castrated nude mice. Once the tumor volume reached 1000 mm³, xenografts were harvested. About 100mm³ tumor trunks were minced and re-inoculated into castrated mice to generate the next passage xenografts (Figure 5.2A). These experiments were repeated 5 cycles to obtain P1-P5 passages of LnNE tumors. The rest of the tissue samples from each passage were used for immunohistochemistry and primary culture to monitor cell morphology and neuroendocrine marker expression changes.

In the castrated mice where LNCaP xenografts do not form, the tumor take of LnNE P1 was 13 weeks but progressively reduced to 3.5 weeks at the P5 passage (Figure 5.2B). Tumor doubling times were also reduced from 3.3 weeks at P1 to 2.3 weeks at P5 (Figure 5.2C-D). In addition, serum SYP concentrations increased in correlation with the LnNE tumor volumes (Figure 5.2E). Immunohistochemistry showed that SYP was negative in the LNCaP xenografts from non-castrated mice, but became positive in LnNE P1 with increased intensity in LnNE P4 and P5 tumors (Figure 5.2F). The AR remained positive in all tumors. However, AR-negative cell population increased in LnNE P4 and P5 tumors. PSA expression was reduced starting in LnNE P1 tumors, but was totally abolished in LnNE P3-P5 tumors. These results indicate that LnNE xenografts are progressively transformed into NEPC under long-term androgen depletion.

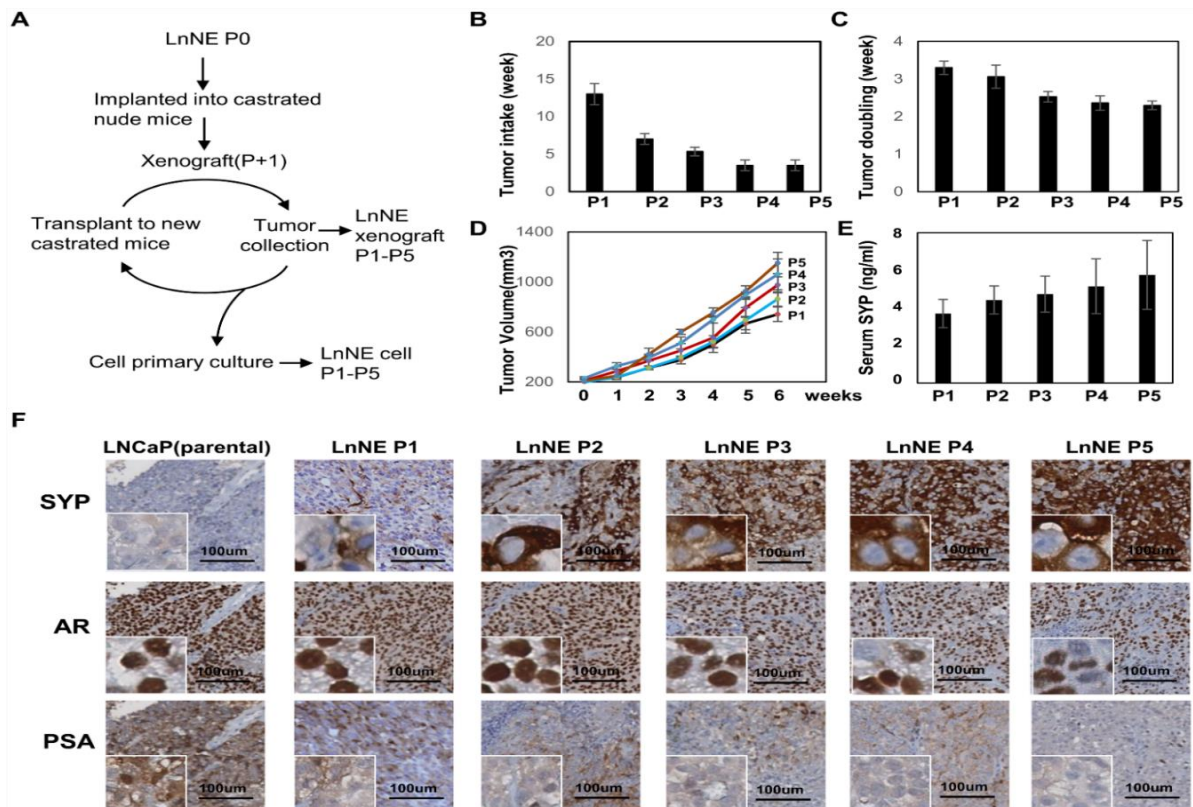


Figure 5.2 Establishment of LnNE neuroendocrine prostate cancer xenografts

(A) A schematic diagram showing the experimental procedure of P1 to P5 LnNE xenografts and primary cultured LnNE cells. LnNE xenografts were established as described in Material and Method. (B-D) Tumor take (B), tumor doubling time (average duration of tumor volumes that increase from 200 to 400 and from 400 to 800 mm³), and tumor growth curve (D) were measured. (E) Serum SYP concentration were measured 6 weeks after the tumor volumes reached 200mm³. (F) Immunohistochemistry detected SYP, AR and PSA on LNCaP, and LnNE P1-P5 xenografts. Scale bars = 100µm.

5.2.3 Morphology and neuroendocrine phenotypes of LnNE cells

LNCaP cells cultured in androgen depleted medium present with epithelial spear morphology with compact cell bodies and extended fine branches while growing as adherent monolayers (Figure 5.3A). In contrast, LnNE P1-P5 cells formed 3D multicellular spheroids even under the 2D culturing conditions. These cells strongly expressed multiple neuroendocrine makers at both mRNA and proteins levels, similar to those of the well characterized NEPC cell line, NCI-H660 (Figure 5.3B-C). It is worth mentioning that there were dramatic inductions of CHGB, SCG3 and NSE expressions between P2 and P3 cells, implying that from the P3 passage on, LnNE cell/xenografts models have developed full and sustainable neuroendocrine phenotypes. Additionally, PSA expression disappeared at the P2 stage, while AR expression was reduced and

kept in low levels in the LnNE P3-P5 passages, indicating that AR transcriptional activity was abolished and the AR expression could be sustained at low levels during NEPC progression. These findings resemble many clinical NEPC tumors that show both AR and neuroendocrine marker positivity.

DHT treatment to P1 and P2 cells resulted in destruction of multicellular spheroid formation (Figure 5.3D). Cells became adherent to the surface of culturing dish and grew as monolayers similar to LNCaP cells. However, the morphology of LnNE P3, P4, and P5 cells remained in spheroids even in the presence of DHT. Our previous studies reported that the neuroendocrine phenotype of LnNE P0 cells could be reversed when treated with androgens. In this study, we report that cells from early LnNE passages were still responsive to DHT, resulting in the upregulation of AR, PSA and E-Cad protein levels, but downregulation of CHGB, SCG3, and NSE expressions (Figure 5.3E). Once reached to the P5 stage, however, LnNE cells became indifferent to DHT treatment with regard to morphology and biomarker expressions. In summary, we observed NEPC progression of the LnNE model from P0 to P5 under the prolonged castration condition, with the AR signaling diminishing at the P2 stage, neuroendocrine phenotypes fully developed at the P3 stage, and morphology and AdPC/neuroendocrine marker expressions being stabilized at the AR-indifferent P5 stage.

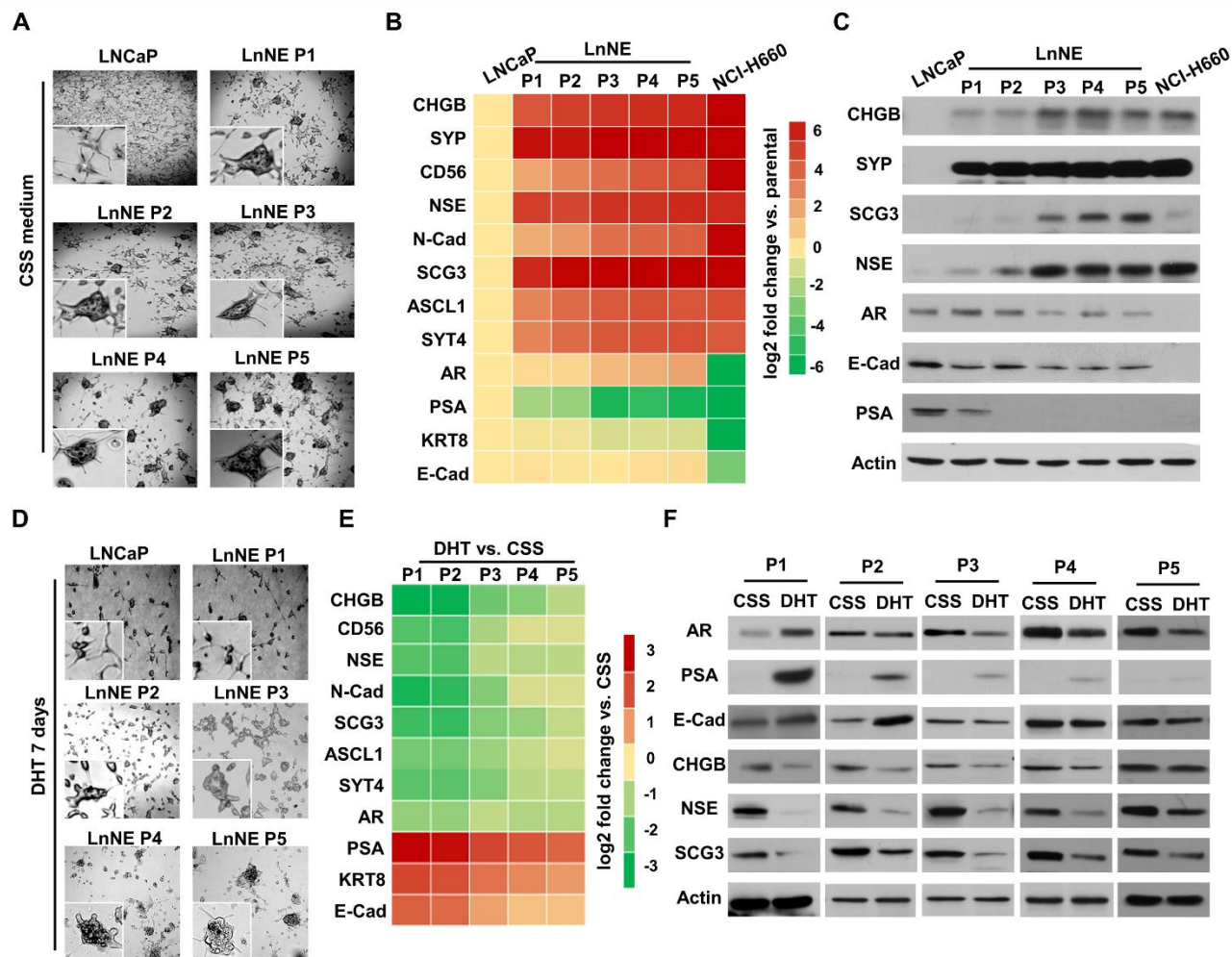


Figure 5.3 LncNE cell morphology and neuroendocrine phenotypes

(A-C) LNCaP and LnNE cell series P1 to P5 were cultured in the RPMI1640 medium containing 10% CSS and NCI-H660 cells were cultured in the HITES medium, as described in the Materials and Methods section, for 2 weeks. (A) Cell morphology changes were examined by the Zeiss fluorescent microscope. (B-C) Total RNA and protein lysates were collected and used to measure the expressions of neuroendocrine and AdPC biomarkers by real-time qPCR (B) and immunoblotting (C). (D-F) LnNE cell series were cultured in the medium containing 10% CSS for 2 weeks followed by vehicle or 10nM DHT treatment for another week. (D) Images of spheroid

morphology were captured by the Zeiss fluorescent microscope. (E) Whole cell RNA and protein were collected and used to measure expressions of neuroendocrine and AdPC biomarkers by real-time qPCR (E) and immunoblotting (F). AR, PSA and NE biomarkers change became insensitive to DHT treatment from LnNE P1 to P5.

5.2.4 Cell proliferation rate and transfection efficacy of LnNE cells

Using BrDU incorporation assays, LnNE cells cultured in androgen depletion medium have a proliferation rate 2-3-fold higher than NCHI-H660 cells (Figure 5.4A). Importantly, the proliferation rate of LnNE cells increased with passage numbers, indicating that the LnNE cells have adapted androgen depletion conditions and gradually gained proliferative abilities in addition to stabilized NEPC biomarker expressions. These observations suggest the concurrence of transdifferentiation and accelerated proliferation during LnNE P0 to P5 progression. Moreover, when transfected with the GFP expression vector by lipofectamine 3000, the transfection efficacy was ~50-70% in LnNE P5 cells, but <2% in HCl-N660 cells (Figure 5.4B). We also transfected plasmid DNA encoding REST in LnNE P5 cells, resulting in ~3,500-fold induction of REST mRNA levels and ~4-164-fold reduction of mRNA levels of neuroendocrine markers (Figure 5.4C). In addition, LnNE P5 cells can be transfected with the siRNA oligo, resulting in 56% depletion of SRRM4 mRNA and 1.8-9.5-fold reduction of mRNA levels of neuroendocrine markers (Figure 5.4D). These results indicate that LnNE cells have a relatively high proliferation

rate *in vitro* and can be transfected with plasmid DNA and siRNA to manipulate gene expression.

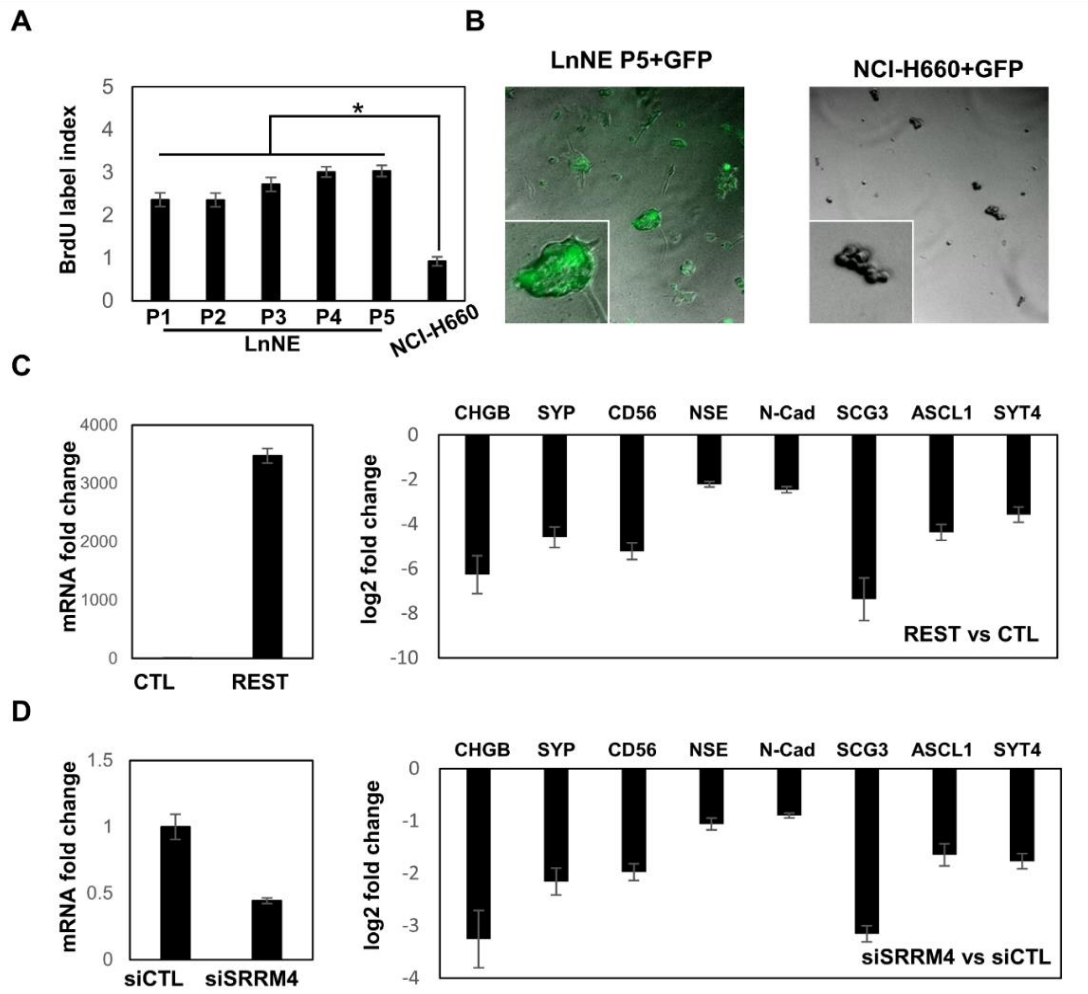


Figure 5.4 LnNE cell proliferation and transfection efficacy

(A) BrdU incorporation assays were performed on LnNE P1 to P5 cells and NCI-H660 cells. BrdU incorporation rates were calculated as described in the materials and methods. (B) LnNE P5 and NCI-H660 cells were transfected with GFP expression vectors. Fluorescence images were captured by the Zeiss fluorescent microscopes 24 hours after transfection to measure transfection efficiency. (C-D) LnNE P5 cells were transfected with (C) REST expression vector or (D) control or siRNA against SRRM4. Total RNA were collected and used to measure NEPC biomarkers

expression by real-time qPCR.

5.2.5 In vitro LnNE spheroids for drug screening

NCI-H660 cells proliferate extremely slowly in *in vitro* culture conditions, but grow rapidly as tumors in mice, implying that NEPC cells favor 3D culture conditions. This is consistent with our observation that the LnNE cells formed spheroids even under the 2D culturing conditions (Figure 5.3). We applied the GravityPLUS Hanging Drop system (InSphero, Brunswick, USA) in a 96-well format to allow LnNE cell growth in 3D conditions (Figure 5.5A). LnNE P5 cells form a single spheroid per well in ~5 days, and the spheroids retained their morphology on flat-bottom 96-well plates for up to 7 days, during which the spheroid proliferation rate can be measured by the spheroid size as well as by BrDU incorporation assays (Figure 5.5B). Additionally, the spheroids can also be collected and paraffin embedded to perform immunohistochemistry (Figure 5.5C). We showed that LnNE P5 spheroids expressed high levels of SYP and AR but no PSA, consistent with the expression profiles of LnNE xenografts, as shown in figure 5.2. These results indicate that multiple LnNE spheroids can be established in 96 well plates simultaneously to allow high throughput screening assays to identify potential small molecules that may inhibit NEPC cell proliferation or modulate NEPC cell morphology.

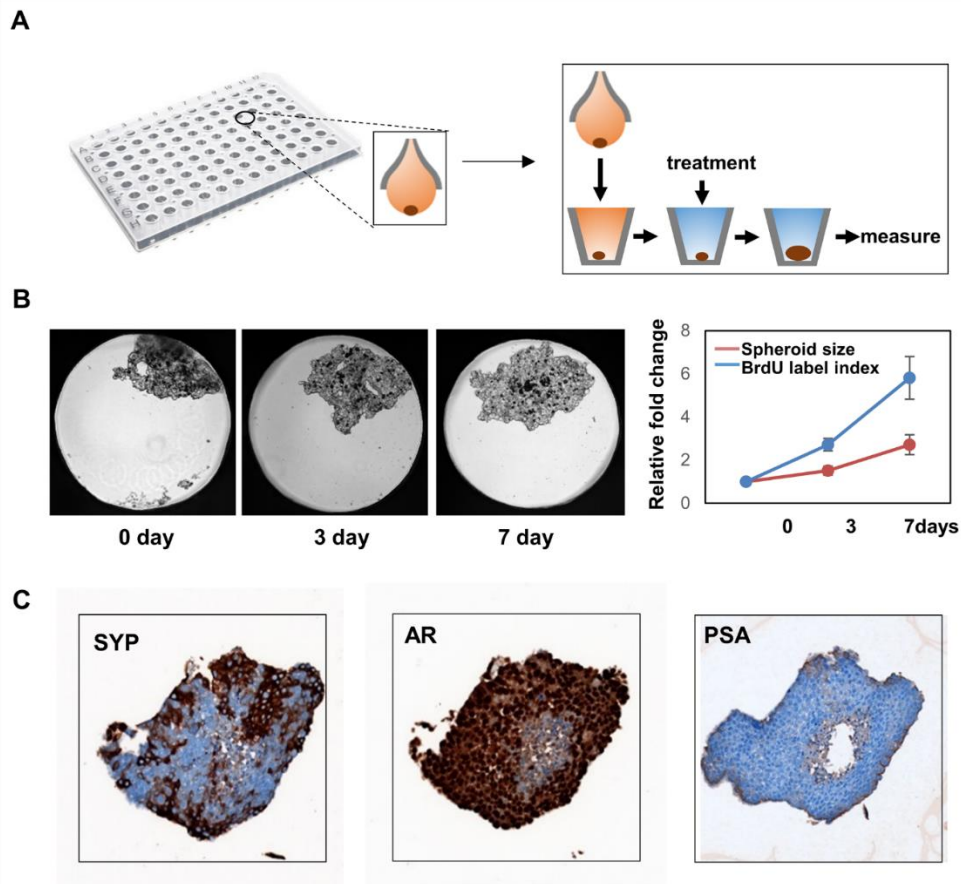


Figure 5.5 3D culture of LnNE cells

(A) LnNE P5 cells were cultured to form 3-D multicellular spheroids as described in the Materials and Methods section. (B) Time-lapse images of spheroids were shown. Relative spheroid sizes and BrDU incorporation rates were measured at indicated time points. (C) Spheroids were collected and paraffin embedded. Immunohistochemistry was performed using indicated antibodies.

5.3 Discussion

In this study we demonstrate that the LnNE can form multicellular spheroids under 2D or 3D culture conditions *in vitro*, as well as xenografts *in vivo*. LnNE has global transcription and RNA

splicing signatures similar to those of NEPC tumors. LnNE tumors are castrate-resistant, and aggressively growing in nude mice. Although the AR protein expression remains, its transcription activity is deactivated, and the neuroendocrine phenotype of LnNE cells cannot be reversed by androgen re-administration. We report that LnNE cells are relatively highly proliferative, easy to be transfected, and are suitable for performing high throughput screening assays.

The LnNE model is generated by introducing exogenous SRRM4 in adenocarcinoma cells. We have previously shown that SRRM4 can confer neuroendocrine phenotypes to AdPC cells through compromising the function of genes such as REST and FOXA1^{114,228}. Other SRRM4 target genes, such as PTPRF and PTK2, have known functionality in regulating cell proliferation or apoptosis¹¹⁴, suggesting that these genes may enable cancer cells to gain growth and survival advantages under chemo- or hormonal therapies. It should also be noted that several SRRM4 target genes are histone acetyltransferases or de-methyltransferases (e.g. MEAF6 and BHC80), which may promote NEPC progression through epigenetic mechanisms²²⁹. Therefore, generation of the LnNE model suggests that NEPC can evolve directly from AdPC under the control of SRRM4. Through regulating RNA splicing and epigenetic mechanisms, SRRM4 induces two cellular processes, including neuroendocrine differentiation and accelerated proliferation, which collaboratively contribute to NEPC establishment. In addition, the phenotypical transitions of LnNE P0 to P5 support the idea that NEPC progression is a gradual and chronic process. Neuroendocrine

differentiation of cancer cells is initially transient and reversible, but becomes permanent, possibly by NEPC-specific factors that promote cell proliferation. It is likely that multiple cycles of differentiation and proliferation are required for establishing NEPC.

SRRM4 strongly induces multiple neuroendocrine markers, among which SYP, CD56, and chromogranins are commonly used for NEPC diagnosis by pathologists. However, a challenge in early NEPC detection is intra-tumoral heterogeneity, as NEPC tumors do not show universal neuroendocrine marker profiles. Our results suggest that SRRM4 may be a more reliable diagnostic marker for NEPC than those previously reported because the immunohistochemistry of the tissue microarray showed that SRRM4 has a higher negatively predictive value in ruling out NEPC tumors, and SRRM4 positivity has higher sensitivity than CD56, SYP, and CHGA individually to NEPC (Chapter 3).

The LnNE model also accepts TP53 depletion, raising the question of whether loss-of-function of TP53 contributes to NEPC progression through either its canonical pathways that regulate cell cycling and apoptosis²³⁰, or through promoting cell lineage plasticity, mediated by Sox2 or Sox11^{100, 101, 231}. Inactivation of TP53 was more frequent in NEPC (67%) when compared to AdPC (31.4-53.3%)^{94, 232, 233}. It is worth mentioning that the upregulation of basal and NE markers in the presence of anti-androgens only occurred when both TP53 and Rb1 were depleted. This is

consistent with our previous results that showed no significant increase of neuroendocrine markers with TP53 inactivation alone¹¹⁴. Our GSEA analyses did not show further enhancement of NEPC gene signatures when TP53 depletion was added to SRRM4 overexpression. In fact, our LnNE model has the RB1 gene intact, and very low Sox2 and Sox11 mRNA levels. Since TP53 depletion enhances cell proliferation and colony formation of LNCaP cells overexpressing SRRM4¹¹⁴, we propose that the loss-of-function of TP53 in the context of SRRM4 overexpression contributes to NEPC progression through enhancing cell proliferation.

The LnNE model preserves AR protein levels, but becomes PSA-negative, supporting the notion that reduced AR function is concurrent with NEPC progression. It has been shown that AR protein expression can be detected by immunohistochemistry in NEPC, but the mRNA levels of AR target genes are significantly reduced⁹⁴. In three independent reports, 27% (6/22), 38% (23/61) and 47% (7/15) of small cell neuroendocrine prostate tumors are AR protein positive, as detected by immunohistochemistry^{234, 235}. These tumors can also express AR target genes, including PSA and NKX3.1. It is therefore reasonable to speculate that other types of NEPC adenocarcinoma with neuroendocrine differentiation may have even higher rates of AR positivity. These findings collectively suggest that the remaining AR expression, along with reduced/abrogated AR functions, may be a common pathological characteristic in tumors with ongoing NEPC progression, or in subsets of NEPC tumors. We also observed that our LnNE model gradually

reduced AR signaling as well as AR-positive cell numbers during P0 to P5 xenograft passaging. It is therefore important to continue to monitor AR expression and function, as this model is grafted onto castrated mice for higher passages.

In summary, we present an NEPC cell/xenograft model that has similar molecular and pathological features to those of NEPC tumors from patient samples. This model could be a useful research tool to study this disease.

5.3.1 Mechanism of NEPC progression

LnNE cells show higher proliferative rates than LNCaP and NHT-660 cell lines, which is consistent with the fact that t-NEPC is highly aggressive and proliferative. The proliferative phenotype is possibly driven by several mechanisms. One possible reason is loss function of TP53/RB1, which leads to an increase of cell cycle and decrease of apoptosis through their canonical pathways. Increased neural peptides, which are synthesized and released by LnNE cells, may also promote PCa cell proliferation. It has been reported that the NE marker ASCL1 can promote cell cycle and neuronal differentiation when expressed in neural progenitor cells²³⁶. The effect of secreted neural peptide on PCa cells still needs to be determined.

A recently research has found that SRRM4-induced exon inclusion can change protein structure and thereby protein-protein interaction in neurogenesis²³⁷. Interestingly, as mentioned in Chapter 4, several genes regulated by SRRM4 are associated with biological processes, including histone modifying, intracellular signaling transduction, protein phosphorylation, and transcription regulation. AS of these genes may affect cell proliferation and apoptosis either through their canonical pathways, or may lead to novel functions caused by structure reprogramming. In the next Chapter, we will study the detailed mechanisms through which AS of SRRM4-targeted genes regulate NEPC progression.

Chapter 6: RNA Splicing of the BHC80 Gene Facilitates Neuroendocrine Prostate Cancer

Progression

6.1 Introduction

Although NEPC is rare as a primary subtype of PCa, it is becoming more prevalent as androgen receptor “quiescent” CRPC, emerging under the selective pressures of more potent ARPI^{83, 84}. However, even after potent ARPI treatment, about 25% of patients harbour NEPC foci at death⁸⁵, implying that certain CRPC tumors are capable of attaining a proliferative NEPC state. Once t-NEPC is diagnosed, patient survival is less than one year²³⁸. A major obstacle in controlling t-NEPC is the lack of understanding of the molecular underpinnings of t-NEPC.

T-NEPC is most likely derived from AdPC through complicated NE differentiation, proliferation, and tumorigenesis processes. Whole-exome sequencing has revealed that t-NEPC and AdPC have similar genomic landscapes⁹⁴, even though they differ significantly in gene expression and cell morphology^{93, 94, 104}. Case studies showed that cell populations of AdPC, AdPC with neuroendocrine differentiation, and t-NEPC co-existed in the same tumors²³⁹. Intermediate morphological and phenotypical transitions in cancer cells between the boundaries of AdPC and NEPC cell populations indicated dynamic neuroendocrine differentiation processes²³⁹. AdPC transformation into t-NEPC is replicable in PDXs, when only castration surgery was performed on the host mice¹⁰⁴. Loss-of-function of TP53, Rb1, and/or PTEN was shown to confer AdPC cells

lineage plasticity under ARPI treatments^{100, 101, 105}. These cancer cells utilize Sox2, EZH2, and Sox11 to epigenetically re-program the AdPC transcriptome and adapt into neuroendocrine lineage. We show that AdPC cells can be transformed into t-NEPC xenografts when a neural RNA splicing factor SRRM4 is introduced exogenously²⁴⁰. Collectively, these results support that t-NEPC originates from AdPC.

AdPC progression to t-NEPC requires not only NE differentiation, but also proliferation. AdPC cells can undergo NE differentiation induced by loss-of-function of the AR, REST, and FoxA1^{104, 169, 240}, or by treatments of cAMP, IL-6, androgen depletion, or hypoxia *in vitro*^{167, 170-174}. However, not all of these protein factors and treatments enable t-NEPC formation. While AR blockade is necessary for t-NEPC establishment, it is insufficient because only ~25% of hormone therapy-treated tumors transform into t-NEPC⁸⁵. Most AR-positive AdPC xenografts (*e.g.*, LNCaP, LAPC4) do not progress to t-NEPC as a result of castration. Cory Abate-Shen et al. reported that in TP53/PTEN knockout mice treated with castration surgery, NE-like cells from focal NE differentiation regions are non-proliferative, in striking contrast to NE-like cells within overt NE differentiation regions that are highly proliferative¹⁰⁵, suggesting a “proliferative switch” represented by a key molecular event of t-NEPC emergence. Several genes such as AURKA, PEG10, MEAF6, and Cyclin D1 have also been implicated in t-NEPC development¹⁸¹⁻¹⁸⁴. However, instead of inducing NE differentiation of AdPC cells, these genes regulate cell

proliferation, invasion, and tumor growth. These results support the idea that AdPC cells with NE differentiation have to be switched into a highly proliferative stage in order to develop into t-NEPC.

AdPC and t-NEPC share similar genomic features but differ dramatically in transcriptomes, suggesting that RNA splicing and epigenetic mechanisms are responsible for t-NEPC development. Through analyzing RNA-seq data from two independent NEPC cohorts^{99, 104}, we report a t-NEPC specific RNA splicing signature from 24 genes²⁴⁰. BHC80 is the only gene that regulates histone methylation and gene transcription²⁴¹. BHC80 was originally found as a component of histone modification complexes where it antagonized the actions of LSD1, CoREST, and HDACs in de-methylating H3K4 to de-repress gene transcription. It is expressed mainly as two isoforms, BHC80-1, and BHC80-2, whereby an alternative exon 14a replaces exon 14 in BHC80-2 (GRCh38/hg38)²⁴². This splicing event disrupts one of the two predicted nuclear localization signals (NLSs), potentially leading to increased cytoplasmic localization. In this study, we report that BHC80-2 is highly expressed in t-NEPC and exerts non-epigenetic activities in stimulating the MyD88-p38-TTP axis to enhance multiple tumor-promoting cytokines during t-NEPC progression.

6.2 Results

6.2.1 RNA splicing of BHC80-2 is upregulated in t-NEPC

RNA-seq data from both the VPC12 and Beltran cohorts indicated that BHC80-2 is dramatically upregulated in t-NEPC, while BHC80-1 remains at similar levels between AdPC and t-NEPC (Figure 6.1A-B).

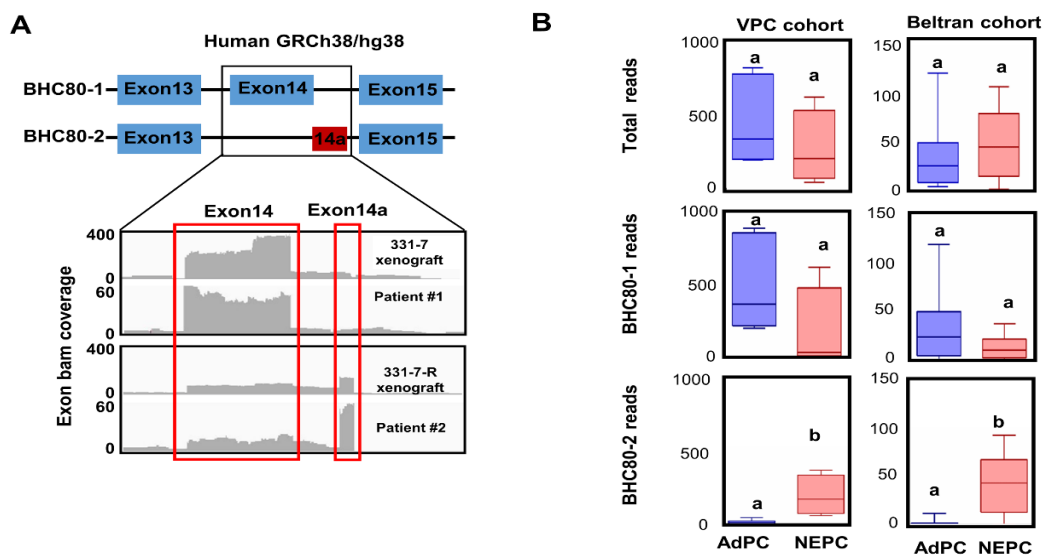


Figure 6.1 Expression of BHC80-2 splice variant is upregulated in NEPC

(A-B) RNA-seq data of PDXs and patients in the VPC and Beltran cohorts were analyzed. (A) Increased inclusion of the alternatively spliced exon14a in both NEPC patient tissues and NEPC PDXs was identified by RNA-seq. (B) Comparison of overall gene reads, reads of BHC80-1 and BHC80-2 splice variants between NEPC and AdPC tumors from both VPC and Beltran cohorts. Values without a common letter are significantly different, $p < 0.05$

To confirm these RNA-seq data, we have also constructed a tissue microarray with CRPC tumor biopsies from an independent patient cohort and have applied RNA *in situ* hybridization (RISH) assays to study BHC80 splicing variants' expression in t-NEPC tissues. The specificity of the BHC80-1 and -2 probes had been validated in multiple control tissue slides (Figure 6.2).

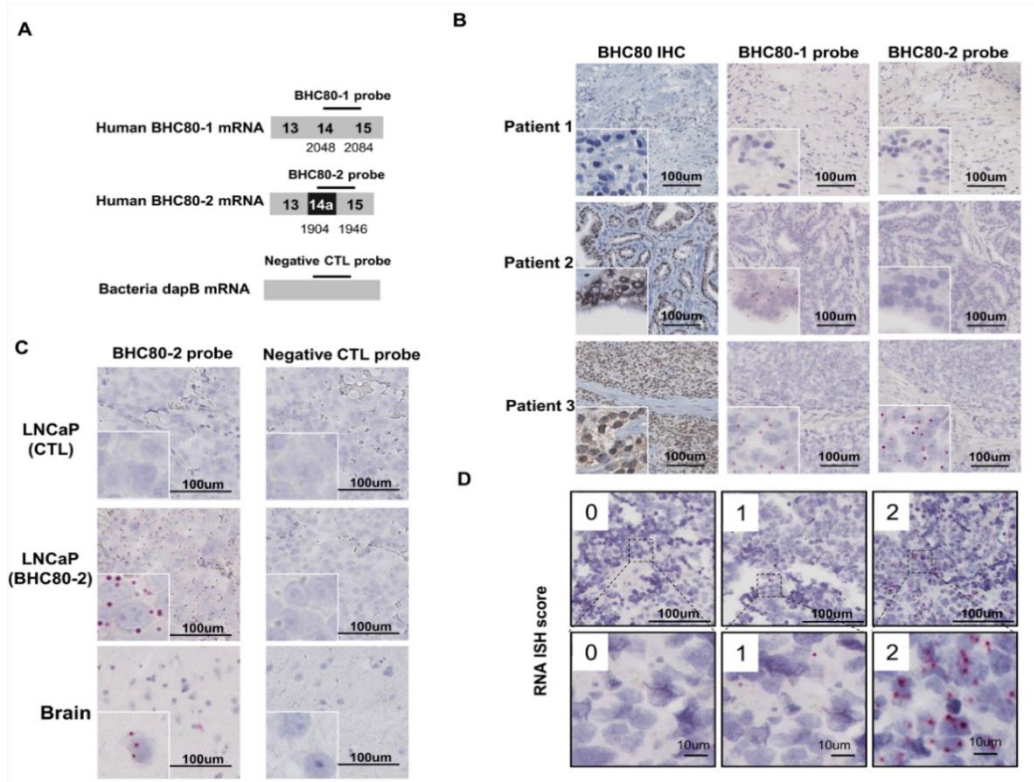


Figure 6.2 Validation of BHC80-1 and BHC80-2 probes

(A) A schematic diagram shows alternative RNA splicing of the BHC80 gene and the locations of BHC80-1(NM_001101802.1) and BHC80-2(NM_016621.3) RISH probes. (B) BHC80-1 and BHC80-2 RISH assays and IHC assays using anti-BHC80 antibody were performed on three different patient tissue. (C) RISH assays using control and BHC80-2 probes were performed on LNCaP(CTL), LNCaP(BHC80-2) xenografts and brain tissue. (D) Representative images of RISH

assays of BHC80-2 with different RISH scores.

RISH results confirm that BHC80-2 is strongly expressed in two groups of t-NEPC (SCNC and AdNE), but weakly expressed in AdPC (Figure 6.3A-B). In contrast, BHC80-1 levels showed no difference among all three tumor groups. Furthermore, the BHC80-2, but not the BHC80-1 RISH signal, was highly correlated with not only the number of NE markers (Pearson correlation $r=0.819$; $p<0.0001$), but also the IHC scores of CHGA, SYP, and CD56 (Pearson correlation $r=0.822$, 0.828 , and 0.699 respectively; $p<0.0001$) (Figure 6.3C-D). It was positively associated with Ki67 index, but negatively correlated with AdPC markers such as AR and PSA. Together, both RNA-seq and RISH results from three independent patient cohorts concluded that RNA splicing of BHC80-2 is upregulated in t-NEPC, while BHC80-1 expression remains the same in AdPC and t-NEPC.

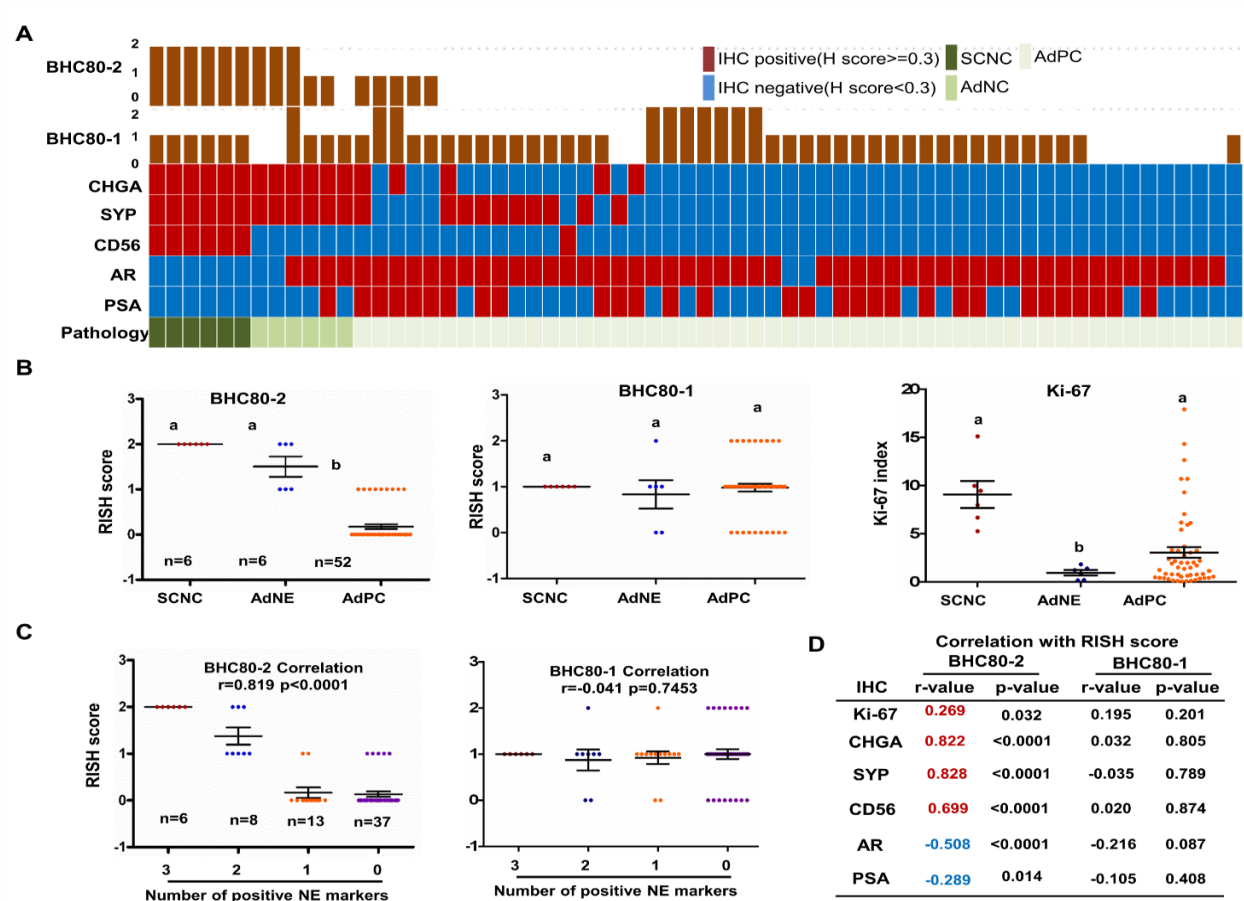


Figure 6.3 Expression of BHC80-2 splice variant is correlated with t-NEPC progression

(A) BHC80-1 and BHC80-2 RISH assays and IHC assays using CHGA, SYP, CD56, AR, PSA, and Ki-67 antibodies were performed on castrate-resistant prostate cancer TMA. RISH scores of BHC80-1 and BHC80-2, as well as tumor histology, were evaluated as described in the Materials and Methods section. Each column represents one of the 64 tissue cores from 32 patients. (B) CRPC tissue cores were grouped into SCNC, AdNE, and AdPC, according to their histology. Distribution of BHC80-1 and BHC80-2 RISH scores, as well as the Ki-67 index in each tumor group are plotted. (C) Scatterplots show BHC80-2 RISH scores in association with the numbers of positive NE markers. BHC80-2 correlation with NE marker numbers were calculated by

Pearson's Chi-square test. (D) BHC80-2 expression in correlation with CHGA, SYP, CD56, AR, and PSA IHC scores and Ki-67 indexes was calculated using Pearson's Chi-square test.

6.2.2 SRRM4 regulates RNA splicing of BHC80-2

Because the RNA splicing factor SRRM4 had been demonstrated to be a driver of t-NEPC, we hypothesize that SRRM4 regulates BHC80-2 RNA splicing. Using RISH assays on the CRPC TMA, we first showed that BHC80-2 and SRRM4 are both highly expressed in SCNC and AdNC, but weakly in AdPC. Their levels are highly correlated (Pearson correlation $r=0.856$; $p<0.0001$) (Figure 6.4A). We have transduced LNCaP adenocarcinoma cells with SRRM4 to generate the LnNE tumor models that show aggressive growth with classic NEPC transcriptomes and phenotypes mimicking patient t-NEPC27. BHC80-2 is negative in parental LNCaP xenografts, but dramatically upregulated in the LnNE tumors (Figure 6.4B). The mRNA levels of BHC80-1 is abundantly expressed in all AdPC and NEPC cell lines, however, BHC80-2 is only expressed in SRRM4-positive VCaP and H660 cell lines (Figure 6.4C). These results from patient tumors, xenograft and cell models confirmed SRRM4 expression correlated with BHC80-2 RNA splicing.

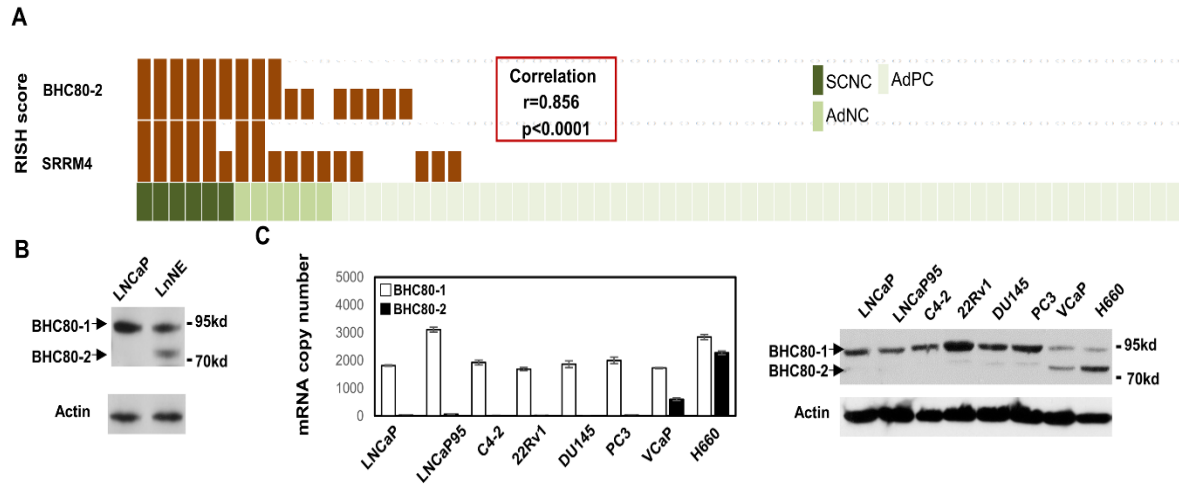


Figure 6.4 SRRM4 expression is correlated with alternative splicing of the BHC80 in PCa cells

(A) BHC80-2 and SRRM4 RISH assays were performed on castrate-resistant prostate cancer TMA. Each column represents one of the 64 tissue cores from 32 patients. BHC80-2 RISH scores, in correlation with SRRM4 RISH scores, were calculated by Pearson's Chi-square test. (B) Total protein of LNCaP and LnNE cell lines were collected and used to measure BHC80-1 and BHC80-2 protein expression by immunoblotting. (C) Multiple PCa cell lines were used to measure BHC80-1, BHC80-2 and SRRM4 expression in both protein and mRNA levels by immunoblotting and real-time PCR assays.

To confirm that SRRM4 directly regulates BHC80-2 splicing, we constructed a BHC80 minigene reporter in which exons 14 and 14a and their flanking ~300bp nucleotides were inserted between exons 13 and 15 (Figure 6.5A), and transfected this minigene into LNCaP and 293T cells. SRRM4

upregulated BHC80-2, but downregulated BHC80-1 mRNA derived from the minigene reporter (Figure 6.5B). Interestingly, U2AF65 stimulates, while PTB inhibits, BHC80-2 splicing, indicating that other splicing factors also participate in BHC80 RNA splicing. However, SRRM4 is a neural-specific splicing factor that also regulates PTB RNA splicing and functions, leading us to focus on SRRM4-mediated BHC80-2 RNA splicing. RNA chromatin immunoprecipitation (RNA-ChIP) showed that SRRM4 was recruited to the region next to the 3' splice site of BHC80 intron 14 (designated as region P1), but not the control region (designated P2) (Figure 6.5C-D). The UGC motif was predicted to be a consensus SRRM4 recognition site and our RNA-pulldown assays confirmed that purified SRRM4 protein from LNCaP cells interacted directly with the wild type, but not the mutant UGC motif from intron 14 of the BHC80 gene (Figure 6.5E). Furthermore, site-directed mutagenesis (UGC to UAC) of the UGC motif within the BHC80 minigene showed that failure of SRRM4-mediated exon 14a inclusion (Figure 6.5F). These results together confirm that SRRM4 directly regulates BHC80-2 RNA splicing in PCa cells.

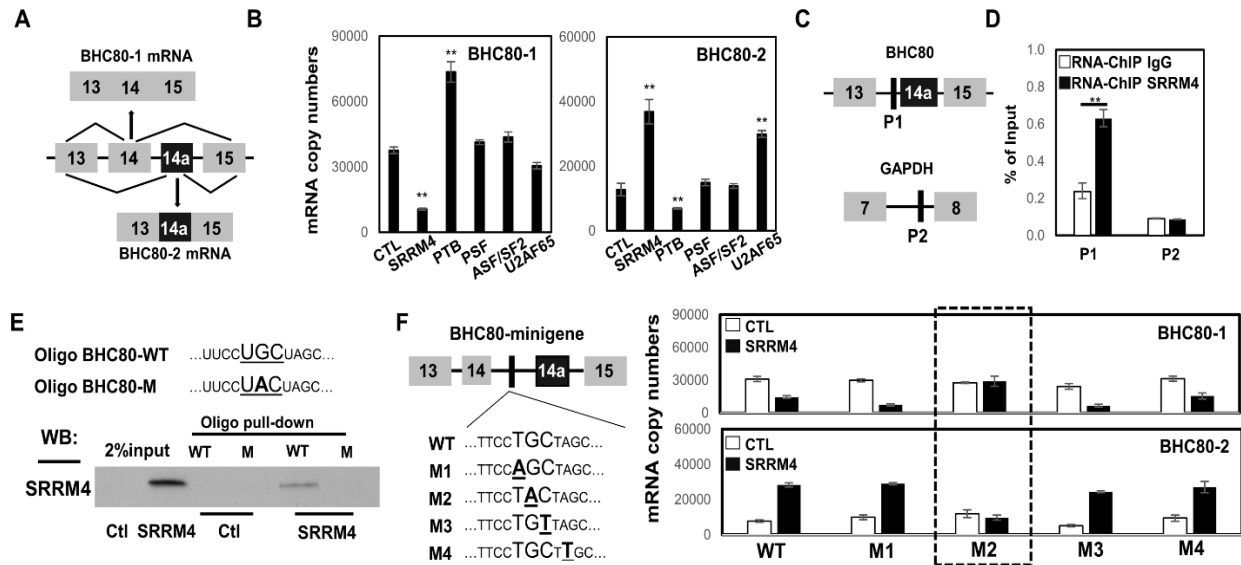


Figure 6.5 SRRM4 regulates alternative splicing of the BHC80 in PCa cells

(A) A schematic diagram shows the BHC80 minigene reporter and the splice variants derived from the minigene. (B) The BHC80-minigene reporter was co-transfected with plasmids encoding indicated splicing factors into LNCaP cells. Total RNA was extracted to measure BHC80-1 and BHC80-2 mRNA levels by real-time qPCR. (C) A schematic diagram of the P1 and P2 regions used in RNA-ChIP assays. (D) LNCaP cells were transfected with the Flag-SRRM4 plasmid. RNA-ChIP assays were performed using control or Flag antibody. Eluted RNA fragments were used as templates for real-time qPCR. Signals were calculated as percentage of input. (E) Flag-SRRM4 was purified from LNCaP cells to perform RNA pulldown assays. Oligo associated proteins were detected by immunoblotting. (F) LNCaP cells were transfected with control, BHC80-minigene or BHC80-minigene with M1-M4 mutations in the presence of +/-SRRM4. Total RNA was collected and used to measure BHC80-1 and BHC80-2 mRNA levels by real-time

qPCR. All results were derived from three independent experiments that were performed in triplicate. Data were presented as the mean \pm S.D. **, $p < 0.01$ compared with controls.

6.2.3 BHC80-2 promotes PCa cell growth and tumor progression

Because BHC80-2 is barely expressed in AdPC and strongly expressed during t-NEPC progression, we introduced Flag-tagged BHC80-2 and BHC80-1 into LNCaP, PC3, and TRAMP-C1 AdPC cell models by lentivirus to study BHC80-2 functions. RNAi of BHC80-2 was not performed because depletion of BHC80-2 does not follow t-NEPC progression and the exon 14a, unique to BHC80-2, is only 24bp in length. Neither BHC80 isoforms altered AR signaling, nor induced NE markers and neuronal morphologies (Figure 6.6).

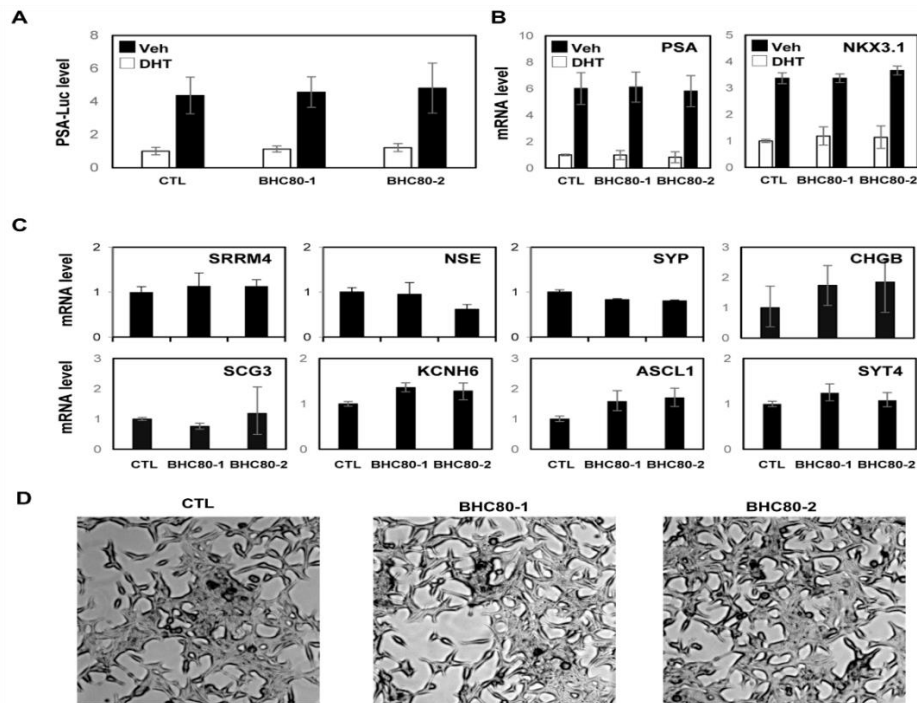


Figure 6.6 BHC80-2 does not confer LNCaP cell NEPC phenotype

(A) LNCaP cells were transfected with control, BHC80-1 or BHC80-2 expression vectors together with PSA-luciferase and renilla reporters. Cells were then treated with vehicle or 10nM of DHT for 24h. Luciferase activities were measured. (B-C) Total RNA was also collected for real-time PCR assays to measure the expression of PSA and Nkx3.1 in (B) and different NE markers in (C). (D) Morphology of LNCaP(CTL), LNCaP(BHC80-1) and LNCaP(BHC80-2) cells were captured by microscopy.

However, BHC80-2, but not BHC80-1, stimulated cell proliferation, migration, invasion, and colony formation independent of androgens (Figure 6.7A-D). BHC80-2-transduced LNCaP xenografts progressed more rapidly to CRPC stage, as demonstrated by tumor volumes and serum PSA levels (Figure 6.7E). BHC80-2 also stimulates TRAMP-C1 xenograft growth (Figure 6.7F). These results indicate that gain-of-function of BHC80-2 in PCa cells stimulates cell growth and xenograft progression independent of androgens.

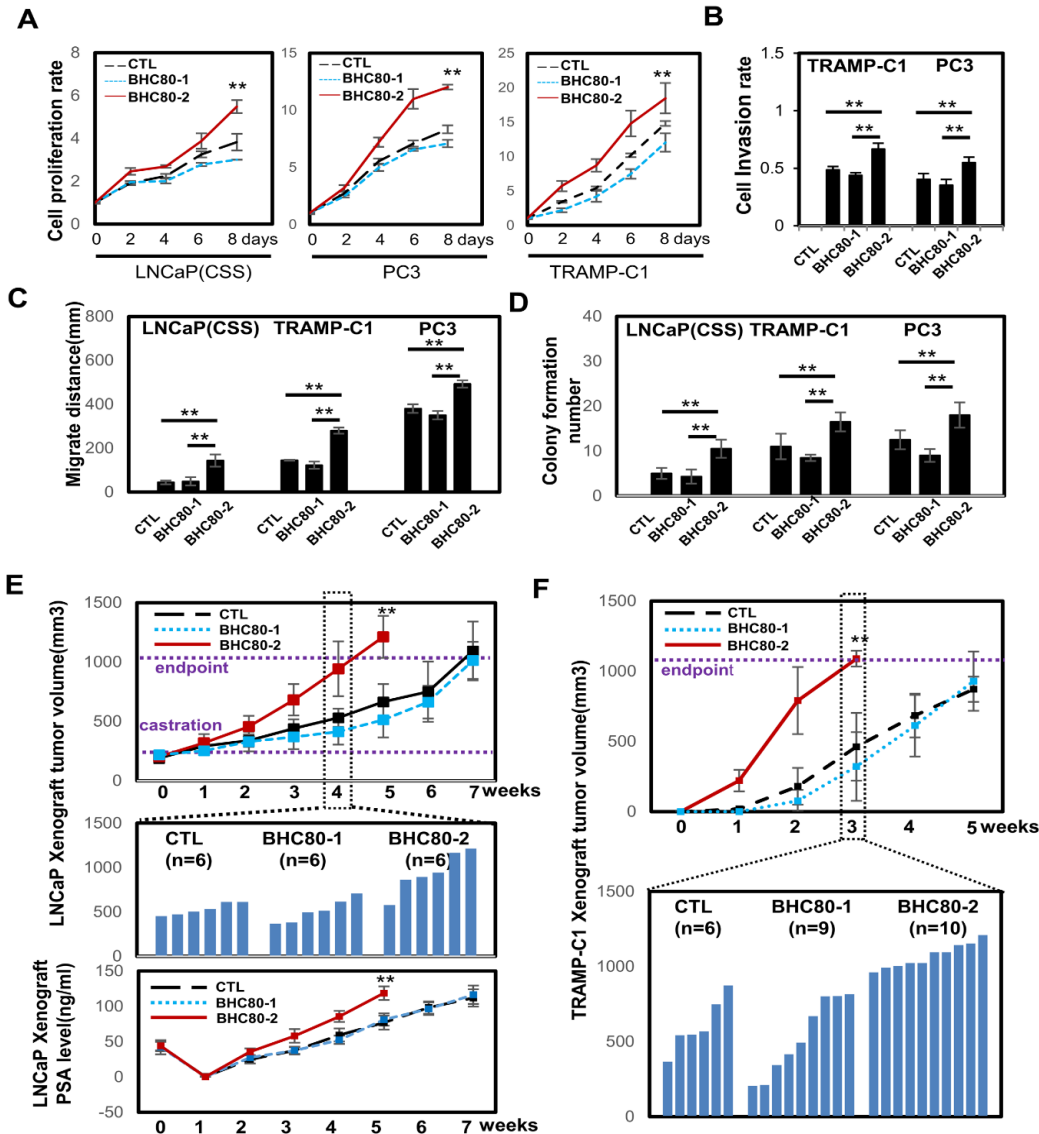


Figure 6.7 BHC80-2 increases PCa proliferation, invasion, and xenograft growth

(A-D) LNCaP, PC3 and TRAMP-C1 cell lines were stably introduced control, BHC80-1 and BHC80-2 by lentivirus. (A) Cell proliferation rate was measured by MTS assay and presented as relative fold change to day 0. (B) Cell invasion ability of PC3 and TRAMP cell lines was measured by using the Matrigel Invasion Chambers. (C) Wound healing assays measured PC3 and TRAMP-C1 cell migration rate within 16 hours and LNCaP cell migration rate within 24 hours. (D) Colony

formation assays were performed on cell lines as indicated. Colonies were stained with crystal violet and colony numbers were counted. All results are presented as the mean \pm S.D. (n = 3; **, p < 0.01). (E) LNCaP(CTL), LNCaP(BHC80-1) and LNCaP(BHC80-2) cells were used to establish xenografts as described in the Materials and Methods section. Tumor volume and serum PSA concentrations were measured at different time points. (F) TRAMP-C1(CTL), TRAMP-C1(BHC80-1) and TRAMP-C1(BHC80-2) xenografts were established and tumor volumes were measured.

6.2.4 BHC80-2 targets the MyD88 signaling in PCa cells

To decipher the BHC80-2 signal pathways, we first profiled BHC80-2 transcriptome using Ampliseq transcriptome sequencing analyses described previously³⁰. While 3119 genes were differentially expressed in LNCaP(BHC80-2) cells compared to LNCaP(CTL) cells, 349 genes were differentially expressed between LNCaP(BHC80-1) and LNCaP(BHC80-2) cells (p<0.05, fold change cutoff >2) (Figure 6.8A). A total of 177 genes were specifically regulated by BHC80-2. Gene ontology (GO) analysis (<http://david.abcc.ncifcrf.gov/>) revealed that the key cellular processes were mainly related to immune response, anti-apoptosis and cell migration. Seven GO annotation function groups were enriched and the expression of representative genes within these groups were plotted. (Figure 6.8B-D)

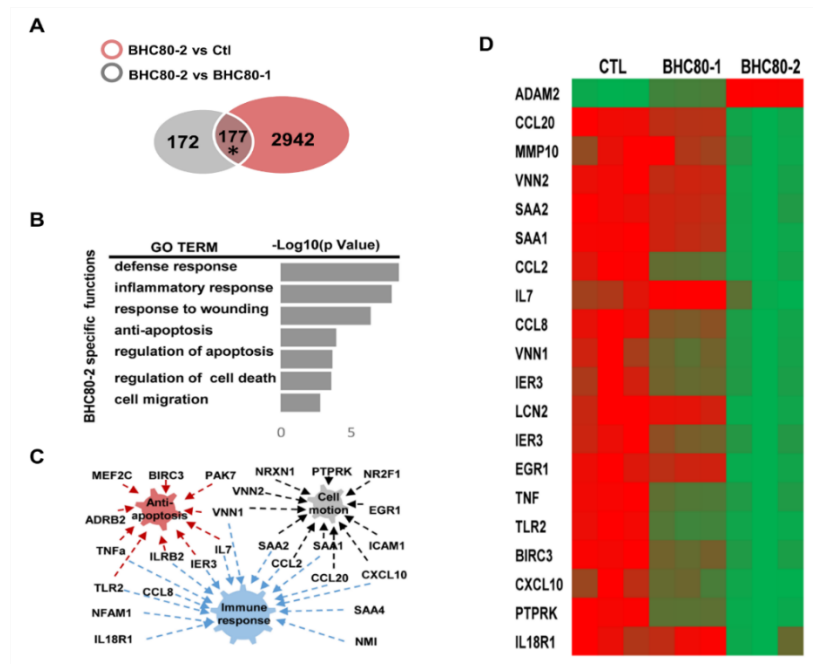


Figure 6.8 Genes and cellular function regulated by BHC80-2

(A) Total RNA of LNCaP(CTL), LNCaP(BHC80-1) and LNCaP(BHC80-2) cells were isolated and used for Ampliseq transcriptome sequencing analyses to get total transcriptomes data. A Venn diagram of results shows the comparison of transcriptomes among these cells (fold change>2 and adjusted p< 0.05). Totally 177 genes were regulated by BHC80-2 specifically (B) Top-ranked gene functions by BHC80-2 specifically were analyzed by DAVID software. Go terms were listed in the table. (C) IPA downstream analysis identified that genes associated with immune response, anti-apoptosis and cell motion are regulated by BHC80-2. (D) A heatmap shows the expression of top-ranked BHC80-2 regulated genes.

The BHC80-2 transcriptome was also analyzed by the Ingenuity Pathway Analysis (IPA) software for upstream regulators and identified TNF α , MyD88, NF-kB, IL-1a, IL-1b, and TLR4 (Z score>2

and $p < 0.001$) and for downstream effectors; and identified CCL2, CCL20, CXCL10, TLR2, et al. (Figure 6.9A-B). These bioinformatics predictions were validated by real-time PCR assays showing that BHC80-2, but not BHC80-1, induced CCL20, CXCL10, CCL2, and TNF α expressions (Figure 6.9C). Conditioned media from LNCaP(BHC80-2) cells significantly enhanced PCa cell proliferation and invasion (Figure 6.9D). These effects can be attenuated by CCL2, TNF α , and CXCL10 neutralizing antibodies or a MyD88 inhibitor (MyD88i) (Figure 6.9E). Further investigation showed that MyD88i, but not a TLR4 inhibitor, reduced BHC80-2 activities in upregulating CCL2, CXCL10, and TNF α (Figure 6.9F-G). Collectively, these results reveal a new function of BHC80-2 that specifically activates the MyD88 signaling to enhance CCL2, TNF α , and CXCL10 secretion, thereby stimulating PCa cell growth and invasion.

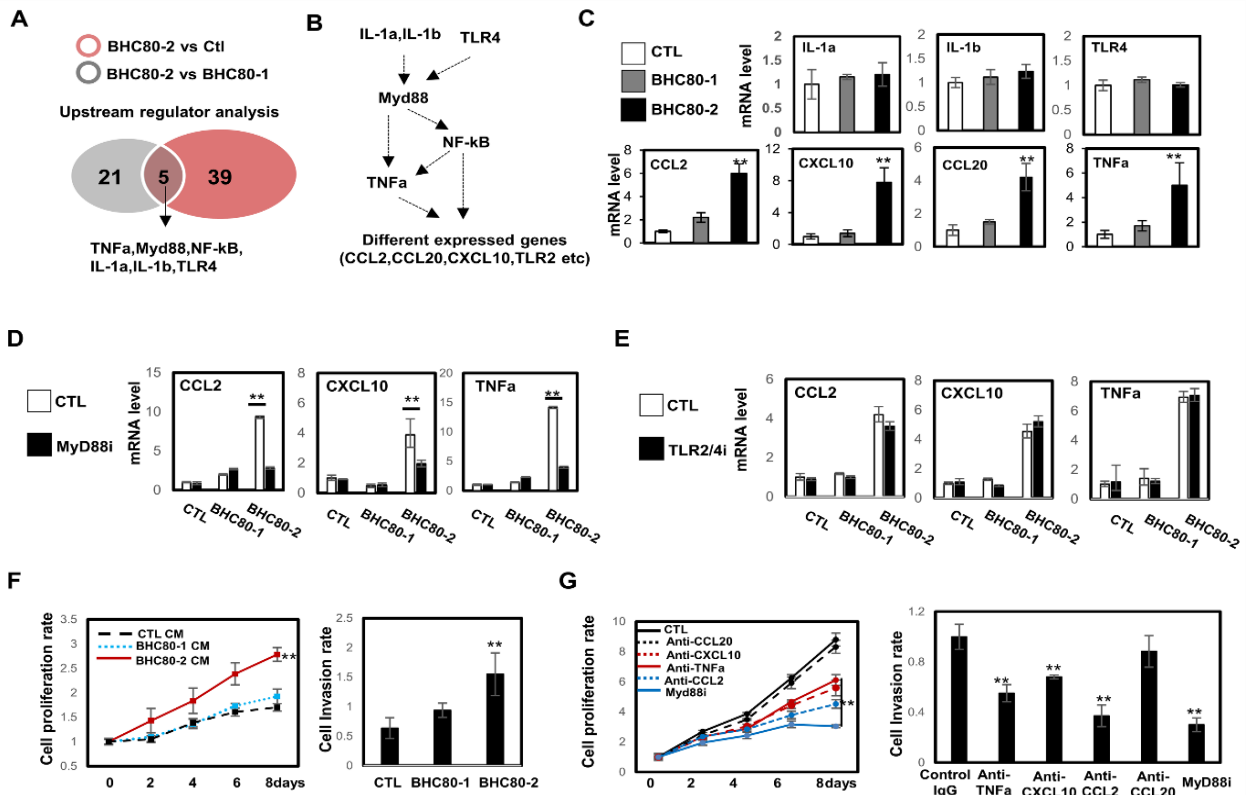


Figure 6.9 BHC80-2 regulates target cytokines expression through MyD88

(A) Total gene expressions data of LNCaP(CTL), LNCaP(BHC80-1), and LNCaP(BHC80-2) cells were used for upstream regulator analysis by using IPA software. A Venn diagram shows the common upstream regulators among these cells ($Z\text{-score} > 2$ and adjusted $p < 0.001$). (B) Interaction among five specific signals detected by IPA as the main upstream regulator of BHC80-2 transcriptome. (C) Genes specifically associated with BHC80-2 were validated by real-time qPCR. (D) LNCaP(CTL), LNCaP(BHC80-1), and LNCaP(BHC80-2) cells were treated with control, or MyD88 inhibitor (MyD88i), or (E) control, or 30ug/ml TLR2/4 inhibitor OxPAPC (TLR2/4i) for 24 hours. CCL2, CXCL10, and TNF α mRNA levels were measured by real-time qPCR. (F) Conditioned medium collected from LNCaP and PC3 cells expressing CTL, BHC80-1, and BHC80-2 were used to treat parental LNCaP and PC3 cells. LNCaP cell proliferation and PC3 invasion rates were measured. (G) LNCaP(BHC80-2) and PC3(BHC80-2) cells were treated with control, CCL2, CXCL10, TNF α , and CCL20 neutralizing antibodies. LNCaP cell proliferation and PC3 cell invasion rates were measured. All results were derived from three independent experiments that were performed in triplicate. Data were presented as the mean \pm S.D. **, $p < 0.01$ compared with controls.

6.2.5 A novel non-epigenetic action of BHC80-2 triggers the MyD88-p38-TTP pathway

We observed that BHC80-2 regulated gene expression through two mechanisms: i) BHC80-2

increased the RNA stability of CXCL10, TNF α , and CCL2, but not CCL20, as TLR2 genes demonstrated (Figure 6.10A); and ii) BHC80-2 increased the transcription initiation rates of genes such as CCL20 and TLR2, as demonstrated by our nuclear run-on assays (Figure 6.10B). MyD88 was demonstrated to stabilize CXCL10 and TNF α mRNAs in immune cells through the MyD88-p38-TTP pathway (Figure 6.10C). Specifically, MyD88 serves as an activator of p38, which, in turn, reduces the affinity of TTP to its binding motifs of substrate RNAs, and stabilizes cytokine mRNAs^{243, 244}. We showed that BHC80-2, but not BHC80-1, stimulated p38 phosphorylation, which could be inhibited by MyD88 inhibitor (Figure 6.10D). Consistently, the p38 inhibitor SB203580 (p38i) suppressed CXCL10, TNF α , and CCL2, but not CCL20 and TLR2 mRNA expression induced by BHC80-2 (Figure 6.10E). RNA-ChIP showed that BHC80-2 reduced TTP affinity to CXCL10, TNF α and CCL2 mRNAs without changing expression of TTP (Figure 6.10F).

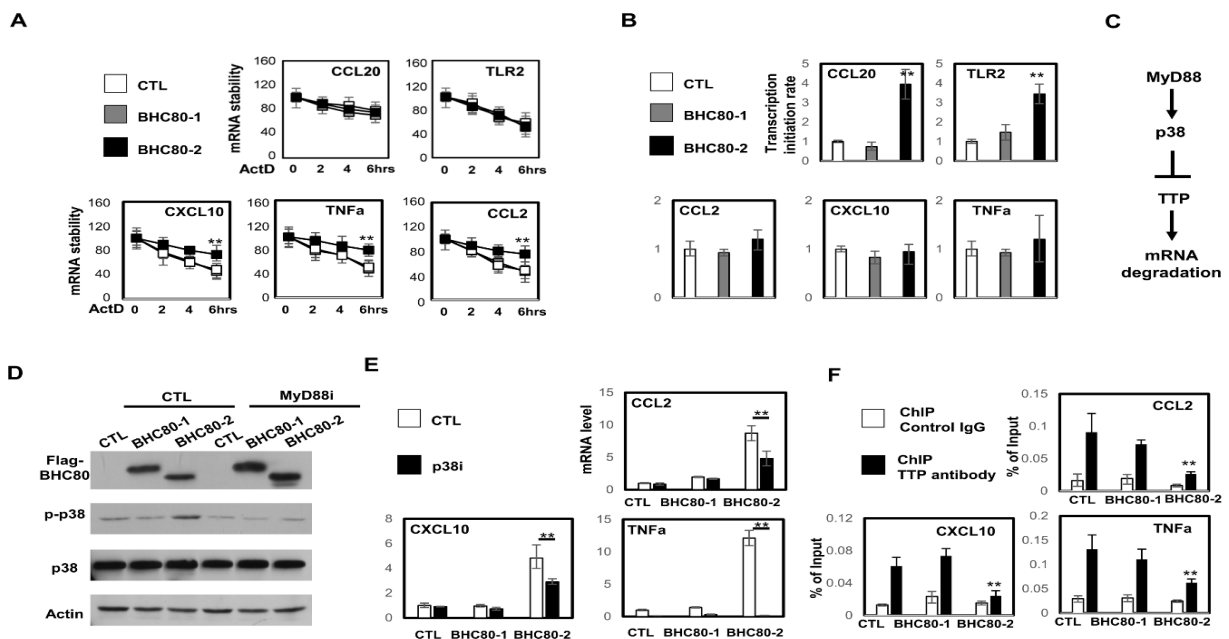


Figure 6.10 BHC80-2 regulates the RNA stability of target cytokines through the MyD88-p38-TTP pathway

(A) LNCaP(CTL), LNCaP(BHC80-1) and LNCaP(BHC80-2) cells were treated with RNA synthesis inhibitor actinomycin D (ActD) for 0-6 hours. CCL2, CXCL10, TNF α , CCL20, and TLR2 mRNA levels were measured by real-time qPCR. (B) LNCaP(CTL), LNCaP(BHC80-1), and LNCaP(BHC80-2) cells were used to perform RNA run-on assays. Nascent CCL20, TLR2, CXCL10, TNF α , and CCL2 mRNAs were purified and measured by real-time qPCR. (C) A schematic diagram shows how MyD88 regulates the RNA stability through the MyD88-p38-TTP pathway. (D) LNCaP(CTL), LNCaP(BHC80-1) and LNCaP(BHC80-2) cells were incubated with control or Myd88i for 24 hours. Phospho-p38 and total p38 protein levels were detected by immunoblotting. (E) LNCaP(CTL), LNCaP(BHC80-1), and LNCaP(BHC80-2) cells were incubated with vehicle or 10uM of p38-specific inhibitor SB203580 (p38i) for 24hours. CXCL10, TNF α , CCL2, CCL20, and TLR2 mRNA levels were measured by real-time qPCR. (F) RNA-ChIP assays were performed using the TTP antibody. Eluted RNA fragments were used as templates for real-time qPCR. Signals were calculated as percentage of input. All results were derived from three independent experiments that were performed in triplicate. Data were presented as the mean \pm S.D. **, $p < 0.01$ compared with controls.

To determine whether the cytosolic actions of BHC80-2 are due to the destruction of the predicted

nuclear localization signaling (NLS) peptide by RNA splicing (Figure 6.11A), we applied immunofluorescence microscopy to show that BHC80-1 is only expressed in the nucleus, while BHC80-2 and BHC80-1, with mutations within the NLS (BHC80-1m carrying glycine 429 to asparagine and arginine 430 to alanine), are localized in both the cytoplasm and the nucleus. These results were confirmed by immunoblotting assays using cytoplasm and nuclear fractions of LNCap cells transfected with BHC80-1, BHC80-1m, and BHC80-2 (Figure 6.11B). In addition, both co-immunoprecipitation and proximate ligation assays (PLA) confirmed that BHC80-2 and BHC80-1m interact with MyD88 (Figure 6.11C-D). Together, these results revealed a novel non-epigenetic action of BHC80-2 – that BHC80-2 is localized in cytoplasm and activates MyD88 to enhance the RNA stability of multiple tumor-promoting cytokines via the MyD88-p38-TTP axis.

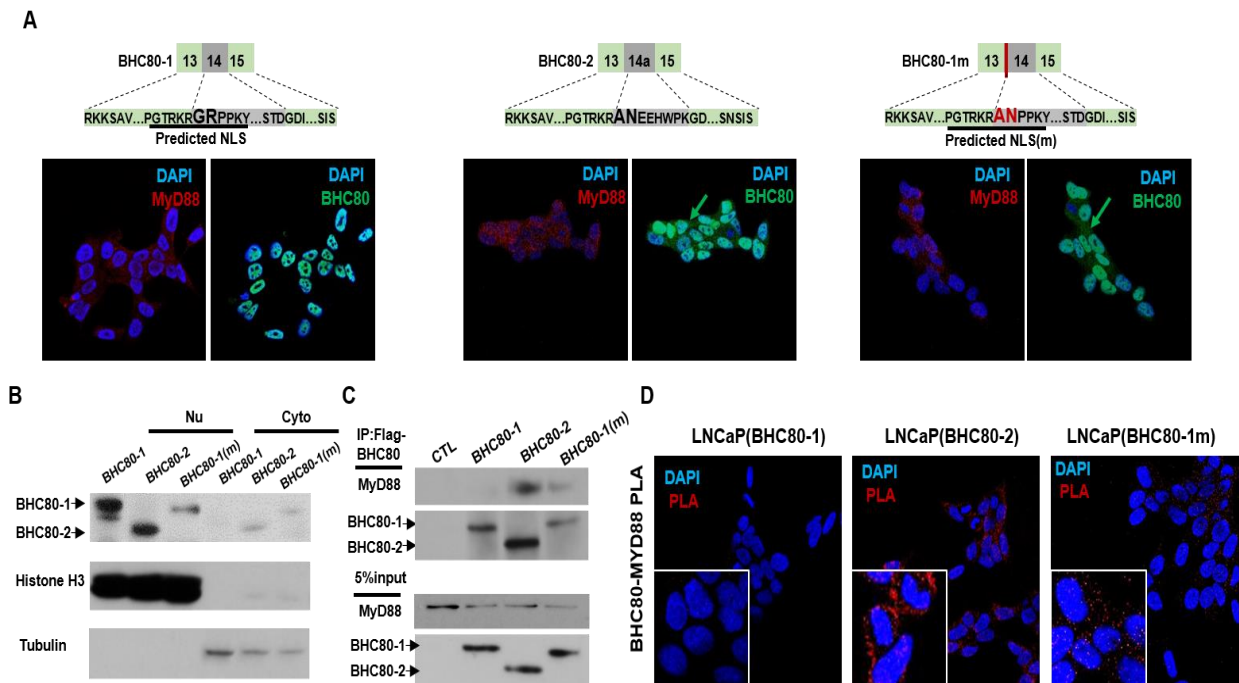


Figure 6.11 BHC80-2 directly interacted with Myd88

(A) A schematic diagram of protein sequence differences among BHC80-1, BHC80-2, and BHC80-1m. Immunofluorescence assays with BHC80 and MyD88 antibodies on indicated cells were examined via fluorescence microscope. (B) LNCaP (BHC80-1), LNCaP (BHC80-2), and LNCaP (BHC80-1m) cells were used to separate cytoplasmic and nuclear protein fractions. BHC80-1, BHC80-2, and BHC80-1m proteins was detected by immunoblotting. Histone 3 (H3) and tubulin were used as markers to confirm the efficacy of protein fractionation. (C) LNCaP(CTL), LNCaP(BHC80-1), LNCaP(BHC80-2), and LNCaP(BHC80-1m) cells were used to perform immunoprecipitation assays with Flag tag antibody. The associated proteins were detected by MyD88 and Flag antibodies. (D) PLA assays using Flag-BHC80 and MyD88 antibodies were performed on LNCaP(BHC80-1), LNCaP(BHC80-2), and LNCaP(BHC80-1m) cells as described in the Materials and Methods section. Red dots represent BHC80 and MyD88 interactions. NLS: nuclear localization signaling. Nu: nuclear. Cyto: cytoplasmic

6.2.6 Blocking BHC80-2 signaling inhibits NEPC cell spheroid growth

To further confirm the importance of BHC80-2 signaling for t-NEPC development, we applied inhibitors of BHC80-2 downstream effectors to our established NEPC 3D cell-spheroid models. NEPC cells differ significantly from AdPC cells in that they form 3D structures in suspension and cluster into multi-cellular spheroids, as exemplified by primary cultured NEPC cells and NEPC cell lines (e.g. NCI-H660). Spheroids derived from LNCaP(BHC80-2) cells grew significantly

faster than LNCaP(CTL) and LNCaP(BHC80-1) spheroids, as determined by spheroid sizes and MTS assays (Figure 6.12A). LNCaP(BHC80-2) spheroid growth was suppressed by MyD88i or CCL2 antibodies in both time- and dose-dependent manners (Figure 6.12B). The suppressive effects of MyD88i and CCL2 antibodies were reproducible in the LnNE and NCI-H660 spheroids (Figure 6.12C). These results confirmed that blocking BHC80-2 signaling inhibits NEPC cell spheroid growth, and implies that suppressing the BHC80-2 signaling may possibly prevent tumor progression to t-NEPC growth.

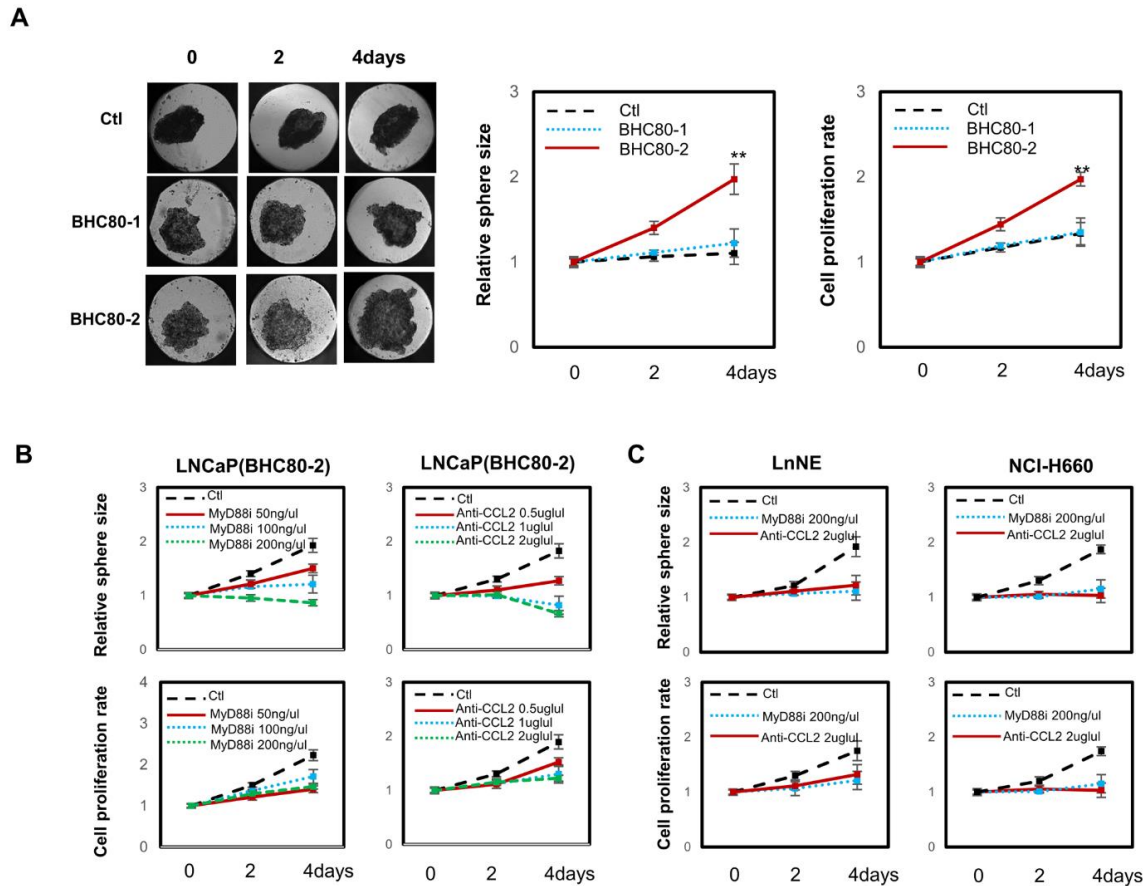


Figure 6.12 Blocking BHC80-2 signaling via MyD88 and CCL20 suppresses PCa spheroid growth

(A) LNCaP(CTL), LNCaP(BHC80-1), and LNCaP(BHC80-2) cells were cultured to form 3-D multi-cellular spheroids as described in the Materials and Methods section. Time-lapse images were presented. Relative spheroid size changes and proliferation rates were measured during 0-4 days. (B-C) LNCaP(BHC80-2) cells (B), LnNE cells and NCI-H660 cells (C) were cultured and allowed to generate 3-D micro-spheroids followed by treatments of increasing doses of MyD88 inhibitor or CCL2 neutralizing antibody for 0-4 days. Relative spheroid size changes and proliferation rates were measured during 0-4 days.

6.3 Discussion

We report here a novel non-epigenetic action of the BHC80 gene that demonstrates AdPC progression to t-NEPC. Functionally re-directed by the neural splicing factor SRRM4, the RNA splice variant of BHC80-2 is highly expressed during t-NEPC development. It can be localized in the cytoplasm of cancer cells, and trigger the MyD88-p38-TTP signal pathway, resulting in the stimulation of tumor-promoting cytokines, and acceleration of cell proliferation and xenograft growth, androgen independently. These findings highlight the idea that the RNA splicing mechanism regulates immune responses of cancer cells to counteract anti-cancer therapies and progress to t-NEPC.

The development of t-NEPC involves both differentiation and proliferation, two distinguishable

and coordinated cellular processes controlled by multiple genes. While NE differentiation initiates tumor progression toward t-NEPC, it is the proliferation that allows for t-NEPC establishment. It has been shown that between 30-100% of prostate tumors bearing NE-positive cells, depending on patient cohorts and detection methods^{175, 245}, along with NE differentiation of PCa, has not been confirmed to be correlated with poor patient outcomes^{176, 245, 246}. Detection of AdPC cells with NE markers is also insufficient for a pathologist to diagnose as t-NEPC, unless the Ki67 proliferation index and morphological alterations are also observed. The significance of proliferation during t-NEPC is even greater if proliferation driver genes specific for t-NEPC are identified and used as therapeutic targets. Our studies demonstrated that RNA splicing of BHC80-2 is a t-NEPC-specific event, which is endorsed by BHC80-2 expression in correlation with not only tumor cell morphology, Ki67 index, and NE marker status. BHC80-2 stimulates androgen-independent cell proliferation and tumor growth, highlighting that BHC80-2 is a t-NEPC proliferation driver gene, and may have the potential to be a therapeutic target.

BHC80 was originally found as a component of histone modification complexes where it antagonized the actions of LSD1, CoREST, and HDACs in de-methylating H3K4, resulting in de-repression of gene transcription^{241, 247, 248}. However, there has been no evidence confirming whether BHC80-1 and BHC80-2 function differently. Our studies report, for the first time, a non-epigenetic action unique to cytosolic BHC80-2 via the MyD88-p38-TTP pathway. SRRM4-

mediated inclusion of exon 14a destroys one of the NLSs, creating an opportunity for BHC80-2 to be localized in cytosol and to trigger MyD88 signaling. However, we cannot exclude the possibility that BHC80-2 in the nucleus functions differently than BHC80-1 in the nucleus, and also contributes to t-NEPC development. Although we did observe that BHC80-2 regulation of CCL20 and TLR2 occurs at the transcription levels, CCL20 neutralizing antibody did not antagonize BHC80-2-induced cell proliferation and invasion (Figure 6.4G), and the TLR inhibitor did not alter CCL2, CXCL10, and TNF α expressions (Figure 6.4E). Therefore, we did not pursue this research direction. Nevertheless, BHC80-2-induced CCL20 and TLR2 may still contribute to t-NEPC progression by altering the tumor microenvironment through leucocyte recruitment.

That BHC80-2 promotes t-NEPC development also supports the idea that inflammation contributes to carcinogenesis and tumor progression^{249, 250}. The adapter protein MyD88 mediates various tumor-promoting signals triggered by microbial or endogenous ligands of cell surface receptors such as TLRs and IL-1Rs through downstream effectors such as NF κ B, AKT, JNK, and p38²⁵¹. Our new findings demonstrate that BHC80-2 bypasses cell surface receptors to activate MyD88 and stimulate cytokine expression. MyD88 may induce its target gene expression by either enhancing the RNA stability of short-lived mRNAs containing AU-rich elements in their 3' UTR^{243, 244}, or by upregulating gene transcription initiation²⁵². It is now clear that BHC80-2 enhances the RNA stability of CCL2, CXCL10, and TNF α through the MyD88-p38-TTP pathway

(Figure 6.10 and 6.11), and these cytokines are key mediators for BHC80-2 to promote tumor progression to t-NEPC.

In summary, we report novel non-epigenetic functions of BHC80-2 that promote therapy-resistant prostate cancer progression to t-NEPC by enhancing androgen-independent cell proliferation and tumor growth. Our studies provide new insights into the molecular mechanisms whereby AdPC cells utilize alternative RNA splicing to trigger immune responses of cancer cells for t-NEPC development.

Chapter 7: Closing Remarks

7.1 Conclusion

Although ARPI improved overall prostate cancer survival, t-NEPC becomes more prevalent when ARPI is comprehensively used. The median survival of NEPC patients is less than one year. What is even worse is that NEPC is difficult to diagnose because it secretes low/no PSA, a biomarker used by clinicians to monitor the efficacy of ARPI therapy. Currently, there is few effective diagnosis or curative treatment for NEPC, due to the lack of understanding of this cancer. It is therefore urgent to investigate how ARPI drives the emergence of NEPC in order to aid new discoveries that can allow for earlier diagnosis and/or effective management of this lethal disease. Based on our publications and our substantial preliminary results, we hypothesized that increased SRRM4 expression in prostate tumors drives AdPC progression to t-NEPC. We have designed three specific aims to test this hypothesis: 1) SRRM4 expression is correlated with t-NEPC progression and can be used as a diagnostic marker of t-NEPC, 2) SRRM4 is a driver of t-NEPC, and 3) SRRM4 facilitates progression of t-NEPC.

In Chapter 3, whole-transcriptome sequencing data were extracted from prostate tumors from two independent cohorts: the VPC and Beltran cohort(s). A novel bioinformatics tool, COMPAS, was invented to analyze alternative RNA splicing on RNA-sequencing data. COMPAS identified most of the splice events that were predicted to be regulated by the RNA splicing factor SRRM4. We

applied RNA *in situ hybridization* and IHC assays to measure the expressions of SRRM4, NEPC markers (SYP, CD56, and CHGA), and AdPC markers (AR, PSA) in a series of TMA constructed from CRPC, treatment-naïve tumors, and tumors treated with NHT for 0-12 months. In this chapter, we report that SRRM4 in CRPC tumors is highly expressed in NEPC, and strongly correlated with SYP, CD56, and CHGA expressions. Patients with SRRM4-positive tumors had a median overall survival rate of 12.3 months, as compared to 23 months for patients with SRRM4-negative tumors. Based on these findings, we concluded that SRRM4 expression in castrate-resistant tumors is highly correlated with NEPC and poor patient survival. It may serve as a diagnosis and prognosis biomarker of NEPC.

In Chapter 4, *in vitro* and *in vivo* evidence confirmed that one important SRRM4 target gene was REST, a key regulator of neurogenesis and differentiation. Moreover, SRRM4 strongly stimulated AdPC cells to express NEPC biomarkers, and this effect was exacerbated by ARPI. ARPI combined with a gain of SRRM4-induced adenocarcinoma cells to assume multicellular spheroid morphology and was essential in establishing progressive NEPC xenografts. These actions of SRRM4 were further enhanced by loss-of-function of TP53. These results indicated that SRRM4 drives t-NEPC progression.

In Chapter 5, we generated an NEPC model, LnNE, which was derived from AdPC cells by

overexpressing SRRM4, and knocking down TP53. LnNE had a global similarity in transcription and RNA splicing to that of tumors from NEPC patients. LnNE xenografts are castrate-resistant, highly aggressive, express multiple neuroendocrine markers, preserve AR expression, and are PSA-negative. Its neuroendocrine phenotype cannot be reversed by androgen treatment. LnNE cells grow as multi-cellular spheroids under 2-dimensional culture conditions similar to the NEPC cell line NCI-H660, but have a higher proliferation rate and are easier to be transfected. LnNE cells can also adapt to 3-dimensional culture conditions in a 96-plate format, allowing for high throughput screening assays. In summary, the LnNE model is useful to study the mechanisms of NEPC progression and to discover potential therapies for NEPC.

In Chapter 6, by analyzing whole transcriptome data of LNCaP and LnNE cells, we identified a BHC80 splice variant, BHC80-2, that functions as a key facilitator of t-NEPC development. Functionally reprogrammed by the neural RNA splicing factor SRRM4, BHC80-2 does not confer the NEPC phenotype to cancer cells, but rather stimulates cell proliferation and invasion to accelerate tumor progression. In contrast to the epigenetic role of BHC80 in histone demethylation, we defined a novel non-epigenetic action of BHC80-2 whereby cytosolic BHC80-2 protein triggers the MyD88-p38-TTP pathway to increase the RNA stability of a set of tumor-promoting cytokines. Blocking BHC80-2 signaling suppresses NEPC cell spheroid growth, identifying BHC80-2 as a potential therapeutic target for t-NEPC.

In conclusion, my study demonstrated that SRRM4 expression is correlated with NE differentiation, and patients with SRRM4 expression have a relatively low overall survival rate. SRRM4 drives NE differentiation of AdPC, and facilitates t-NEPC progression under ARPI treatment by regulating the alternative splicing of REST and the BHC80 gene. These findings suggest that SRRM4 has the potential to become a diagnostic biomarker, and a therapeutic target of t-NEPC.

7.2 Research significance

T-NEPC is a highly aggressive, lethal subtype of prostate cancer. In order to treat t-NEPC as effectively as possible, it is imperative that more reliable biomarkers and new therapeutic targets are developed, to improve the management of the disease. Our research began with identifying a t-NEPC-specific splicing factor, SRRM4, and establishing its clinical correlation with t-NEPC progression. This was followed by demonstrating its functional importance in driving NE transdifferentiation of AdPC under ARPI conditions, and eventually deciphering the mechanism through which SRRM4 can facilitate t-NEPC progression.

To investigate SRRM4 expression and function in t-NEPC, we have applied multiple *in vivo* and *in vitro* approaches. We have developed a novel bioinformatics tool called COMPAS to analyze the whole transcriptome data of two independent t-NEPC cohorts: the VPC and Beltran cohort(s).

We also included 382 PCa tissue cores cohorts in our study, which strengthened the findings on SRRM4 and BHC80-2. Beyond basic IHC staining, RISH assays were used to detect SRRM4 and BHC80-2 directly on TMAs, and were instrumental in validating and enhancing the clinical relevance of our findings.

Our established pipeline was used to study the mechanisms by which SRRM4 regulates REST and BHC80 gene splicing. We have constructed REST and BHC80 minigenes, which can mimic the process of endogenous gene splicing. Using wild and site-direct-mutant minigenes, combined with RNA-IP and RNA-pulldown assays, we demonstrated that SRRM4 can directly bind to the UGC motif of pre-RNA and induce the inclusion of neuro-specific exons.

We have established LNCaP-derived NEPC xenografts. Based on this achievement, we have generated a NEPC cell model, the LnNE cell line. This cell line shows similar transcription and splicing signatures as t-NEPC tumors. Through analyzing the whole transcriptome sequencing data of the LnNE cell model, we have found that BHC80 is a crucial downstream target gene of SRRM4. This cell model was also applied in testing the treatment efficacy of MyD88 and CCL2 inhibitors.

This study has, for the first time, identified SRRM4 as a novel driver gene of t-NEPC, and demonstrated that SRRM4 drives NE transdifferentiation, and facilitates t-NEPC progression, by

regulating the alternate splicing of REST and BHC80 genes separately. We demonstrated that SRRM4 is upregulated in t-NEPC tumors and its expression is correlated with NE marker expression and t-NEPC progression. SRRM4 drives the NE transdifferentiation of AdPC, and establishes NEPC xenografts by compromising the repressing function of REST through alternative splicing. Meanwhile, SRRM4 can also induce the expression of the BHC80-2 splicing variant, which triggers the MyD88-p38-TTP pathway to increase the RNA stability of a set of tumor-promoting cytokines.

In short, our studies indicated that SRRM4 is a t-NEPC biomarker, a powerful driver, and a potential therapeutic target, of t-NEPC. These studies will not only enhance our understanding of the mechanisms underlying t-NEPC development, but also provide insights for personalized medicine-based strategies for PCa patients. It rationalizes the design of SRRM4 inhibitors for patients with t-NEPC.

7.3 Limitations and Future Directions

Using the bioinformatics tool COMPAS, we identified that t-NEPC has a NEPC specific splicing signature and 24 genes that commonly spliced by SRRM4. However we could not exclude the possibility that other SRRM4 target genes that may be missed because of the limitation of the algorithm and the sample sequencing quality. In fact, because the sequencing quality, BHC80 is

omitted. So the amount of SRRM4 target genes may not limited to 24. More SRRM4 target gene could be found if using more advanced bioinformatics tools.

To investigate the relationship between SRRM4 and t-NEPC patient prognosis, we included 32 CRPC patients in our study, and compared the median overall survival between NEPC and AdPC (Chapter 3). The small number of t-NEPC patients limited the significance of our conclusion. More PCa specimens, especially t-NEPC tissues from the tumor bank, would further strengthen the findings from Chapter 3 on SRRM4. In addition, we did not study whether SRRM4 expression is a risk factor for AdPC to finally progress into t-NEPC, because acquiring tumor biopsy samples at different time points in the same patient is beyond our capability.

The mechanisms of induction of SRRM4 remain unknown. No NEPC-specific mutations were found in the SRRM4 promoter, therefore induction of the SRRM4 gene expression may involve epigenetic mechanisms. It has been reported that REST4 can increase SRRM4 expression in neural cells. However, we did not observe this phenomenon in our studies (Chapter 4). Meanwhile, overexpression of other NEPC-associated transcription factors and epigenetic modifiers, such as EZH2 and SOX2, also did not alter the SRRM4 expression level in LNCaP cells. We hypothesize that some uncharacterized mutations may be a prerequisite for, and cooperate with, other epigenetic changes that contribute to SRRM4 expression.

NEPC usually has low/no expression of the AR and PSA. The LnNE model preserves AR protein levels, but becomes PSA-negative, indicating a middle stage of NE transdifferentiation (Chapter 5). We may not exclude the possibility that long-term ARPI treatment will finally abolish AR protein expression. However, it is also possible that genomic contexts may also affect loss of AdPC characteristics and t-NEPC formation. Because of the heterogeneity of PCa, we need to test the effects of SRRM4 on multiple PCa cell models in addition to LNCaP, as well as the conditional PTEN null mouse model to confirm that SRRM4 is a driver gene.

BHC80-1 is universally expressed in different cell lineages, and is a well-known histone modifier, controlling fundamental cellular functions. While gain-of-function of BHC80-2 was thoroughly investigated, depletion of BHC80-1 was not yet achieved. We applied the CRISPR-Cas9 system to generate the endogenous BHC80-1 knockout PCa cell lines, and then constructed PCa cell lines that expressed only BHC80-1 and BHC80-2. However knockout of BHC80-1 is lethal to PCa cell lines. Going forward, we may apply shRNA targeting 3'UTR region of BHC80 pre-mRNA to knock down endogenous BHC80-1 and BHC80-2 mRNA in LNCaP(BHC80-1) and LNCaP(BHC80-2) cell lines. Cell studies on these cell lines will certainly broaden our understanding of the functions of BHC80-2.

BHC80-1 and BHC80-2 share the same functional PHD domain, which suggests that BHC80-2 may also exert genomic actions to regulate cell growth and tumor progression. The coding region of exon 14a in BHC80-2 may alter protein interactions within the BRAF/HDAC complex when compared with exon 14 in BHC80-1 (Chapter 6). As well, other mechanism or splicing factors may also enhance BHC80-2 splicing. However, this project demonstrated how SRRM4 reprograms BHC80-2 to facilitate NEPC tumor progression.

An important future plan involves developing drugs that are SRRM4 inhibitors. In our research that is beyond the scope of this study, by performing RNA-pulldown assays using fragments of SRRM4 protein, we have characterized a ~50aa and a ~30aa region of SRRM4 that is responsible for its RNA binding and splicing activity. However, the RNA-binding region is highly enriched with serine and arginine, which makes this fragment highly charged and hard to be crystalized using traditional methods. The design of inhibitors to block these SRRM4 activities is provided through collaborations with Dr. Artem Cherkasov (Director of Pharmacology/Drug Design Core, VPC).

Besides the prostate, tumors of other organs may also show neuroendocrine phenotypes, such as small cell lung cancer and small cell pancreatic cancer. Loss of REST, and overexpression of SRRM4, have been reported in small cell lung cancer cell lines^{210, 253, 254}. Whether SRRM4 drives

or participates in the formation and progression of these cancers still need further investigation. In addition, REST has been reported as an oncogene in neural tumors. Several studies have found that high REST expression is associated with shorter overall survival and disease-free survival in glioma^{255, 256}. Since neural tumors show a de-differentiation phenotype, SRRM4 is expected to be downregulated in glioma. Further investigation of SRRM4 function may provide insights for therapeutic strategies for not only t-NEPC, but also other neural-related tumors.

Bibliography

1. Pishgar F, Ebrahimi H, Saeedi Moghaddam S, Fitzmaurice C, Amini E. Global, Regional and National Burden of Prostate Cancer, 1990 to 2015: Results from the GBD Study 2015. *J Urol.* 2017.
2. Global Burden of Disease Cancer C, Fitzmaurice C, Allen C, Barber RM, Barregard L, Bhutta ZA, Brenner H, Dicker DJ, Chimed-Orchir O, Dandona R, Dandona L, Fleming T, Forouzanfar MH, Hancock J, Hay RJ, Hunter-Merrill R, Huynh C, Hosgood HD, Johnson CO, Jonas JB, Khubchandani J, Kumar GA, Kutz M, Lan Q, Larson HJ, Liang X, Lim SS, Lopez AD, MacIntyre MF, Marczak L, Marquez N, Mokdad AH, Pinho C, Pourmalek F, Salomon JA, Sanabria JR, Sandar L, Sartorius B, Schwartz SM, Shackelford KA, Shibuya K, Stanaway J, Steiner C, Sun J, Takahashi K, Vollset SE, Vos T, Wagner JA, Wang H, Westerman R, Zeeb H, Zoeckler L, Abd-Allah F, Ahmed MB, Alabed S, Alam NK, Aldhahri SF, Alem G, Alemayohu MA, Ali R, Al-Raddadi R, Amare A, Amoako Y, Artaman A, Asayesh H, Atnafu N, Awasthi A, Saleem HB, Barac A, Bedi N, Bensenor I, Berhane A, Bernabe E, Betsu B, Binagwaho A, Boneya D, Campos-Nonato I, Castaneda-Orjuela C, Catala-Lopez F, Chiang P, Chibueze C, Chittheer A, Choi JY, Cowie B, Damtew S, das Neves J, Dey S, Dharmaratne S, Dhillon P, Ding E, Driscoll T, Ekwueme D, Endries AY, Farvid M, Farzadfar F, Fernandes J, Fischer F, TT GH, Gebru A, Gopalani S, Hailu A, Horino M, Horita N, Husseini A, Huybrechts I, Inoue M, Islami F, Jakovljevic M, James S, Javanbakht M, Jee SH, Kasaeian A, Kedir MS, Khader YS, Khang YH, Kim D, Leigh J, Linn

S, Lunevicius R, El Razek HMA, Malekzadeh R, Malta DC, Marcenes W, Markos D, Melaku YA, Meles KG, Mendoza W, Mengiste DT, Meretoja TJ, Miller TR, Mohammad KA, Mohammadi A, Mohammed S, Moradi-Lakeh M, Nagel G, Nand D, Le Nguyen Q, Nolte S, Ogbo FA, Oladimeji KE, Oren E, Pa M, Park EK, Pereira DM, Plass D, Qorbani M, Radfar A, Rafay A, Rahman M, Rana SM, Soreide K, Satpathy M, Sawhney M, Sepanlou SG, Shaikh MA, She J, Shiue I, Shore HR, Shrimel MG, So S, Soneji S, Stathopoulou V, Stroumpoulis K, Sufiyan MB, Sykes BL, Tabares-Seisdedos R, Tadese F, Tedla BA, Tessema GA, Thakur JS, Tran BX, Ukwaja KN, Uzochukwu BSC, Vlassov VV, Weiderpass E, Wubshet Terefe M, Yebo HG, Yimam HH, Yonemoto N, Younis MZ, Yu C, Zaidi Z, Zaki MES, Zenebe ZM, Murray CJL, Naghavi M.

Global, Regional, and National Cancer Incidence, Mortality, Years of Life Lost, Years Lived With Disability, and Disability-Adjusted Life-years for 32 Cancer Groups, 1990 to 2015: A Systematic Analysis for the Global Burden of Disease Study. *JAMA Oncol.* 2017;3 (4) : 524-548.

3. Bubendorf L, Schopfer A, Wagner U, Sauter G, Moch H, Willi N, Gasser TC, Mihatsch MJ. Metastatic patterns of prostate cancer: an autopsy study of 1,589 patients. *Hum Pathol.* 2000;31 (5) : 578-583.

4. Feldman BJ, Feldman D. The development of androgen-independent prostate cancer. *Nat Rev Cancer.* 2001;1 (1) : 34-45.

5. Pienta KJ, Bradley D. Mechanisms underlying the development of androgen-independent prostate cancer. *Clin Cancer Res.* 2006;12 (6) : 1665-1671.

6. Marker PC, Donjacour AA, Dahiya R, Cunha GR. Hormonal, cellular, and molecular control of prostatic development. *Dev Biol.* 2003;253 (2) : 165-174.
7. Hayward SW, Cunha GR. The prostate: development and physiology. *Radiol Clin North Am.* 2000;38 (1) : 1-14.
8. Wang Y, Hayward S, Cao M, Thayer K, Cunha G. Cell differentiation lineage in the prostate. *Differentiation.* 2001;68 (4-5) : 270-279.
9. Hayward SW, Baskin LS, Haughney PC, Foster BA, Cunha AR, Dahiya R, Prins GS, Cunha GR. Stromal development in the ventral prostate, anterior prostate and seminal vesicle of the rat. *Acta Anat (Basel).* 1996;155 (2) : 94-103.
10. Cunha GR, Hayward SW, Wang YZ. Role of stroma in carcinogenesis of the prostate. *Differentiation.* 2002;70 (9-10) : 473-485.
11. McNeal JE. Normal histology of the prostate. *Am J Surg Pathol.* 1988;12 (8) : 619-633.
12. McNeal JE. The zonal anatomy of the prostate. *Prostate.* 1981;2 (1) : 35-49.
13. McNeal JE. Origin and development of carcinoma in the prostate. *Cancer.* 1969;23 (1) : 24-34.
14. Abate-Shen C, Shen MM. Molecular genetics of prostate cancer. *Genes Dev.* 2000;14 (19) : 2410-2434.
15. Elzanaty S, Erenpreiss J, Becker C. Seminal plasma albumin: origin and relation to the male reproductive parameters. *Andrologia.* 2007;39 (2) : 60-65.

16. Armbruster DA. Prostate-specific antigen: biochemistry, analytical methods, and clinical application. *Clin Chem.* 1993;39(2): 181-195.
17. Brinkmann AO. Molecular mechanisms of androgen action--a historical perspective. *Methods Mol Biol.* 2011;776(3-24).
18. Lonergan PE, Tindall DJ. Androgen receptor signaling in prostate cancer development and progression. *J Carcinog.* 2011;10(20).
19. Cunha GR, Donjacour AA, Cooke PS, Mee S, Bigsby RM, Higgins SJ, Sugimura Y. The endocrinology and developmental biology of the prostate. *Endocr Rev.* 1987;8(3): 338-362.
20. Heidenreich A, Bastian PJ, Bellmunt J, Bolla M, Joniau S, van der Kwast T, Mason M, Matveev V, Wiegel T, Zattoni F, Mottet N, European Association of U. EAU guidelines on prostate cancer. part 1: screening, diagnosis, and local treatment with curative intent-update 2013. *Eur Urol.* 2014;65(1): 124-137.
21. Welch HG, Albertsen PC. Prostate cancer diagnosis and treatment after the introduction of prostate-specific antigen screening: 1986-2005. *J Natl Cancer Inst.* 2009;101(19): 1325-1329.
22. Gann PH. Risk factors for prostate cancer. *Rev Urol.* 2002;4 Suppl 5(S3-S10).
23. Kumar B, Koul S, Khandrika L, Meacham RB, Koul HK. Oxidative stress is inherent in prostate cancer cells and is required for aggressive phenotype. *Cancer Res.* 2008;68(6): 1777-1785.

24. Elkahwaji JE, Hauke RJ, Brawner CM. Chronic bacterial inflammation induces prostatic intraepithelial neoplasia in mouse prostate. *Br J Cancer*. 2009;101 (10): 1740-1748.
25. De Marzo AM, Platz EA, Sutcliffe S, Xu J, Gronberg H, Drake CG, Nakai Y, Isaacs WB, Nelson WG. Inflammation in prostate carcinogenesis. *Nat Rev Cancer*. 2007;7 (4): 256-269.
26. Cano P, Godoy A, Escamilla R, Dhir R, Onate SA. Stromal-epithelial cell interactions and androgen receptor-coregulator recruitment is altered in the tissue microenvironment of prostate cancer. *Cancer Res*. 2007;67 (2): 511-519.
27. Balic I, Graham ST, Troyer DA, Higgins BA, Pollock BH, Johnson-Pais TL, Thompson IM, Leach RJ. Androgen receptor length polymorphism associated with prostate cancer risk in Hispanic men. *J Urol*. 2002;168 (5): 2245-2248.
28. Bratt O, Drevin L, Akre O, Garmo H, Stattin P. Family History and Probability of Prostate Cancer, Differentiated by Risk Category: A Nationwide Population-Based Study. *J Natl Cancer Inst*. 2016;108 (10).
29. Kheirandish P, Chinegwundoh F. Ethnic differences in prostate cancer. *Br J Cancer*. 2011;105 (4): 481-485.
30. Eeles R, Goh C, Castro E, Bancroft E, Guy M, Al Olama AA, Easton D, Kote-Jarai Z. The genetic epidemiology of prostate cancer and its clinical implications. *Nat Rev Urol*. 2014;11 (1): 18-31.

31. Na R, Zheng SL, Han M, Yu H, Jiang D, Shah S, Ewing CM, Zhang L, Novakovic K, Petkewicz J, Gulukota K, Helseth DL, Jr., Quinn M, Humphries E, Wiley KE, Isaacs SD, Wu Y, Liu X, Zhang N, Wang CH, Khandekar J, Hulick PJ, Shevrin DH, Cooney KA, Shen Z, Partin AW, Carter HB, Carducci MA, Eisenberger MA, Denmeade SR, McGuire M, Walsh PC, Helfand BT, Brendler CB, Ding Q, Xu J, Isaacs WB. Germline Mutations in ATM and BRCA1/2 Distinguish Risk for Lethal and Indolent Prostate Cancer and are Associated with Early Age at Death. *Eur Urol.* 2017;71 (5) : 740-747.
32. McMichael AJ. Food, nutrition, physical activity and cancer prevention. Authoritative report from World Cancer Research Fund provides global update. *Public Health Nutr.* 2008;11 (7) : 762-763.
33. Cao Y, Ma J. Body mass index, prostate cancer-specific mortality, and biochemical recurrence: a systematic review and meta-analysis. *Cancer Prev Res (Phila).* 2011;4 (4) : 486-501.
34. Nuclear Receptors Nomenclature C. A unified nomenclature system for the nuclear receptor superfamily. *Cell.* 1999;97 (2) : 161-163.
35. Wang D, Tindall DJ. Androgen action during prostate carcinogenesis. *Methods Mol Biol.* 2011;776 (25-44).
36. Migliaccio A, Castoria G, Auricchio F. Analysis of androgen receptor rapid actions in cellular signaling pathways: receptor/Src association. *Methods Mol Biol.* 2011;776 (361-370).

37. Nazareth LV, Weigel NL. Activation of the human androgen receptor through a protein kinase A signaling pathway. *J Biol Chem.* 1996;271 (33): 19900-19907.
38. Birtle AJ, Freeman A, Masters JR, Payne HA, Harland SJ, Registry BSoOC. Clinical features of patients who present with metastatic prostate carcinoma and serum prostate-specific antigen (PSA) levels < 10 ng/mL: the "PSA negative" patients. *Cancer.* 2003;98 (11): 2362-2367.
39. Mottet N, Bellmunt J, Bolla M, Briers E, Cumberbatch MG, De Santis M, Fossati N, Gross T, Henry AM, Joniau S, Lam TB, Mason MD, Matveev VB, Moldovan PC, van den Bergh RCN, Van den Broeck T, van der Poel HG, van der Kwast TH, Rouviere O, Schoots IG, Wiegel T, Cornford P. EAU-ESTRO-SIOG Guidelines on Prostate Cancer. Part 1: Screening, Diagnosis, and Local Treatment with Curative Intent. *Eur Urol.* 2017;71 (4): 618-629.
40. Stamey TA, Yang N, Hay AR, McNeal JE, Freiha FS, Redwine E. Prostate-specific antigen as a serum marker for adenocarcinoma of the prostate. *N Engl J Med.* 1987;317 (15): 909-916.
41. Carter HB, Albertsen PC, Barry MJ, Etzioni R, Freedland SJ, Greene KL, Holmberg L, Kantoff P, Konety BR, Murad MH, Penson DF, Zietman AL. Early detection of prostate cancer: AUA Guideline. *J Urol.* 2013;190 (2): 419-426.
42. Lilja H, Ulmert D, Vickers AJ. Prostate-specific antigen and prostate cancer: prediction, detection and monitoring. *Nat Rev Cancer.* 2008;8 (4): 268-278.
43. Cooperberg MR, Broering JM, Carroll PR. Time trends and local variation in primary treatment of localized prostate cancer. *J Clin Oncol.* 2010;28 (7): 1117-1123.

44. van der Kwast TH, Lopes C, Santonja C, Pihl CG, Neetens I, Martikainen P, Di Lollo S, Bubendorf L, Hoedemaeker RF, Members of the pathology committee of the European Randomised Study of Screening for Prostate C. Guidelines for processing and reporting of prostatic needle biopsies. *J Clin Pathol*. 2003;56(5): 336-340.
45. Humphrey PA. Gleason grading and prognostic factors in carcinoma of the prostate. *Mod Pathol*. 2004;17(3): 292-306.
46. Gleason DF, Mellinger GT, Veterans Administration Cooperative Urological Research G. Prediction of Prognosis for Prostatic Adenocarcinoma by Combined Histological Grading and Clinical Staging. *J Urol*. 2017;197(2S): S134-S139.
47. van Poppel H. Locally advanced and high risk prostate cancer: The best indication for initial radical prostatectomy? *Asian J Urol*. 2014;1(1): 40-45.
48. Epstein JI, Egevad L, Amin MB, Delahunt B, Srigley JR, Humphrey PA, Grading C. The 2014 International Society of Urological Pathology (ISUP) Consensus Conference on Gleason Grading of Prostatic Carcinoma: Definition of Grading Patterns and Proposal for a New Grading System. *Am J Surg Pathol*. 2016;40(2): 244-252.
49. Epstein JI, Zelefsky MJ, Sjoberg DD, Nelson JB, Egevad L, Magi-Galluzzi C, Vickers AJ, Parwani AV, Reuter VE, Fine SW, Eastham JA, Wiklund P, Han M, Reddy CA, Ciezki JP, Nyberg T, Klein EA. A Contemporary Prostate Cancer Grading System: A Validated Alternative to the Gleason Score. *Eur Urol*. 2016;69(3): 428-435.

50. Schroder FH, Hermanek P, Denis L, Fair WR, Gospodarowicz MK, Pavone-Macaluso M. The TNM classification of prostate cancer. *Prostate Suppl.* 1992;4 (129-138).
51. Cuzick J, Swanson GP, Fisher G, Brothman AR, Berney DM, Reid JE, Mesher D, Speights VO, Stankiewicz E, Foster CS, Moller H, Scardino P, Warren JD, Park J, Younus A, Flake DD, 2nd, Wagner S, Gutin A, Lanchbury JS, Stone S, Transatlantic Prostate G. Prognostic value of an RNA expression signature derived from cell cycle proliferation genes in patients with prostate cancer: a retrospective study. *Lancet Oncol.* 2011;12 (3): 245-255.
52. Nguyen HG, Welty CJ, Cooperberg MR. Diagnostic associations of gene expression signatures in prostate cancer tissue. *Curr Opin Urol.* 2015;25 (1): 65-70.
53. Knezevic D, Goddard AD, Natraj N, Cherbavaz DB, Clark-Langone KM, Snable J, Watson D, Falzarano SM, Magi-Galluzzi C, Klein EA, Quale C. Analytical validation of the Oncotype DX prostate cancer assay - a clinical RT-PCR assay optimized for prostate needle biopsies. *BMC Genomics.* 2013;14 (690).
54. Neves AF, Araujo TG, Biase WK, Meola J, Alcantara TM, Freitas DG, Goulart LR. Combined analysis of multiple mRNA markers by RT-PCR assay for prostate cancer diagnosis. *Clin Biochem.* 2008;41 (14-15): 1191-1198.
55. Gittelman MC, Hertzman B, Bailen J, Williams T, Koziol I, Henderson RJ, Efros M, Bidair M, Ward JF. PCA3 molecular urine test as a predictor of repeat prostate biopsy outcome in men

- with previous negative biopsies: a prospective multicenter clinical study. *J Urol*. 2013;190 (1) : 64-69.
56. Ramos CG, Valdevenito R, Vergara I, Anabalon P, Sanchez C, Fulla J. PCA3 sensitivity and specificity for prostate cancer detection in patients with abnormal PSA and/or suspicious digital rectal examination. First Latin American experience. *Urol Oncol*. 2013;31 (8) : 1522-1526.
57. Wilt TJ, Brawer MK, Jones KM, Barry MJ, Aronson WJ, Fox S, Gingrich JR, Wei JT, Gilhooly P, Grob BM, Nsouli I, Iyer P, Cartagena R, Snider G, Roehrborn C, Sharifi R, Blank W, Pandya P, Andriole GL, Culkin D, Wheeler T, Prostate Cancer Intervention versus Observation Trial Study G. Radical prostatectomy versus observation for localized prostate cancer. *N Engl J Med*. 2012;367 (3) : 203-213.
58. Wallen EM. Treatment for localized prostate cancer: surgical approaches. *N C Med J*. 2006;67 (2) : 146-148.
59. Dall'Era MA, Albertsen PC, Bangma C, Carroll PR, Carter HB, Cooperberg MR, Freedland SJ, Klotz LH, Parker C, Soloway MS. Active surveillance for prostate cancer: a systematic review of the literature. *Eur Urol*. 2012;62 (6) : 976-983.
60. D'Amico AV, Whittington R, Malkowicz SB, Schultz D, Blank K, Broderick GA, Tomaszewski JE, Renshaw AA, Kaplan I, Beard CJ, Wein A. Biochemical outcome after radical prostatectomy, external beam radiation therapy, or interstitial radiation therapy for clinically localized prostate cancer. *JAMA*. 1998;280 (11) : 969-974.

61. Chang AJ, Autio KA, Roach M, 3rd, Scher HI. High-risk prostate cancer-classification and therapy. *Nat Rev Clin Oncol*. 2014;11 (6) : 308-323.
62. Amling CL, Blute ML, Bergstralh EJ, Seay TM, Slezak J, Zincke H. Long-term hazard of progression after radical prostatectomy for clinically localized prostate cancer: continued risk of biochemical failure after 5 years. *J Urol*. 2000;164 (1) : 101-105.
63. Sharifi N, Gulley JL, Dahut WL. Androgen deprivation therapy for prostate cancer. *JAMA*. 2005;294 (2) : 238-244.
64. Cookson MS, Roth BJ, Dahm P, Engstrom C, Freedland SJ, Hussain M, Lin DW, Lowrance WT, Murad MH, Oh WK, Penson DF, Kibel AS. Castration-resistant prostate cancer: AUA Guideline. *J Urol*. 2013;190 (2) : 429-438.
65. Cornford P, Bellmunt J, Bolla M, Briers E, De Santis M, Gross T, Henry AM, Joniau S, Lam TB, Mason MD, van der Poel HG, van der Kwast TH, Rouviere O, Wiegel T, Mottet N. EAU-ESTRO-SIOG Guidelines on Prostate Cancer. Part II: Treatment of Relapsing, Metastatic, and Castration-Resistant Prostate Cancer. *Eur Urol*. 2017;71 (4) : 630-642.
66. Ryan CJ, Smith MR, de Bono JS, Molina A, Logothetis CJ, de Souza P, Fizazi K, Mainwaring P, Piulats JM, Ng S, Carles J, Mulders PF, Basch E, Small EJ, Saad F, Schrijvers D, Van Poppel H, Mukherjee SD, Suttman H, Gerritsen WR, Flaig TW, George DJ, Yu EY, Efsthathiou E, Pantuck A, Winquist E, Higano CS, Taplin ME, Park Y, Kheoh T, Griffin T, Scher HI, Rathkopf

- DE, Investigators C-A-. Abiraterone in metastatic prostate cancer without previous chemotherapy. *N Engl J Med.* 2013;368 (2): 138-148.
67. Raymond LW, Carr JP, Only C. Abiraterone in metastatic prostate cancer. *N Engl J Med.* 2013;368 (15): 1457-1458.
68. Beer TM, Armstrong AJ, Rathkopf DE, Loriot Y, Sternberg CN, Higano CS, Iversen P, Bhattacharya S, Carles J, Chowdhury S, Davis ID, de Bono JS, Evans CP, Fizazi K, Joshua AM, Kim CS, Kimura G, Mainwaring P, Mansbach H, Miller K, Noonberg SB, Perabo F, Phung D, Saad F, Scher HI, Taplin ME, Venner PM, Tombal B, Investigators P. Enzalutamide in metastatic prostate cancer before chemotherapy. *N Engl J Med.* 2014;371 (5): 424-433.
69. Elsada A, Pearce F, George E, Adler A. NICE guidance on enzalutamide for metastatic hormone-relapsed prostate cancer. *Lancet Oncol.* 2014;15 (10): 1058-1059.
70. Pal SK, Sartor O. Prostate cancer: the best fit for enzalutamide in metastatic prostate cancer. *Nat Rev Clin Oncol.* 2014;11 (9): 504-506.
71. Karantanos T, Corn PG, Thompson TC. Prostate cancer progression after androgen deprivation therapy: mechanisms of castrate resistance and novel therapeutic approaches. *Oncogene.* 2013;32 (49): 5501-5511.
72. Smith MR, Kabbinavar F, Saad F, Hussain A, Gittelman MC, Bilhartz DL, Wynne C, Murray R, Zinner NR, Schulman C, Linnartz R, Zheng M, Goessl C, Hei YJ, Small EJ, Cook R, Higano

- CS. Natural history of rising serum prostate-specific antigen in men with castrate nonmetastatic prostate cancer. *J Clin Oncol.* 2005;23 (13): 2918-2925.
73. Locke JA, Guns ES, Lubik AA, Adomat HH, Hendy SC, Wood CA, Ettinger SL, Gleave ME, Nelson CC. Androgen levels increase by intratumoral de novo steroidogenesis during progression of castration-resistant prostate cancer. *Cancer Res.* 2008;68 (15): 6407-6415.
74. Guo Z, Yang X, Sun F, Jiang R, Linn DE, Chen H, Chen H, Kong X, Melamed J, Tepper CG, Kung HJ, Brodie AM, Edwards J, Qiu Y. A novel androgen receptor splice variant is up-regulated during prostate cancer progression and promotes androgen depletion-resistant growth. *Cancer Res.* 2009;69 (6): 2305-2313.
75. Hu R, Dunn TA, Wei S, Isharwal S, Veltri RW, Humphreys E, Han M, Partin AW, Vessella RL, Isaacs WB, Bova GS, Luo J. Ligand-independent androgen receptor variants derived from splicing of cryptic exons signify hormone-refractory prostate cancer. *Cancer Res.* 2009;69 (1): 16-22.
76. Linja MJ, Savinainen KJ, Saramaki OR, Tammela TL, Vessella RL, Visakorpi T. Amplification and overexpression of androgen receptor gene in hormone-refractory prostate cancer. *Cancer Res.* 2001;61 (9): 3550-3555.
77. Marcelli M, Ittmann M, Mariani S, Sutherland R, Nigam R, Murthy L, Zhao Y, DiConcini D, Puxeddu E, Esen A, Eastham J, Weigel NL, Lamb DJ. Androgen receptor mutations in prostate cancer. *Cancer Res.* 2000;60 (4): 944-949.

78. Visakorpi T, Hyytinen E, Koivisto P, Tanner M, Keinanen R, Palmberg C, Palotie A, Tammela T, Isola J, Kallioniemi OP. In vivo amplification of the androgen receptor gene and progression of human prostate cancer. *Nat Genet.* 1995;9(4): 401-406.
79. Korpala M, Korn JM, Gao X, Rakiec DP, Ruddy DA, Doshi S, Yuan J, Kovats SG, Kim S, Cooke VG, Monahan JE, Stegmeier F, Roberts TM, Sellers WR, Zhou W, Zhu P. An F876L mutation in androgen receptor confers genetic and phenotypic resistance to MDV3100 (enzalutamide). *Cancer Discov.* 2013;3(9): 1030-1043.
80. Vlachostergios PJ, Puca L, Beltran H. Emerging Variants of Castration-Resistant Prostate Cancer. *Curr Oncol Rep.* 2017;19(5): 32.
81. Watson PA, Arora VK, Sawyers CL. Emerging mechanisms of resistance to androgen receptor inhibitors in prostate cancer. *Nat Rev Cancer.* 2015;15(12): 701-711.
82. Nadal R, Schweizer M, Kryvenko ON, Epstein JI, Eisenberger MA. Small cell carcinoma of the prostate. *Nat Rev Urol.* 2014;11(4): 213-219.
83. Hirano D, Okada Y, Minei S, Takimoto Y, Nemoto N. Neuroendocrine differentiation in hormone refractory prostate cancer following androgen deprivation therapy. *Eur Urol.* 2004;45(5): 586-592; discussion 592.
84. Sasaki T, Komiya A, Suzuki H, Shimbo M, Ueda T, Akakura K, Ichikawa T. Changes in chromogranin a serum levels during endocrine therapy in metastatic prostate cancer patients. *Eur Urol.* 2005;48(2): 224-229; discussion 229-230.

85. Aparicio A, Logothetis CJ, Maity SN. Understanding the lethal variant of prostate cancer: power of examining extremes. *Cancer Discov.* 2011;1 (6) : 466-468.
86. Beltran H, Tomlins S, Aparicio A, Arora V, Rickman D, Ayala G, Huang J, True L, Gleave ME, Soule H, Logothetis C, Rubin MA. Aggressive variants of castration-resistant prostate cancer. *Clin Cancer Res.* 2014;20(11) : 2846-2850.
87. Parimi V, Goyal R, Poropatich K, Yang XJ. Neuroendocrine differentiation of prostate cancer: a review. *Am J Clin Exp Urol.* 2014;2 (4) : 273-285.
88. Terry S, Beltran H. The many faces of neuroendocrine differentiation in prostate cancer progression. *Front Oncol.* 2014;4 (60).
89. Furtado P, Lima MV, Nogueira C, Franco M, Tavora F. Review of small cell carcinomas of the prostate. *Prostate Cancer.* 2011;2011 (543272).
90. Santoni M, Conti A, Burattini L, Berardi R, Scarpelli M, Cheng L, Lopez-Beltran A, Cascinu S, Montironi R. Neuroendocrine differentiation in prostate cancer: novel morphological insights and future therapeutic perspectives. *Biochim Biophys Acta.* 2014;1846 (2) : 630-637.
91. Smith BA, Sokolov A, Uzunangelov V, Baertsch R, Newton Y, Graim K, Mathis C, Cheng D, Stuart JM, Witte ON. A basal stem cell signature identifies aggressive prostate cancer phenotypes. *Proc Natl Acad Sci U S A.* 2015;112 (47) : E6544-6552.

92. Klimstra DS, Beltran H, Lilenbaum R, Bergsland E. The spectrum of neuroendocrine tumors: histologic classification, unique features and areas of overlap. *Am Soc Clin Oncol Educ Book*. 2015: 92-103.
93. Lotan TL, Gupta NS, Wang W, Toubaji A, Haffner MC, Chaux A, Hicks JL, Meeker AK, Bieberich CJ, De Marzo AM, Epstein JI, Netto GJ. ERG gene rearrangements are common in prostatic small cell carcinomas. *Mod Pathol*. 2011;24(6): 820-828.
94. Beltran H, Prandi D, Mosquera JM, Benelli M, Puca L, Cyrta J, Marotz C, Giannopoulou E, Chakravarthi BV, Varambally S, Tomlins SA, Nanus DM, Tagawa ST, Van Allen EM, Elemento O, Sboner A, Garraway LA, Rubin MA, Demichelis F. Divergent clonal evolution of castration-resistant neuroendocrine prostate cancer. *Nat Med*. 2016;22(3): 298-305.
95. Helpap B, Kollermann J, Oehler U. Neuroendocrine differentiation in prostatic carcinomas: histogenesis, biology, clinical relevance, and future therapeutical perspectives. *Urol Int*. 1999;62(3): 133-138.
96. Bluemn EG, Coleman IM, Lucas JM, Coleman RT, Hernandez-Lopez S, Tharakan R, Bianchi-Frias D, Dumpit RF, Kaipainen A, Corella AN, Yang YC, Nyquist MD, Mostaghel E, Hsieh AC, Zhang X, Corey E, Brown LG, Nguyen HM, Pienta K, Ittmann M, Schweizer M, True LD, Wise D, Rennie PS, Vessella RL, Morrissey C, Nelson PS. Androgen Receptor Pathway-Independent Prostate Cancer Is Sustained through FGF Signaling. *Cancer Cell*. 2017;32(4): 474-489 e476.

97. Priemer DS, Montironi R, Wang L, Williamson SR, Lopez-Beltran A, Cheng L. Neuroendocrine Tumors of the Prostate: Emerging Insights from Molecular Data and Updates to the 2016 World Health Organization Classification. *Endocr Pathol.* 2016;27(2): 123-135.
98. Wang HT, Yao YH, Li BG, Tang Y, Chang JW, Zhang J. Neuroendocrine Prostate Cancer (NEPC) progressing from conventional prostatic adenocarcinoma: factors associated with time to development of NEPC and survival from NEPC diagnosis-a systematic review and pooled analysis. *J Clin Oncol.* 2014;32(30): 3383-3390.
99. Beltran H, Rickman DS, Park K, Chae SS, Sboner A, MacDonald TY, Wang Y, Sheikh KL, Terry S, Tagawa ST, Dhir R, Nelson JB, de la Taille A, Allory Y, Gerstein MB, Perner S, Pienta KJ, Chinnaiyan AM, Wang Y, Collins CC, Gleave ME, Demichelis F, Nanus DM, Rubin MA. Molecular characterization of neuroendocrine prostate cancer and identification of new drug targets. *Cancer Discov.* 2011;1(6): 487-495.
100. Ku SY, Rosario S, Wang Y, Mu P, Seshadri M, Goodrich ZW, Goodrich MM, Labbe DP, Gomez EC, Wang J, Long HW, Xu B, Brown M, Loda M, Sawyers CL, Ellis L, Goodrich DW. Rb1 and Trp53 cooperate to suppress prostate cancer lineage plasticity, metastasis, and antiandrogen resistance. *Science.* 2017;355(6320): 78-83.
101. Mu P, Zhang Z, Benelli M, Karthaus WR, Hoover E, Chen CC, Wongvipat J, Ku SY, Gao D, Cao Z, Shah N, Adams EJ, Abida W, Watson PA, Prandi D, Huang CH, de Stanchina E, Lowe SW, Ellis L, Beltran H, Rubin MA, Goodrich DW, Demichelis F, Sawyers CL. SOX2 promotes

lineage plasticity and antiandrogen resistance in TP53- and RB1-deficient prostate cancer. *Science*. 2017;355 (6320) : 84-88.

102. Dardenne E, Beltran H, Benelli M, Gayvert K, Berger A, Puca L, Cyrta J, Sboner A, Noorzad Z, MacDonald T, Cheung C, Yuen KS, Gao D, Chen Y, Eilers M, Mosquera JM, Robinson BD, Elemento O, Rubin MA, Demichelis F, Rickman DS. N-Myc Induces an EZH2-Mediated Transcriptional Program Driving Neuroendocrine Prostate Cancer. *Cancer Cell*. 2016;30 (4) : 563-577.

103. Tran C, Ouk S, Clegg NJ, Chen Y, Watson PA, Arora V, Wongvipat J, Smith-Jones PM, Yoo D, Kwon A, Wasielewska T, Welsbie D, Chen CD, Higano CS, Beer TM, Hung DT, Scher HI, Jung ME, Sawyers CL. Development of a second-generation antiandrogen for treatment of advanced prostate cancer. *Science*. 2009;324 (5928) : 787-790.

104. Lin D, Wyatt AW, Xue H, Wang Y, Dong X, Haegert A, Wu R, Brahmhatt S, Mo F, Jong L, Bell RH, Anderson S, Hurtado-Coll A, Fazli L, Sharma M, Beltran H, Rubin M, Cox M, Gout PW, Morris J, Goldenberg L, Volik SV, Gleave ME, Collins CC, Wang Y. High fidelity patient-derived xenografts for accelerating prostate cancer discovery and drug development. *Cancer Res*. 2014;74 (4) : 1272-1283.

105. Zou M, Toivanen R, Mitrofanova A, Floch N, Hayati S, Sun Y, Le Magnen C, Chester D, Mostaghel EA, Califano A, Rubin MA, Shen MM, Abate-Shen C. Transdifferentiation as a

Mechanism of Treatment Resistance in a Mouse Model of Castration-Resistant Prostate Cancer.

Cancer Discov. 2017;7(7): 736-749.

106. DeCaprio JA, Ludlow JW, Figge J, Shew JY, Huang CM, Lee WH, Marsilio E, Paucha E, Livingston DM. SV40 large tumor antigen forms a specific complex with the product of the retinoblastoma susceptibility gene. Cell. 1988;54(2): 275-283.

107. Linzer DI, Levine AJ. Characterization of a 54K dalton cellular SV40 tumor antigen present in SV40-transformed cells and uninfected embryonal carcinoma cells. Cell. 1979;17(1): 43-52.

108. Kaplan-Lefko PJ, Chen TM, Ittmann MM, Barrios RJ, Ayala GE, Huss WJ, Maddison LA, Foster BA, Greenberg NM. Pathobiology of autochthonous prostate cancer in a pre-clinical transgenic mouse model. Prostate. 2003;55(3): 219-237.

109. Gingrich JR, Barrios RJ, Morton RA, Boyce BF, DeMayo FJ, Finegold MJ, Angelopoulou R, Rosen JM, Greenberg NM. Metastatic prostate cancer in a transgenic mouse. Cancer Res. 1996;56(18): 4096-4102.

110. Garabedian EM, Humphrey PA, Gordon JI. A transgenic mouse model of metastatic prostate cancer originating from neuroendocrine cells. Proc Natl Acad Sci U S A. 1998;95(26): 15382-15387.

111. Clermont PL, Lin D, Crea F, Wu R, Xue H, Wang Y, Thu KL, Lam WL, Collins CC, Wang Y, Helgason CD. Polycomb-mediated silencing in neuroendocrine prostate cancer. Clin Epigenetics. 2015;7(40).

112. Bishop JL, Thaper D, Vahid S, Davies A, Ketola K, Kuruma H, Jama R, Nip KM, Angeles A, Johnson F, Wyatt AW, Fazli L, Gleave ME, Lin D, Rubin MA, Collins CC, Wang Y, Beltran H, Zoubeidi A. The Master Neural Transcription Factor BRN2 Is an Androgen Receptor-Suppressed Driver of Neuroendocrine Differentiation in Prostate Cancer. *Cancer Discov.* 2017;7(1): 54-71.
113. Ci X, Hao J, Dong X, Choi SY, Xue H, Wu R, Qu S, Gout PW, Zhang F, Haegert AM, Fazli L, Crea F, Ong CJ, Zoubeidi A, He HH, Gleave ME, Collins CC, Lin D, Wang Y. Heterochromatin Protein 1alpha Mediates Development and Aggressiveness of Neuroendocrine Prostate Cancer. *Cancer Res.* 2018;78(10): 2691-2704.
114. Li Y, Donmez N, Sahinalp C, Xie N, Wang Y, Xue H, Mo F, Beltran H, Gleave M, Wang Y, Collins C, Dong X. SRRM4 Drives Neuroendocrine Transdifferentiation of Prostate Adenocarcinoma Under Androgen Receptor Pathway Inhibition. *Eur Urol.* 2017;71(1): 68-78.
115. Black DL. Mechanisms of alternative pre-messenger RNA splicing. *Annu Rev Biochem.* 2003;72(291-336).
116. Kan Z, Rouchka EC, Gish WR, States DJ. Gene structure prediction and alternative splicing analysis using genomically aligned ESTs. *Genome Res.* 2001;11(5): 889-900.
117. Lander ES, Linton LM, Birren B, Nusbaum C, Zody MC, Baldwin J, Devon K, Dewar K, Doyle M, FitzHugh W, Funke R, Gage D, Harris K, Heaford A, Howland J, Kann L, Lehoczky J, LeVine R, McEwan P, McKernan K, Meldrim J, Mesirov JP, Miranda C, Morris W, Naylor J,

Raymond C, Rosetti M, Santos R, Sheridan A, Sougnez C, Stange-Thomann Y, Stojanovic N, Subramanian A, Wyman D, Rogers J, Sulston J, Ainscough R, Beck S, Bentley D, Burton J, Clee C, Carter N, Coulson A, Deadman R, Deloukas P, Dunham A, Dunham I, Durbin R, French L, Grafham D, Gregory S, Hubbard T, Humphray S, Hunt A, Jones M, Lloyd C, McMurray A, Matthews L, Mercer S, Milne S, Mullikin JC, Mungall A, Plumb R, Ross M, Shownkeen R, Sims S, Waterston RH, Wilson RK, Hillier LW, McPherson JD, Marra MA, Mardis ER, Fulton LA, Chinwalla AT, Pepin KH, Gish WR, Chissoe SL, Wendl MC, Delehaunty KD, Miner TL, Delehaunty A, Kramer JB, Cook LL, Fulton RS, Johnson DL, Minx PJ, Clifton SW, Hawkins T, Branscomb E, Predki P, Richardson P, Wenning S, Slezak T, Doggett N, Cheng JF, Olsen A, Lucas S, Elkin C, Uberbacher E, Frazier M, Gibbs RA, Muzny DM, Scherer SE, Bouck JB, Sodergren EJ, Worley KC, Rives CM, Gorrell JH, Metzker ML, Naylor SL, Kucherlapati RS, Nelson DL, Weinstock GM, Sakaki Y, Fujiyama A, Hattori M, Yada T, Toyoda A, Itoh T, Kawagoe C, Watanabe H, Totoki Y, Taylor T, Weissenbach J, Heilig R, Saurin W, Artiguenave F, Brottier P, Bruls T, Pelletier E, Robert C, Wincker P, Smith DR, Doucette-Stamm L, Rubenfield M, Weinstock K, Lee HM, Dubois J, Rosenthal A, Platzer M, Nyakatura G, Taudien S, Rump A, Yang H, Yu J, Wang J, Huang G, Gu J, Hood L, Rowen L, Madan A, Qin S, Davis RW, Federspiel NA, Abola AP, Proctor MJ, Myers RM, Schmutz J, Dickson M, Grimwood J, Cox DR, Olson MV, Kaul R, Raymond C, Shimizu N, Kawasaki K, Minoshima S, Evans GA, Athanasiou M, Schultz R, Roe BA, Chen F, Pan H, Ramser J, Lehrach H, Reinhardt R, McCombie WR, de la Bastide M,

Dedhia N, Blocker H, Hornischer K, Nordsiek G, Agarwala R, Aravind L, Bailey JA, Bateman A, Batzoglou S, Birney E, Bork P, Brown DG, Burge CB, Cerutti L, Chen HC, Church D, Clamp M, Copley RR, Doerks T, Eddy SR, Eichler EE, Furey TS, Galagan J, Gilbert JG, Harmon C, Hayashizaki Y, Haussler D, Hermjakob H, Hokamp K, Jang W, Johnson LS, Jones TA, Kasif S, Kasprzyk A, Kennedy S, Kent WJ, Kitts P, Koonin EV, Korf I, Kulp D, Lancet D, Lowe TM, McLysaght A, Mikkelsen T, Moran JV, Mulder N, Pollara VJ, Ponting CP, Schuler G, Schultz J, Slater G, Smit AF, Stupka E, Szustakowki J, Thierry-Mieg D, Thierry-Mieg J, Wagner L, Wallis J, Wheeler R, Williams A, Wolf YI, Wolfe KH, Yang SP, Yeh RF, Collins F, Guyer MS, Peterson J, Felsenfeld A, Wetterstrand KA, Patrinos A, Morgan MJ, de Jong P, Catanese JJ, Osoegawa K, Shizuya H, Choi S, Chen YJ, Szustakowki J, International Human Genome Sequencing C. Initial sequencing and analysis of the human genome. *Nature*. 2001;409(6822): 860-921.

118. Modrek B, Resch A, Grasso C, Lee C. Genome-wide detection of alternative splicing in expressed sequences of human genes. *Nucleic Acids Res*. 2001;29(13): 2850-2859.

119. Modrek B, Lee C. A genomic view of alternative splicing. *Nat Genet*. 2002;30(1): 13-19.

120. Pan Q, Shai O, Lee LJ, Frey BJ, Blencowe BJ. Deep surveying of alternative splicing complexity in the human transcriptome by high-throughput sequencing. *Nat Genet*. 2008;40(12): 1413-1415.

121. Matlin AJ, Clark F, Smith CW. Understanding alternative splicing: towards a cellular code. *Nat Rev Mol Cell Biol*. 2005;6(5): 386-398.

122. David CJ, Manley JL. The search for alternative splicing regulators: new approaches offer a path to a splicing code. *Genes Dev.* 2008;22 (3) : 279-285.
123. Gao K, Masuda A, Matsuura T, Ohno K. Human branch point consensus sequence is yUnAy. *Nucleic Acids Res.* 2008;36 (7) : 2257-2267.
124. Wang Z, Burge CB. Splicing regulation: from a parts list of regulatory elements to an integrated splicing code. *RNA.* 2008;14 (5) : 802-813.
125. Barash Y, Calarco JA, Gao W, Pan Q, Wang X, Shai O, Blencowe BJ, Frey BJ. Deciphering the splicing code. *Nature.* 2010;465 (7294) : 53-59.
126. Irimia M, Blencowe BJ. Alternative splicing: decoding an expansive regulatory layer. *Curr Opin Cell Biol.* 2012;24 (3) : 323-332.
127. Buljan M, Chalancon G, Eustermann S, Wagner GP, Fuxreiter M, Bateman A, Babu MM. Tissue-specific splicing of disordered segments that embed binding motifs rewires protein interaction networks. *Mol Cell.* 2012;46 (6) : 871-883.
128. Romero PR, Zaidi S, Fang YY, Uversky VN, Radivojac P, Oldfield CJ, Cortese MS, Sickmeier M, LeGall T, Obradovic Z, Dunker AK. Alternative splicing in concert with protein intrinsic disorder enables increased functional diversity in multicellular organisms. *Proc Natl Acad Sci U S A.* 2006;103 (22) : 8390-8395.

129. Ellis JD, Barrios-Rodiles M, Colak R, Irimia M, Kim T, Calarco JA, Wang X, Pan Q, O'Hanlon D, Kim PM, Wrana JL, Blencowe BJ. Tissue-specific alternative splicing remodels protein-protein interaction networks. *Mol Cell*. 2012;46(6): 884-892.
130. Weatheritt RJ, Davey NE, Gibson TJ. Linear motifs confer functional diversity onto splice variants. *Nucleic Acids Res*. 2012;40(15): 7123-7131.
131. Johnson JM, Castle J, Garrett-Engele P, Kan Z, Loerch PM, Armour CD, Santos R, Schadt EE, Stoughton R, Shoemaker DD. Genome-wide survey of human alternative pre-mRNA splicing with exon junction microarrays. *Science*. 2003;302(5653): 2141-2144.
132. Sveen A, Agesen TH, Nesbakken A, Rognum TO, Lothe RA, Skotheim RI. Transcriptome instability in colorectal cancer identified by exon microarray analyses: Associations with splicing factor expression levels and patient survival. *Genome Med*. 2011;3(5): 32.
133. Taggart AJ, DeSimone AM, Shih JS, Filloux ME, Fairbrother WG. Large-scale mapping of branchpoints in human pre-mRNA transcripts in vivo. *Nat Struct Mol Biol*. 2012;19(7): 719-721.
134. Sveen A, Kilpinen S, Ruusulehto A, Lothe RA, Skotheim RI. Aberrant RNA splicing in cancer; expression changes and driver mutations of splicing factor genes. *Oncogene*. 2016;35(19): 2413-2427.
135. Skotheim RI, Nees M. Alternative splicing in cancer: noise, functional, or systematic? *Int J Biochem Cell Biol*. 2007;39(7-8): 1432-1449.
136. Ward AJ, Cooper TA. The pathobiology of splicing. *J Pathol*. 2010;220(2): 152-163.

137. He C, Zhou F, Zuo Z, Cheng H, Zhou R. A global view of cancer-specific transcript variants by subtractive transcriptome-wide analysis. *PLoS One*. 2009;4(3): e4732.
138. Lopez-Bigas N, Audit B, Ouzounis C, Parra G, Guigo R. Are splicing mutations the most frequent cause of hereditary disease? *FEBS Lett*. 2005;579(9): 1900-1903.
139. Lim KH, Ferraris L, Filloux ME, Raphael BJ, Fairbrother WG. Using positional distribution to identify splicing elements and predict pre-mRNA processing defects in human genes. *Proc Natl Acad Sci U S A*. 2011;108(27): 11093-11098.
140. Omenn GS, Guan Y, Menon R. A new class of protein cancer biomarker candidates: differentially expressed splice variants of ERBB2 (HER2/neu) and ERBB1 (EGFR) in breast cancer cell lines. *J Proteomics*. 2014;107(103-112).
141. Wang ET, Sandberg R, Luo S, Khrebtkova I, Zhang L, Mayr C, Kingsmore SF, Schroth GP, Burge CB. Alternative isoform regulation in human tissue transcriptomes. *Nature*. 2008;456(7221): 470-476.
142. Calarco JA, Zhen M, Blencowe BJ. Networking in a global world: establishing functional connections between neural splicing regulators and their target transcripts. *RNA*. 2011;17(5): 775-791.
143. Li Q, Lee JA, Black DL. Neuronal regulation of alternative pre-mRNA splicing. *Nat Rev Neurosci*. 2007;8(11): 819-831.

144. Jensen KB, Dredge BK, Stefani G, Zhong R, Buckanovich RJ, Okano HJ, Yang YY, Darnell RB. Nova-1 regulates neuron-specific alternative splicing and is essential for neuronal viability. *Neuron*. 2000;25 (2) : 359-371.
145. Coutinho-Mansfield GC, Xue Y, Zhang Y, Fu XD. PTB/nPTB switch: a post-transcriptional mechanism for programming neuronal differentiation. *Genes Dev*. 2007;21 (13) : 1573-1577.
146. Schoenherr CJ, Anderson DJ. The neuron-restrictive silencer factor (NRSF): a coordinate repressor of multiple neuron-specific genes. *Science*. 1995;267 (5202) : 1360-1363.
147. Chong JA, Tapia-Ramirez J, Kim S, Toledo-Aral JJ, Zheng Y, Boutros MC, Altshuler YM, Frohman MA, Kraner SD, Mandel G. REST: a mammalian silencer protein that restricts sodium channel gene expression to neurons. *Cell*. 1995;80 (6) : 949-957.
148. Andres ME, Burger C, Peral-Rubio MJ, Battaglioli E, Anderson ME, Grimes J, Dallman J, Ballas N, Mandel G. CoREST: a functional corepressor required for regulation of neural-specific gene expression. *Proc Natl Acad Sci U S A*. 1999;96 (17) : 9873-9878.
149. Grimes JA, Nielsen SJ, Battaglioli E, Miska EA, Speh JC, Berry DL, Atouf F, Holdener BC, Mandel G, Kouzarides T. The co-repressor mSin3A is a functional component of the REST-CoREST repressor complex. *J Biol Chem*. 2000;275 (13) : 9461-9467.
150. Huang Y, Myers SJ, Dingledine R. Transcriptional repression by REST: recruitment of Sin3A and histone deacetylase to neuronal genes. *Nat Neurosci*. 1999;2 (10) : 867-872.

151. Naruse Y, Aoki T, Kojima T, Mori N. Neural restrictive silencer factor recruits mSin3 and histone deacetylase complex to repress neuron-specific target genes. *Proc Natl Acad Sci U S A*. 1999;96(24): 13691-13696.
152. Tachibana M, Sugimoto K, Fukushima T, Shinkai Y. Set domain-containing protein, G9a, is a novel lysine-preferring mammalian histone methyltransferase with hyperactivity and specific selectivity to lysines 9 and 27 of histone H3. *J Biol Chem*. 2001;276(27): 25309-25317.
153. Zhang Q, Piston DW, Goodman RH. Regulation of corepressor function by nuclear NADH. *Science*. 2002;295(5561): 1895-1897.
154. Zhang Y, Sun ZW, Iratni R, Erdjument-Bromage H, Tempst P, Hampsey M, Reinberg D. SAP30, a novel protein conserved between human and yeast, is a component of a histone deacetylase complex. *Mol Cell*. 1998;1(7): 1021-1031.
155. Roopra A, Sharling L, Wood IC, Briggs T, Bachfischer U, Paquette AJ, Buckley NJ. Transcriptional repression by neuron-restrictive silencer factor is mediated via the Sin3-histone deacetylase complex. *Mol Cell Biol*. 2000;20(6): 2147-2157.
156. Alland L, David G, Shen-Li H, Potes J, Muhle R, Lee HC, Hou H, Jr., Chen K, DePinho RA. Identification of mammalian Sds3 as an integral component of the Sin3/histone deacetylase corepressor complex. *Mol Cell Biol*. 2002;22(8): 2743-2750.
157. Chen ZF, Paquette AJ, Anderson DJ. NRSF/REST is required in vivo for repression of multiple neuronal target genes during embryogenesis. *Nat Genet*. 1998;20(2): 136-142.

158. Paquette AJ, Perez SE, Anderson DJ. Constitutive expression of the neuron-restrictive silencer factor (NRSF)/REST in differentiating neurons disrupts neuronal gene expression and causes axon pathfinding errors in vivo. *Proc Natl Acad Sci U S A*. 2000;97 (22): 12318-12323.
159. Zhang X, Coleman IM, Brown LG, True LD, Kollath L, Lucas JM, Lam HM, Dumpit R, Corey E, Chery L, Lakely B, Higano CS, Montgomery B, Roudier M, Lange PH, Nelson PS, Vessella RL, Morrissey C. SRRM4 Expression and the Loss of REST Activity May Promote the Emergence of the Neuroendocrine Phenotype in Castration-Resistant Prostate Cancer. *Clin Cancer Res*. 2015;21 (20): 4698-4708.
160. Lapuk AV, Wu C, Wyatt AW, McPherson A, McConeghy BJ, Brahmabhatt S, Mo F, Zoubeidi A, Anderson S, Bell RH, Haegert A, Shukin R, Wang Y, Fazli L, Hurtado-Coll A, Jones EC, Hach F, Hormozdiari F, Hajirasouliha I, Boutros PC, Bristow RG, Zhao Y, Marra MA, Fanjul A, Maher CA, Chinnaiyan AM, Rubin MA, Beltran H, Sahinalp SC, Gleave ME, Volik SV, Collins CC. From sequence to molecular pathology, and a mechanism driving the neuroendocrine phenotype in prostate cancer. *J Pathol*. 2012;227 (3): 286-297.
161. Chang YT, Lin TP, Campbell M, Pan CC, Lee SH, Lee HC, Yang MH, Kung HJ, Chang PC. REST is a crucial regulator for acquiring EMT-like and stemness phenotypes in hormone-refractory prostate cancer. *Sci Rep*. 2017;7 (42795).

162. Lee N, Park SJ, Haddad G, Kim DK, Park SM, Park SK, Choi KY. Interactomic analysis of REST/NRSF and implications of its functional links with the transcription suppressor TRIM28 during neuronal differentiation. *Sci Rep.* 2016;6 (39049).
163. Tawadros T, Martin D, Abderrahmani A, Leisinger HJ, Waeber G, Haefliger JA. IB1/JIP-1 controls JNK activation and increased during prostatic LNCaP cells neuroendocrine differentiation. *Cell Signal.* 2005;17 (8) : 929-939.
164. Qureshi IA, Mehler MF. Regulation of non-coding RNA networks in the nervous system--what's the REST of the story? *Neurosci Lett.* 2009;466 (2) : 73-80.
165. Palm K, Belluardo N, Metsis M, Timmusk T. Neuronal expression of zinc finger transcription factor REST/NRSF/XBR gene. *J Neurosci.* 1998;18 (4) : 1280-1296.
166. Palm K, Metsis M, Timmusk T. Neuron-specific splicing of zinc finger transcription factor REST/NRSF/XBR is frequent in neuroblastomas and conserved in human, mouse and rat. *Brain Res Mol Brain Res.* 1999;72 (1) : 30-39.
167. Zhu Y, Liu C, Cui Y, Nadiminty N, Lou W, Gao AC. Interleukin-6 induces neuroendocrine differentiation (NED) through suppression of RE-1 silencing transcription factor (REST). *Prostate.* 2014;74 (11) : 1086-1094.
168. Chen R, Li Y, Buttyan R, Dong X. Implications of PI3K/AKT inhibition on REST protein stability and neuroendocrine phenotype acquisition in prostate cancer cells. *Oncotarget.* 2017;8 (49) : 84863-84876.

169. Kim J, Jin H, Zhao JC, Yang YA, Li Y, Yang X, Dong X, Yu J. FOXA1 inhibits prostate cancer neuroendocrine differentiation. *Oncogene*. 2017;36(28): 4072-4080.
170. Deeble PD, Murphy DJ, Parsons SJ, Cox ME. Interleukin-6- and cyclic AMP-mediated signaling potentiates neuroendocrine differentiation of LNCaP prostate tumor cells. *Mol Cell Biol*. 2001;21(24): 8471-8482.
171. Bang YJ, Pirnia F, Fang WG, Kang WK, Sartor O, Whitesell L, Ha MJ, Tsokos M, Sheahan MD, Nguyen P, Niklinski WT, Myers CE, Trepel JB. Terminal neuroendocrine differentiation of human prostate carcinoma cells in response to increased intracellular cyclic AMP. *Proc Natl Acad Sci U S A*. 1994;91(12): 5330-5334.
172. Cox ME, Deeble PD, Lakhani S, Parsons SJ. Acquisition of neuroendocrine characteristics by prostate tumor cells is reversible: implications for prostate cancer progression. *Cancer Res*. 1999;59(15): 3821-3830.
173. Lin TP, Chang YT, Lee SY, Campbell M, Wang TC, Shen SH, Chung HJ, Chang YH, Chiu AW, Pan CC, Lin CH, Chu CY, Kung HJ, Cheng CY, Chang PC. REST reduction is essential for hypoxia-induced neuroendocrine differentiation of prostate cancer cells by activating autophagy signaling. *Oncotarget*. 2016;7(18): 26137-26151.
174. Deng X, Elzey BD, Poulson JM, Morrison WB, Ko SC, Hahn NM, Ratliff TL, Hu CD. Ionizing radiation induces neuroendocrine differentiation of prostate cancer cells in vitro, in vivo and in prostate cancer patients. *Am J Cancer Res*. 2011;1(7): 834-844.

175. di Sant'Agnesse PA. Neuroendocrine differentiation in carcinoma of the prostate. Diagnostic, prognostic, and therapeutic implications. *Cancer*. 1992;70 (1 Suppl): 254-268.
176. Abrahamsson PA. Neuroendocrine differentiation in prostatic carcinoma. *Prostate*. 1999;39 (2): 135-148.
177. Vashchenko N, Abrahamsson PA. Neuroendocrine differentiation in prostate cancer: implications for new treatment modalities. *Eur Urol*. 2005;47 (2): 147-155.
178. Sainz RM, Mayo JC, Tan DX, Leon J, Manchester L, Reiter RJ. Melatonin reduces prostate cancer cell growth leading to neuroendocrine differentiation via a receptor and PKA independent mechanism. *Prostate*. 2005;63 (1): 29-43.
179. Wright ME, Tsai MJ, Aebersold R. Androgen receptor represses the neuroendocrine transdifferentiation process in prostate cancer cells. *Mol Endocrinol*. 2003;17 (9): 1726-1737.
180. Mori S, Murakami-Mori K, Bonavida B. Interleukin-6 induces G1 arrest through induction of p27(Kip1), a cyclin-dependent kinase inhibitor, and neuron-like morphology in LNCaP prostate tumor cells. *Biochem Biophys Res Commun*. 1999;257 (2): 609-614.
181. Lee AR, Li Y, Xie N, Gleave ME, Cox ME, Collins CC, Dong X. Alternative RNA splicing of the MEAF6 gene facilitates neuroendocrine prostate cancer progression. *Oncotarget*. 2017;8 (17): 27966-27975.
182. Mosquera JM, Beltran H, Park K, MacDonald TY, Robinson BD, Tagawa ST, Perner S, Bismar TA, Erbersdobler A, Dhir R, Nelson JB, Nanus DM, Rubin MA. Concurrent AURKA and

MYCN gene amplifications are harbingers of lethal treatment-related neuroendocrine prostate cancer. *Neoplasia*. 2013;15(1): 1-10.

183. Akamatsu S, Wyatt AW, Lin D, Lysakowski S, Zhang F, Kim S, Tse C, Wang K, Mo F, Haegert A, Brahmabhatt S, Bell R, Adomat H, Kawai Y, Xue H, Dong X, Fazli L, Tsai H, Lotan TL, Kossai M, Mosquera JM, Rubin MA, Beltran H, Zoubeidi A, Wang Y, Gleave ME, Collins CC. The Placental Gene PEG10 Promotes Progression of Neuroendocrine Prostate Cancer. *Cell Rep*. 2015;12(6): 922-936.

184. Tsai H, Morais CL, Alshalalfa M, Tan HL, Haddad Z, Hicks J, Gupta N, Epstein JI, Netto GJ, Isaacs WB, Luo J, Mehra R, Vessella RL, Karnes RJ, Schaeffer EM, Davicioni E, De Marzo AM, Lotan TL. Cyclin D1 Loss Distinguishes Prostatic Small-Cell Carcinoma from Most Prostatic Adenocarcinomas. *Clin Cancer Res*. 2015;21(24): 5619-5629.

185. Dominguez-Brauer C, Thu KL, Mason JM, Blaser H, Bray MR, Mak TW. Targeting Mitosis in Cancer: Emerging Strategies. *Mol Cell*. 2015;60(4): 524-536.

186. Culine S, El Demery M, Lamy PJ, Iborra F, Avances C, Pinguet F. Docetaxel and cisplatin in patients with metastatic androgen independent prostate cancer and circulating neuroendocrine markers. *J Urol*. 2007;178(3 Pt 1): 844-848; discussion 848.

187. Aparicio AM, Harzstark AL, Corn PG, Wen S, Araujo JC, Tu SM, Pagliaro LC, Kim J, Millikan RE, Ryan C, Tannir NM, Zurita AJ, Mathew P, Arap W, Troncso P, Thall PF, Logothetis

- CJ. Platinum-based chemotherapy for variant castrate-resistant prostate cancer. *Clin Cancer Res.* 2013;19(13): 3621-3630.
188. Meulenbeld HJ, Bleuse JP, Vinci EM, Raymond E, Vitali G, Santoro A, Dogliotti L, Berardi R, Cappuzzo F, Tagawa ST, Sternberg CN, Jannuzzo MG, Mariani M, Petroccione A, de Wit R. Randomized phase II study of danusertib in patients with metastatic castration-resistant prostate cancer after docetaxel failure. *BJU Int.* 2013;111(1): 44-52.
189. Beltran H, Rubin MA. New strategies in prostate cancer: translating genomics into the clinic. *Clin Cancer Res.* 2013;19(3): 517-523.
190. Molife LR, Yan L, Vitfell-Rasmussen J, Zernhelt AM, Sullivan DM, Cassier PA, Chen E, Biondo A, Tetteh E, Siu LL, Patnaik A, Papadopoulos KP, de Bono JS, Tolcher AW, Minton S. Phase 1 trial of the oral AKT inhibitor MK-2206 plus carboplatin/paclitaxel, docetaxel, or erlotinib in patients with advanced solid tumors. *J Hematol Oncol.* 2014;7(1).
191. Rybak AP, Tang D. SOX2 plays a critical role in EGFR-mediated self-renewal of human prostate cancer stem-like cells. *Cell Signal.* 2013;25(12): 2734-2742.
192. Ren C, Ren T, Yang K, Wang S, Bao X, Zhang F, Guo W. Inhibition of SOX2 induces cell apoptosis and G1/S arrest in Ewing's sarcoma through the PI3K/Akt pathway. *J Exp Clin Cancer Res.* 2016;35(44).
193. Dobin A, Davis CA, Schlesinger F, Drenkow J, Zaleski C, Jha S, Batut P, Chaisson M, Gingeras TR. STAR: ultrafast universal RNA-seq aligner. *Bioinformatics.* 2013;29(1): 15-21.

194. Trapnell C, Pachter L, Salzberg SL. TopHat: discovering splice junctions with RNA-Seq. *Bioinformatics*. 2009;25 (9): 1105-1111.
195. Katz Y, Wang ET, Airoidi EM, Burge CB. Analysis and design of RNA sequencing experiments for identifying isoform regulation. *Nat Methods*. 2010;7 (12): 1009-1015.
196. Li H, Xie N, Chen R, Verreault M, Fazli L, Gleave ME, Barbier O, Dong X. UGT2B17 Expedites Progression of Castration-Resistant Prostate Cancers by Promoting Ligand-Independent AR Signaling. *Cancer Res*. 2016;76 (22): 6701-6711.
197. Yu Y, Yang O, Fazli L, Rennie PS, Gleave ME, Dong X. Progesterone receptor expression during prostate cancer progression suggests a role of this receptor in stromal cell differentiation. *Prostate*. 2015;75 (10): 1043-1050.
198. Xie N, Liu L, Li Y, Yu C, Lam S, Shynlova O, Gleave M, Challis JR, Lye S, Dong X. Expression and function of myometrial PSF suggest a role in progesterone withdrawal and the initiation of labor. *Mol Endocrinol*. 2012;26 (8): 1370-1379.
199. Zhang MX, Ou H, Shen YH, Wang J, Wang J, Coselli J, Wang XL. Regulation of endothelial nitric oxide synthase by small RNA. *Proc Natl Acad Sci U S A*. 2005;102 (47): 16967-16972.
200. Raj B, Irimia M, Braunschweig U, Sterne-Weiler T, O'Hanlon D, Lin ZY, Chen GI, Easton LE, Ule J, Gingras AC, Eyraas E, Blencowe BJ. A global regulatory mechanism for activating an exon network required for neurogenesis. *Mol Cell*. 2014;56 (1): 90-103.

201. Nakano Y, Jahan I, Bonde G, Sun X, Hildebrand MS, Engelhardt JF, Smith RJ, Cornell RA, Fritsch B, Banfi B. A mutation in the *Srrm4* gene causes alternative splicing defects and deafness in the Bronx waltzer mouse. *PLoS Genet.* 2012;8(10): e1002966.
202. Altman DG, Bland JM. Diagnostic tests. 1: Sensitivity and specificity. *BMJ.* 1994;308(6943): 1552.
203. Wang DB, Kinoshita Y, Kinoshita C, Uo T, Sopher BL, Cudaback E, Keene CD, Bilousova T, Gyls K, Case A, Jayadev S, Wang HG, Garden GA, Morrison RS. Loss of endophilin-B1 exacerbates Alzheimer's disease pathology. *Brain.* 2015;138(Pt 7): 2005-2019.
204. Wang DB, Uo T, Kinoshita C, Sopher BL, Lee RJ, Murphy SP, Kinoshita Y, Garden GA, Wang HG, Morrison RS. Bax interacting factor-1 promotes survival and mitochondrial elongation in neurons. *J Neurosci.* 2014;34(7): 2674-2683.
205. Cai C, Chen S, Ng P, Bublely GJ, Nelson PS, Mostaghel EA, Marck B, Matsumoto AM, Simon NI, Wang H, Chen S, Balk SP. Intratumoral de novo steroid synthesis activates androgen receptor in castration-resistant prostate cancer and is upregulated by treatment with CYP17A1 inhibitors. *Cancer Res.* 2011;71(20): 6503-6513.
206. Raj B, O'Hanlon D, Vessey JP, Pan Q, Ray D, Buckley NJ, Miller FD, Blencowe BJ. Cross-regulation between an alternative splicing activator and a transcription repressor controls neurogenesis. *Mol Cell.* 2011;43(5): 843-850.

207. Conteduca V, Burgio SL, Menna C, Carretta E, Rossi L, Bianchi E, Masini C, Amadori D, De Giorgi U. Chromogranin A is a potential prognostic marker in prostate cancer patients treated with enzalutamide. *Prostate*. 2014;74(16): 1691-1696.
208. Burgio SL, Conteduca V, Menna C, Carretta E, Rossi L, Bianchi E, Kopf B, Fabbri F, Amadori D, De Giorgi U. Chromogranin A predicts outcome in prostate cancer patients treated with abiraterone. *Endocr Relat Cancer*. 2014;21(3): 487-493.
209. Calarco JA, Superina S, O'Hanlon D, Gabut M, Raj B, Pan Q, Skalska U, Clarke L, Gelinas D, van der Kooy D, Zhen M, Ciruna B, Blencowe BJ. Regulation of vertebrate nervous system alternative splicing and development by an SR-related protein. *Cell*. 2009;138(5): 898-910.
210. Shimojo M, Shudo Y, Ikeda M, Kobashi T, Ito S. The small cell lung cancer-specific isoform of RE1-silencing transcription factor (REST) is regulated by neural-specific Ser/Arg repeat-related protein of 100 kDa (nSR100). *Mol Cancer Res*. 2013;11(10): 1258-1268.
211. Scher HI, Fizazi K, Saad F, Taplin ME, Sternberg CN, Miller K, de Wit R, Mulders P, Chi KN, Shore ND, Armstrong AJ, Flaig TW, Flechon A, Mainwaring P, Fleming M, Hainsworth JD, Hirmand M, Selby B, Seely L, de Bono JS, Investigators A. Increased survival with enzalutamide in prostate cancer after chemotherapy. *N Engl J Med*. 2012;367(13): 1187-1197.
212. Svensson C, Ceder J, Iglesias-Gato D, Chuan YC, Pang ST, Bjartell A, Martinez RM, Bott L, Helczynski L, Ulmert D, Wang Y, Niu Y, Collins C, Flores-Morales A. REST mediates

androgen receptor actions on gene repression and predicts early recurrence of prostate cancer.

Nucleic Acids Res. 2014;42 (2) : 999-1015.

213. Gopalakrishnan V. REST and the RESTless: in stem cells and beyond. Future Neurol.

2009;4 (3) : 317-329.

214. Shen R, Dorai T, Szaboles M, Katz AE, Olsson CA, Buttyan R. Transdifferentiation of cultured human prostate cancer cells to a neuroendocrine cell phenotype in a hormone-depleted medium. Urol Oncol. 1997;3 (2) : 67-75.

215. Delk NA, Farach-Carson MC. Interleukin-6: a bone marrow stromal cell paracrine signal that induces neuroendocrine differentiation and modulates autophagy in bone metastatic PCa cells.

Autophagy. 2012;8 (4) : 650-663.

216. Cortes MA, Cariaga-Martinez AE, Lobo MV, Martin Orozco RM, Motino O, Rodriguez-Ubreva FJ, Angulo J, Lopez-Ruiz P, Colas B. EGF promotes neuroendocrine-like differentiation of prostate cancer cells in the presence of LY294002 through increased ErbB2 expression

independent of the phosphatidylinositol 3-kinase-AKT pathway. Carcinogenesis. 2012;33 (6) : 1169-1177.

217. Sauer CG, Roemer A, Grobholz R. Genetic analysis of neuroendocrine tumor cells in prostatic carcinoma. Prostate. 2006;66 (3) : 227-234.

218. Mucci NR, Akdas G, Manely S, Rubin MA. Neuroendocrine expression in metastatic prostate cancer: evaluation of high throughput tissue microarrays to detect heterogeneous protein expression. *Hum Pathol.* 2000;31 (4) : 406-414.
219. Kleb B, Estecio MR, Zhang J, Tzelepi V, Chung W, Jelinek J, Navone NM, Tahir S, Marquez VE, Issa JP, Maity S, Aparicio A. Differentially methylated genes and androgen receptor re-expression in small cell prostate carcinomas. *Epigenetics.* 2016;11 (3) : 184-193.
220. Bartel DP. MicroRNAs: target recognition and regulatory functions. *Cell.* 2009;136 (2) : 215-233.
221. Fabian MR, Sonenberg N, Filipowicz W. Regulation of mRNA translation and stability by microRNAs. *Annu Rev Biochem.* 2010;79 (351-379).
222. Zhao L, Yu H, Yi S, Peng X, Su P, Xiao Z, Liu R, Tang A, Li X, Liu F, Shen S. The tumor suppressor miR-138-5p targets PD-L1 in colorectal cancer. *Oncotarget.* 2016;7 (29) : 45370-45384.
223. Yang R, Liu M, Liang H, Guo S, Guo X, Yuan M, Lian H, Yan X, Zhang S, Chen X, Fang F, Guo H, Zhang C. miR-138-5p contributes to cell proliferation and invasion by targeting Survivin in bladder cancer cells. *Mol Cancer.* 2016;15 (1) : 82.
224. de Bono JS, Logothetis CJ, Molina A, Fizazi K, North S, Chu L, Chi KN, Jones RJ, Goodman OB, Jr., Saad F, Staffurth JN, Mainwaring P, Harland S, Flaig TW, Hutson TE, Cheng T, Patterson H, Hainsworth JD, Ryan CJ, Sternberg CN, Ellard SL, Flechon A, Saleh M, Scholz M, Efstathiou

- E, Zivi A, Bianchini D, Loriot Y, Chieffo N, Kheoh T, Haqq CM, Scher HI, Investigators C-A-. Abiraterone and increased survival in metastatic prostate cancer. *N Engl J Med*. 2011;364 (21): 1995-2005.
225. Carney DN, Gazdar AF, Bepler G, Guccion JG, Marangos PJ, Moody TW, Zweig MH, Minna JD. Establishment and identification of small cell lung cancer cell lines having classic and variant features. *Cancer Res*. 1985;45 (6): 2913-2923.
226. Johnson BE, Whang-Peng J, Naylor SL, Zbar B, Brauch H, Lee E, Simmons A, Russell E, Nam MH, Gazdar AF. Retention of chromosome 3 in extrapulmonary small cell cancer shown by molecular and cytogenetic studies. *J Natl Cancer Inst*. 1989;81 (16): 1223-1228.
227. Lai SL, Brauch H, Knutsen T, Johnson BE, Nau MM, Mitsudomi T, Tsai CM, Whang-Peng J, Zbar B, Kaye FJ, et al. Molecular genetic characterization of neuroendocrine lung cancer cell lines. *Anticancer Res*. 1995;15 (2): 225-232.
228. Kim J, Jin H, Zhao JC, Yang YA, Li Y, Yang X, Dong X, Yu J. FOXA1 inhibits prostate cancer neuroendocrine differentiation. *Oncogene*. 2017.
229. Ahn Lee YL, Ning Xie , Martin Gleave , Michael Cox , Colin Collins, Xuesen Dong. Alternative RNA Splicing of the MEAF6 Gene Facilitates Neuroendocrine Prostate Cancer Progression. *Oncotarget*. 2017 doi: 10.18632/oncotarget.15854.
230. Biegging KT, Mello SS, Attardi LD. Unravelling mechanisms of p53-mediated tumour suppression. *Nat Rev Cancer*. 2014;14 (5): 359-370.

231. Zou M, Toivanen R, Mitrofanova A, Floc'h N, Hayati S, Sun Y, Le Magnen C, Chester D, Mostaghel EA, Califano A, Rubin MA, Shen MM, Abate-Shen C. Transdifferentiation as a Mechanism of Treatment Resistance in a Mouse Model of Castration-resistant Prostate Cancer. *Cancer Discov.* 2017.
232. Robinson D, Van Allen EM, Wu YM, Schultz N, Lonigro RJ, Mosquera JM, Montgomery B, Taplin ME, Pritchard CC, Attard G, Beltran H, Abida W, Bradley RK, Vinson J, Cao X, Vats P, Kunju LP, Hussain M, Feng FY, Tomlins SA, Cooney KA, Smith DC, Brennan C, Siddiqui J, Mehra R, Chen Y, Rathkopf DE, Morris MJ, Solomon SB, Durack JC, Reuter VE, Gopalan A, Gao J, Loda M, Lis RT, Bowden M, Balk SP, Gaviola G, Sougnez C, Gupta M, Yu EY, Mostaghel EA, Cheng HH, Mulcahy H, True LD, Plymate SR, Dvinge H, Ferraldeschi R, Flohr P, Miranda S, Zafeiriou Z, Tunariu N, Mateo J, Perez-Lopez R, Demichelis F, Robinson BD, Schiffman M, Nanus DM, Tagawa ST, Sigaras A, Eng KW, Elemento O, Sboner A, Heath EI, Scher HI, Pienta KJ, Kantoff P, de Bono JS, Rubin MA, Nelson PS, Garraway LA, Sawyers CL, Chinnaiyan AM. Integrative clinical genomics of advanced prostate cancer. *Cell.* 2015;161 (5) : 1215-1228.
233. Chen H, Sun Y, Wu C, Magyar CE, Li X, Cheng L, Yao JL, Shen S, Osunkoya AO, Liang C, Huang J. Pathogenesis of prostatic small cell carcinoma involves the inactivation of the P53 pathway. *Endocr Relat Cancer.* 2012;19 (3) : 321-331.

234. Scheble VJ, Braun M, Wilbertz T, Stiedl AC, Petersen K, Schilling D, Reischl M, Seitz G, Fend F, Kristiansen G, Perner S. ERG rearrangement in small cell prostatic and lung cancer. *Histopathology*. 2010;56(7): 937-943.
235. Wang L, Williamson SR, Zhang S, Huang J, Montironi R, Davison DD, Wang M, Yao JL, Lopez-Beltran A, Osunkoya AO, MacLennan GT, Baldrige LA, Du X, Cheng L. Increased androgen receptor gene copy number is associated with TMPRSS2-ERG rearrangement in prostatic small cell carcinoma. *Mol Carcinog*. 2015;54(9): 900-907.
236. Castro DS, Martynoga B, Parras C, Ramesh V, Pacary E, Johnston C, Drechsel D, Lebel-Potter M, Garcia LG, Hunt C, Dolle D, Bithell A, Ettwiller L, Buckley N, Guillemot F. A novel function of the proneural factor *Ascl1* in progenitor proliferation identified by genome-wide characterization of its targets. *Genes Dev*. 2011;25(9): 930-945.
237. Szekely G, Fritz E, Bandarra J, Heggie W, Sellergren B. Removal of potentially genotoxic acetamide and arylsulfonate impurities from crude drugs by molecular imprinting. *J Chromatogr A*. 2012;1240(52-58).
238. Palmgren JS, Karavadia SS, Wakefield MR. Unusual and underappreciated: small cell carcinoma of the prostate. *Semin Oncol*. 2007;34(1): 22-29.
239. Aparicio A, Tzelepi V, Araujo JC, Guo CC, Liang S, Troncoso P, Logothetis CJ, Navone NM, Maity SN. Neuroendocrine prostate cancer xenografts with large-cell and small-cell features

derived from a single patient's tumor: morphological, immunohistochemical, and gene expression profiles. *Prostate*. 2011;71 (8): 846-856.

240. Li Y, Donmez N, Sahinalp C, Xie N, Wang Y, Xue H, Mo F, Beltran H, Gleave M, Wang Y, Collins C, Dong X. SRRM4 Drives Neuroendocrine Transdifferentiation of Prostate Adenocarcinoma Under Androgen Receptor Pathway Inhibition. *Eur Urol*. 2016.

241. Lan F, Collins RE, De Cegli R, Alpatov R, Horton JR, Shi X, Gozani O, Cheng X, Shi Y. Recognition of unmethylated histone H3 lysine 4 links BHC80 to LSD1-mediated gene repression. *Nature*. 2007;448 (7154): 718-722.

242. Iwase S, Januma A, Miyamoto K, Shono N, Honda A, Yanagisawa J, Baba T. Characterization of BHC80 in BRAF-HDAC complex, involved in neuron-specific gene repression. *Biochem Biophys Res Commun*. 2004;322 (2): 601-608.

243. Hitti E, Iakovleva T, Brook M, Deppenmeier S, Gruber AD, Radzioch D, Clark AR, Blackshear PJ, Kotlyarov A, Gaestel M. Mitogen-activated protein kinase-activated protein kinase 2 regulates tumor necrosis factor mRNA stability and translation mainly by altering tristetraprolin expression, stability, and binding to adenine/uridine-rich element. *Mol Cell Biol*. 2006;26 (6): 2399-2407.

244. Carballo E, Lai WS, Blackshear PJ. Feedback inhibition of macrophage tumor necrosis factor- α production by tristetraprolin. *Science*. 1998;281 (5379): 1001-1005.

245. Noordzij MA, van der Kwast TH, van Steenbrugge GJ, Hop WJ, Schroder FH. The prognostic influence of neuroendocrine cells in prostate cancer: results of a long-term follow-up study with patients treated by radical prostatectomy. *Int J Cancer*. 1995;62 (3) : 252-258.
246. Abrahamsson PA, Cockett AT, di Sant'Agnese PA. Prognostic significance of neuroendocrine differentiation in clinically localized prostatic carcinoma. *Prostate Suppl*. 1998;8 (37-42).
247. Shi YJ, Matson C, Lan F, Iwase S, Baba T, Shi Y. Regulation of LSD1 histone demethylase activity by its associated factors. *Mol Cell*. 2005;19 (6) : 857-864.
248. Klajn A, Ferrai C, Stucchi L, Prada I, Podini P, Baba T, Rocchi M, Meldolesi J, D'Alessandro R. The rest repression of the neurosecretory phenotype is negatively modulated by BHC80, a protein of the BRAF/HDAC complex. *J Neurosci*. 2009;29 (19) : 6296-6307.
249. Zitvogel L, Tesniere A, Kroemer G. Cancer despite immunosurveillance: immunoselection and immunosubversion. *Nat Rev Immunol*. 2006;6 (10) : 715-727.
250. Hanahan D, Weinberg RA. Hallmarks of cancer: the next generation. *Cell*. 2011;144 (5) : 646-674.
251. Salcedo R, Cataisson C, Hasan U, Yuspa SH, Trinchieri G. MyD88 and its divergent toll in carcinogenesis. *Trends Immunol*. 2013;34 (8) : 379-389.
252. Narayanan KB, Park HH. Toll/interleukin-1 receptor (TIR) domain-mediated cellular signaling pathways. *Apoptosis*. 2015;20 (2) : 196-209.

253. Coulson JM, Edgson JL, Woll PJ, Quinn JP. A splice variant of the neuron-restrictive silencer factor repressor is expressed in small cell lung cancer: a potential role in derepression of neuroendocrine genes and a useful clinical marker. *Cancer Res.* 2000;60(7): 1840-1844.
254. Kreisler A, Strissel PL, Strick R, Neumann SB, Schumacher U, Becker CM. Regulation of the NRSF/REST gene by methylation and CREB affects the cellular phenotype of small-cell lung cancer. *Oncogene.* 2010;29(43): 5828-5838.
255. Wagoner MP, Roopra A. A REST derived gene signature stratifies glioblastomas into chemotherapy resistant and responsive disease. *BMC Genomics.* 2012;13(686).
256. Kamal MM, Sathyan P, Singh SK, Zinn PO, Marisetty AL, Liang S, Gumin J, El-Mesallamy HO, Suki D, Colman H, Fuller GN, Lang FF, Majumder S. REST regulates oncogenic properties of glioblastoma stem cells. *Stem Cells.* 2012;30(3): 405-414.